Regulation of Brain Adenosine and Adenine-Nucleotide Levels Under Excitotoxic Conditions and in Sleep Regulation

A Thesis submitted to the
University of Manitoba

In Partial fulfilment of the requirements for the degree of

Doctor of Philosophy
In Pharmacology and Therapeutics

By P. Nickolas Shepel

February 2002

THE UNIVERSITY OF MANITOBA

FACULTY OF GRADUATE STUDIES

*****

COPYRIGHT PERMISSION PAGE

Regulation of Brain Adenosine and Adenine-Nucleotide Levels Under Excitotoxic Conditions and in Sleep Regulation

BY

P. Nickolas Shepel

A Thesis/Practicum submitted to the Faculty of Graduate Studies of The University of Manitoba in partial fulfillment of the requirements of the degree

of

DOCTOR OF PHILOSOPHY

Table of Contents

Abbreviations 6

Preface 8

Work Not Included in the Thesis 9

Abstract 14

Acknowledgements 16

General Introduction 18

A. The Experimental Models Used 19
Excitotoxicity 19
Sleep Deprivation 23

B. Glutamate – An Excitatory Amino Acid 23
Ionotropic Glutamate Receptors 24
AMPA 24
Kainate 25
NMDA 26

Metabotropic Glutamate Receptors 28

Glutamate Transporters 29

C. Adenosine: A Neuromodulator 30
Adenosine Receptors 30
A_1 30
A_2 31
A_3 31

Adenosine Enzymes 32
Adenosine Kinase 32
Adenosine Deaminase 33
5′-Nucleotidase 34

Adenosine Transporters 34

Chapter 1 – Measurement of Adenosine and Adenine-Based Nucleotide Levels in Rat Brain Tissue Fixed by Microwave Irradiation. 35

Abstract 36

Introduction 37

Methods 39
- Animals 39
- Surgical Procedures 39
- Microwave Irradiation 39
- Brain Dissections 40
- Tissue Preparation 40
- HPLC Analysis of Adenosine 42
- HPLC Analysis of Nucleotides 43
- Protein Analysis 43
- Identification and Quantification of Purines 44
- Pooling of Striatal Subregion Data 44

Results 46
- Analysis of Nucleotides 46
- Analysis of Adenosine 47
- Protein Analysis 48
- Tissue Homogenization Model 49

Discussion 52

Chapter 2 – Effects of Glutamate Receptor Stimulation on Adenosine And Energy Charge Levels in Rat Brain. 55

Abstract 56

Introduction 57

Methods 60
- Animals 60
- Surgical Procedures 60
- Chemicals 60
- Intrastriatal Injections 60
- Brain Dissections 61
- Purine and Protein Analyses 61
- Data Analysis and Statistics 61

Results 63
- Intrastriatal L-Glutamate Injection 63

Antagonism of Glutamate Effects 64
Analysis of Adenosine and Nucleotide Levels 65
Purine Levels at the Injection Site 66
Cortical Stimulation Studies 69
Effects of Glutamate Uptake Inhibition 72
Site- and Event-Specificity of Purine Level Changes 73
Effects of mGluR Activation 75
Adenosine Levels and Energy Charge 75

Discussion 78
Adenosine Levels and Energy Charge 78
Adenosine Site- and Event-Specificity 83
The Contralateral Effect 83

Chapter 3 – Effects of Sleep Deprivation on Adenosine and Energy Charge Levels in Rat Brain 86

Abstract 87

Introduction 88

Methods 93
Animals 93
Sleep Deprivation 93
Microwave Irradiation and Dissections 93
Analysis of Purinergic Compounds 95
Between-Study Data Normalization 95

Results 98
24-Hour Sleep Deprivation Studies 98
12-Hour Sleep Deprivation Studies 101

Discussion 104

Chapter 4 - Expression Profiling of Adenosine-Related Genes in Rat Brain: Changes With Diurnal Rhythm and Age – Preliminary Studies. 110

Abstract 111

Introduction 112

Methods 115
Animals 115
Tissue Dissections 115

Experiments 115

Results and Discussion 117
Diurnal Changes in Gene Expression 117
Age-Related Changes in Gene Expression 119
mRNA Isolation From Small Microwaved Tissue Samples 122

Detailed Methods 124

A. Measuring Gene Expression Using Antisense RNA Amplification 124
1. Isolation of Total RNA 124
2. DNase Treatment of Total RNA 126
3. First Strand cDNA Synthesis 127
4. Polymerase Chain Reaction 128
5. Second Strand cDNA Synthesis 129
6. S1 Nuclease Degradation of Single-Stranded cDNA 130
7. Creation of Blunt-Ended cDNA 131
8. Drop Dialysis of Double-Stranded cDNA 132
9. Synthesis of aRNA 133
10. Purification of aRNA 134
11. Hybridization with aRNA 135

B. Mini-Array Analysis of Adenosine-Related Genes 135
1. ^{32}P-Labeled cDNA Probe Synthesis 135
2. Preparation of cDNA Mini-Arrays 136
3. Mini-Array Hybridization 139

C. Measurement of Gene Expression using a Commercial cDNA Array 140
1. ^{32}P-Labeled cDNA Probe Synthesis 140
2. Array Hybridization 141

Final Conclusions and Future Directions 142

Appendix 147

Appendix I. Purine and Protein Analyses 148

A. HPLC Equipment and Chromatograms 149
B. Protein Analysis – Method Validation 150
C. Tissue Homogenization Model 152

Appendix II. Striatal Subregion Purine Analysis 158

A. Basal Purine Levels 159

B. No-Volume Injections 160
C. Tris Vehicle Injections 161
D. Salt Solution Injections 162
E. aCSF Vehicle Injections 163
F. Glutamate Injections (aCSF vehicle) 164
G. Glutamate Injections (with MK-801 ip) 165
H. NMDA Injections (Tris vehicle) 166
I. NMDA Injections (aCSF vehicle) 167
J. Cortex Stimulation 168

Appendix III. Linear Regression Analyses of Adenosine-Energy Charge Relationships 169

A. Adenosine – EC Linear Regression #1 170
B. Adenosine – EC Linear Regression #2 171

Appendix IV. Individual Sleep Deprivation Studies 172

A. 24h Sleep Deprivation - Study #1 173
B. 24h Sleep Deprivation - Study #2 174
C. 24h Sleep Deprivation - Study #3 175
D. 12h Sleep Deprivation - Study #1 176
E. 12h Sleep Deprivation - Study #2 177

Appendix V. Expression Profiling of Adenosine-Related Genes - Supplemental Information 178

A. Oligonucleotide Primers 179
B. Atlas™ Gene Expression Array – Detected Genes 181
C. Reaction Enzymes 184
D. Commercial Nucleotides 185
E. Other Materials 185
F. Buffers 186

References 187

Abbreviations

ACPD: (1S,3R)-1-aminocyclopentane-1,3-dicarboxylic acid*

AMPA: α-amino-3-hydroxy-5-methyl-4-isoxazolepropionate

D-APV: D-2-amino-5-phosphonovalerate

aCSF: artificial cerebrospinal fluid

aRNA: anti-sense RNA

CNQX: 6-cyano-7-nitroquinoxaline-2,3-dione

cAMP: cyclic 3′,5′-adenosine monophosphate

CPP: 3-(2-carboxypiperazine-4-yl)propylphosphonate

DAG: diacylglycerol

DCG-IV : (2S, 1′R, 2′R, 3′R)-2-(2,3-dicarboxycyclopropyl)glycine

DTT: dithiothreitol

GABA: γ-aminobutyric acid

GAPDH: glyceraldehyde-3-phosphate dehydrogenase

GLT: glutamate transporter

GPC: G-protein coupled

HAsp: L-(-)-threo-3-hydroxyaspartic acid

iGluRs: ionotropic glutamate receptors

L-CCG-I : (2S, 1′S, 2′S)-2-(carboxycyclopropyl)glycine

L-AP4: (S)-2-amino-4-phosphonobutyric acid

L-SOP: S-serine-O-phosphate

Ibo: ibotenate

IP_3: inositol-1,4,5-trisphosphate

KA: kainic acid

mGluR: metabotropic glutamate receptor

MK801: 5-methyl-10,11-dihydro-5H-dibenzocyclohepten-5,10-imine maleate

NBQX: 2,3-dihydroxy-6-nitro-7-sulphamoylbenzo(F)-quinoxaline

NMDA: N-methyl-D-aspartate

PCP: phencyclidine

Quis: quisqualate

TCP: N-[1-(2-thienyl)cyclohexyl]-piperidine

TOA: tri-n-octylamine

TTX: tetrodotoxin

* The (1S,3R) enantiomer is the active one at mGLURs whereas the trans ACPD mixture often referred to in literature is usually a racemic mixture of the (1S,3R) and (1R,3S) forms.

Preface

This thesis consists of a General Introduction that summarizes the biological systems we studied and four separate chapters, each outlining separate aspects of our research involving the regulation of adenosine and adenine-based nucleotide levels in brain. Chapter 1 outlines the analytical methods that were developed in order to overcome the challenges of accurately measuring the concentration of purinergic compounds in small brain tissue samples. Using these techniques it was possible for us to study the changes in brain purine levels that occur immediately following acute excitotoxic insults (Chapter 2) and during normal regulation of the homeostatic process of sleep (Chapter 3). In Chapter 4, preliminary experiments designed to measure gene expression changes in small discrete brain regions are described. The objective of this work was to develop methods to characterize the changes in the expression of adenosine-related receptors, enzymes and transporters that might occur both with age and over the circadian cycle in order to gain some insight into components of adenosine regulation that might give rise to the changes in sleep patterns that occur with circadian rhythm and aging.

The Appendix section at the end of the thesis contains detailed supplemental data and methods that were discussed in a summarized form in the chapters. This additional information provides further insight into our interpretation of results and will help facilitate further development of this research.

Work Not Included in the Thesis

Not discussed in this thesis is a significant quantity of work that I carried out in collaboration with other research groups that involved developing methods for nucleotide and adenosine level determination in several different experimental systems. These works were not detailed in this thesis because although I contributed in developing experimental methods I was not directly involved in the study design. In addition, also not included in this thesis are findings from a completely different research project that I carried out which characterized the effects of diadenosine polyphosphate compounds on the function of intracellular ryanodine receptor-regulated Ca^{2+} release channels. Below is a brief description of my collaborative efforts and a list of the resulting publications and abstracts is presented at the end of this section.

Adenosine has been referred to by many as an endogenous neuroprotective molecule given the several protective mechanisms, such as attenuation of excitatory neurotransmission, that it can mediate. In the study by Sinclair et al. (1999), we investigated whether adenosine could act in a paracrine fashion to potentiate its own release during episodes of metabolic stress. Using a cell model known to contain a full complement of adenosine receptors and transporters it was shown that iodoacetic acid-induced metabolic stress increased the release of purinergic compounds, a component of which was adenosine. Under these stress conditions, it was also found that adenosine A_1 receptor stimulation increased purine release by a protein kinase C dependent inhibition of adenosine kinase activity. It was concluded that this

mechanism might serve to facilitate the protective actions of adenosine, in a paracrine fashion, during periods of increased adenosine release.

Several strategies have been proposed to potentiate the endogenous neuroprotective actions of adenosine, under conditions of acute tissue insult, that involve inhibiting adenosine-metabolizing enzymes or blocking adenosine transport across cell membranes. In the study by Parkinson et al. (2000), we tested the hypothesis that nitrobenzylthioinosine (NBMPR), a potent inhibitor of adenosine transport through ENT1-type nucleoside transporters, could protect against neuronal injury during periods of ischemia by increasing tissue adenosine levels and potentiating protective adenosine receptor responses which include the attenuation of proinflammatory cytokine production, namely tumor necrosis factor α (TNF-α). We observed that NBMPR induced a protective effect when given intracerebroventricularly prior to the induction of brain ischemia in rats as indicated by the sparing of hippocampal CA1 pyramidal neurons. Because NBMPR did not affect significantly ischemia-induced increases in tissue adenosine or TNF-α levels, however, we concluded that the protective effect by NBMPR was probably independent of adenosine levels or adenosine receptor-mediated control of TNF-α.

One element implicated in the pathology of Multiple Sclerosis (MS) is the involvement of the cytokine family of signaling molecules, which include TNF-α and interleukin-6 (IL-6). Indeed, in some classes of MS patients (relapsing-remitting) cytokine levels are known to be elevated and these abnormal levels may be due at least in part to altered adenosine homeostasis given that adenosine, through its cell surface receptors, can alter cytokine levels. In the work by Mayne et al. (1999a), we

tested the hypothesis that altered adenosine homeostasis existed in MS patients which might contribute to their elevated cytokine levels. Comparing plasma levels of cytokines and adenosine and peripheral blood mononuclear cells (PBMCs) we observed that MS patients had significantly reduced adenosine A_1 receptor (A_1R) abundance associated with their PBMCs and that their plasma levels of adenosine and TNF-α were significantly reduced and elevated, respectively, compared to controls. Upon verifying that activation of A_1Rs on PBMCs could inhibit mitogen-stimulated production of TNF-α, it was concluded that altered adenosine homeostasis, by contributing to dysregulation of cytokine levels, may contribute in the pathology of MS.

Fixing tissues by microwave irradiation allowed for the accurate and precise determination of metabolically labile metabolites such as adenine-based nucleotides and adenosine. It was not known, however, how this method of tissue fixation would affect tissue RNA and whether measurements of gene expression could be carried out on microwaved tissue. In the study by Mayne et al. (1999b), we investigated whether intact RNA could be extracted from microwaved tissue and whether gene expression measurements could be carried out. In rat brain tissue fixed by microwave irradiation, to a degree that was sufficient to preserve endogenous levels of adenosine, ribosomal RNA was found to be largely degraded, however, messenger RNA (mRNA) was judged to be left in tact given that cDNA synthesis reactions were carried out successfully even with genes expected to be of relatively low abundance. These findings presented the possibility that in addition to using microwave fixation

for the analysis of labile tissue metabolites, one could also investigate the concurrent gene profile in the same tissue.

In addition to my research investigating adenosine and purine nucleotide homeostasis in the brain, I also carried out studies determining the effects of diadenosine polyphosphates (Ap_nAs) on the function of ryanodine receptor-regulated intrcellular Ca^{2+} release channels. Ap_nAs are formed intracellularly during the activation of amino acids by aminoacyl tRNA synthetases and considerable evidence suggests that these compounds may be involved in signaling cellular stress responses. Using radioligand binding studies, I tested the effects of Ap_nAs on ryanodine receptors (RyRs) in different subcellular fractions of rat brain and measured how these effects were altered by other, known RyR modulators including divalent cations (Ca^{2+} and Mg^{2+}) and caffeine. A portion of this work involving the analysis of RyRs in synaptosomal subfractions was included in the review paper by Mattson et al. (2000).

Diadenosine polyphosphates, in addition to their intracellular formation and actions, have also been implicated in having neurotransmitter actions due to their release from neural tissues and their ability to activate cell-surface purine receptors. In the study by Holden et al. (2000), we studied the ability of Ap_nAs to elevate intracellular calcium ($[Ca^{2+}]_i$) levels in neural tissues using cultured fetal astrocytes and fluorescent calcium imaging techniques. We tested the effects of several agents known to alter $[Ca^{2+}]_i$ levels by specific mechanisms on Ap_nA-induced increases in ($[Ca^{2+}]_i$) levels and found that these increases were due partly to Ca^{2+} release from intracellular ryanodine and IP_3–regulated pools and partly to influx of extracellular

Ca^{2+} due to activation of ionotropic purine receptors. These findings suggested that conditions resulting in elevated levels of extracellular Ap_nAs can alter $[Ca^{2+}]_i$ signaling pathways in neuronal tissues.

Publications

Sinclair, C.J.D., **Shepel, P.N.**, Geiger J.D. and Parkinson F.E. (1999) Stimulation of nucleoside efflux and inhibition of adenosine kinase by A_1 adenosine receptor activation. *Biochem Pharmacol.* **59,** 477-483.

Parkinson F.E., Zhang Y.W., **Shepel P.N.**, Greenway S.C., Peeling J., and Geiger J.D. (2000) Effects of nitrobenzylthioinosine on neuronal injury, adenosine levels and adenosine receptor activity in rat forebrain ischemia. *J. Neurochem.* **75,** 795-802.

Mayne M., **Shepel P.N.**, Jiang J., Geiger J.D., and Power C. (1999a) Dysregulation of adenosine A_1 receptor-mediated cytokine expression in peripheral blood mononuclear cells from multiple sclerosis patients. *Ann Neurol.* **45,** 633-639.

Mayne M., **Shepel P.N.**, and Geiger J.D. (1999b) Recovery of high integrity mRNA from brains of rats killed by high-energy focused microwave irradiation. *Brain Res Brain Res Protoc.* **4,** 295-302.

Mattson M.P., LaFerla F.M., Chan, S.L., Leissring M.A., **Shepel P.N.**, and Geiger J.D. (2000) Calcium signaling in the ER: its role in neuronal plasticity and neurodegenerative disorders. *Trends Neurol. Sci.* **23,** 222-229.

Holden C.P., Haughey N.J., Dolhun B., **Shepel P.N.**, Nath A. and Geiger J.D. (2000) Diadenosine pentaphosphate increases levels of intracellular calcium in astrocytes by a mechanism involving release from caffeine/ryanodine- and IP_3-sensitive stores. *J. Neurosci. Res.* **59,** 276-282.

Abstracts Presented at Scientific Meetings

Geiger, J.D., **Shepel, P.N.**, and C.P. Holden. "Diadenosine polyphosphates: Positive modulators of ryanodine receptor calcium release channels." Satellite meeting of the Novartis Foundation Meeting on Dinucleoside Polyphosphates. London, England. March 20-21, 1998.

Shepel, P.N., Holden, C.P., and J.D. Geiger. "Mechanisms of diadenosine polyphosphate modulation of ryanodine receptors in subcellular fractions of rat brain." Joint meeting of the International Society For Neurochemistry and The American Society For Neurochemistry, Boston, Massachusetts, U.S.A. July 20-26, 1997; Abstract S239B.

Abstract

Adenosine and the adenine-based nucleotides ATP, ADP and AMP are purinergic compounds fundamental to cellular energy homeostasis. Produced largely from ATP metabolism, adenosine is referred to as neuroprotective because it accumulates during periods of high-intensity cellular activity, and is known to mediate protective mechanisms that oppose aberrant cellular processes that are initiated under pathological conditions. We used intrastriatal injections of glutamate receptor agonists to investigate the simultaneous changes in purine levels following acute excitotoxic insults to the brain and quantify the relationship between energy charge (EC) depletion and adenosine accumulation. Our results showed that adenosine levels appeared to be regulated in a two-tiered fashion depending on the depolarizing strength of a stimulus. Extensive EC depletion occurring with highly depolarizing stimuli produced higher rates of adenosine formation compared to more weakly depolarizing stimuli. The mechanistic difference between these two modes of adenosine formation appeared to depend on the absence or presence of NMDA receptor activation.

Adenosine as a key regulatory molecule in sleep regulation is proposed to accumulate with prolonged wakefulness as brain ATP stores are gradually depleted. Our analyses of purine levels in cortical, hypothalamic and basal forebrain regions following 12 or 24 h sleep deprivation showed small but consistent decreases in ATP levels in basal forebrain and hypothalamic regions, however, no consistent patterns were observed in adenosine levels.

These studies are the first to quantify the relationship between ATP metabolism and adenosine accumulation in brain and directly measure how the levels of purinergic compounds in brain are altered with sleep deprivation.

Acknowledgements

I would like to begin by acknowledging the Medical Research Council of Canada (now CIHR), the Natural Sciences and Engineering Council of Canada (NSERC) and the American Society for Pharmacological and Experimental Therapeutics (ASPET) for funding support during my graduate studies.

I would like to thank Drs Allan Pack and Mirek Mackiewicz at the University of Pennylvania for making it possible for me to visit their laboratory and begin learning the intricacies of Molecular Biology. My visit there, which included stops in New York and Washington D.C. was an incredible experience!

To my supervisor Dr. Jonathan Geiger I would like to extent my appreciation for his efforts in mentoring my studies. During my time under his supervision I was encouraged to develop my own scientific ideas and was then allowed to pursue them in the laboratory. Today, I credit my graduate studies experience in Jonathan's lab with giving me that ability to think independently and critically about science.

I would like to extent my gratitude to Dr. Clark Holden, a former Post-Doctoral Fellow in Jonathan's lab, for training me in the early years of my graduate studies in my conversion from Analytical Chemist to Pharmacologist. Clark's patience and attention to detail influenced me to adopt good experimental technique early in my studies and facilitated my successes as I continued. At this point I would also like to mention Dr. Michael Mayne and Ms. Julie Fotheringham, two other great people that I had the pleasure to work with while in Jonathan's lab. Although Clark, Julie, Mike and myself no longer work together in the trenches we have a wealth of

memories that we shared and those friendships will undoubtedly continue long after life leads us in our separate directions.

That this thesis is now completed is a tribute to the support given to me by my family during this last year when obstacles in my personal life became seemingly insurmountable. Thank you to my parents Nick and Evelyn, my sisters Mary, Chris and Susan, and Susan's husband George. They have always supported me unconditionally in my efforts to face the challenges of life and my successes today are due in part to their support.

Finally, I would like to thank my Girlfriend, Partner, and Soulmate Sherrie Kelly. She was beside me and supported me throughout most of my graduate studies experience and was always a brilliant energetic light during even the darkest days of the past year. I thank her from the bottom of my heart and hope that in the future I can return her love and support.

General Introduction

General Introduction

Adenosine, an endogenous purine nucleoside ubiquitous to living systems is formed in large part as a breakdown product of the universal biological energy molecule, ATP. Formed in this fashion, adenosine is referred to as a "retaliatory metabolite" [133] as its accumulation during periods of high-energy utilization initiates compensatory mechanisms such as vasodilation [106,149] and attenuation of neuronal signaling [39,233]. Because of its fundamental role as an indicator of cellular metabolic rate, adenosine has been implicated as an important signaling molecule in a variety of physiological processes including sleep and brain responses to ischemic insults. We studied the role of adenosine and high-energy adenine-based nucleotides in *in vivo* models of excitotoxicity, the predominate damaging mechanism in ischemia, and sleep deprivation, a model used to study the mechanisms controlling sleep.

A. Experimental Models Used

Excitotoxicity. Common to mechanisms of acute brain insult such as stroke [12,115] and seizure [13], as well as of chronic neuropathological conditions such as HIV infection [80], Parkinson's [27,54] and Huntington's diseases [23,63,122] is excitotoxicity, a damaging process initiated by abnormally high levels of glutamate release. Glutamate is the primary excitatory neurotransmitter in the central nervous system and under normal conditions is released following nerve depolarization. Under conditions where energy production is compromised, as occurs with cyanide poisoning, or by the more global effect of cutting off nutrient supply as occurs during

stroke, the energy-requiring ion gradients that give rise to the resting membrane potential in excitable cells begin to dissipate with the failure of active transport processes. In the early stages of excitotoxicity, cells swell due to ionic imbalances, membranes depolarize, and glutamate is released (Fig. G.1). This aberrant transmitter release perpetuates further depolarization through activation of ionotropic glutamate receptors (iGluRs) and the resultant large influx of calcium sets in motion destructive apoptotic and necrotic mechanisms. In this context, excitotoxicity may be viewed as a glutamate-initiated cascade of events that leads to increased entropy in brain tissue while cellular energy generation has been compromised.

Adenosine may serve as a protective, inhibitory neuromodulator during the early events in excitotoxicity. In our experimental models, we simulated excitotoxicity by injecting glutamate receptor agonists into rat brain striatum. The striatum serves as a good region for these studies due to its innervation by glutamatergic corticostriatal afferent nerves [189] and its relatively large size and homogeneity of cells (Fig. G.2). The only other major neuronal input to the striatum is the dopaminergic nigrostriatal pathway. Interneurons intrinsic to the striatum are cholinergic and glutamatergic [100,128]. The majority of striatal neurons are GABAergic spiny neurons that leave the striatum forming two parallel output pathways to the globus pallidus and substantia nigra. In brain, the striatum serves as an integration point for neuronal signals coming from both cerebral cortex and substantia nigra and a convergence area for several major neuronal fiber tracts including afferent glutamatergic corticostriatal and dopaminergic nigrostriatal

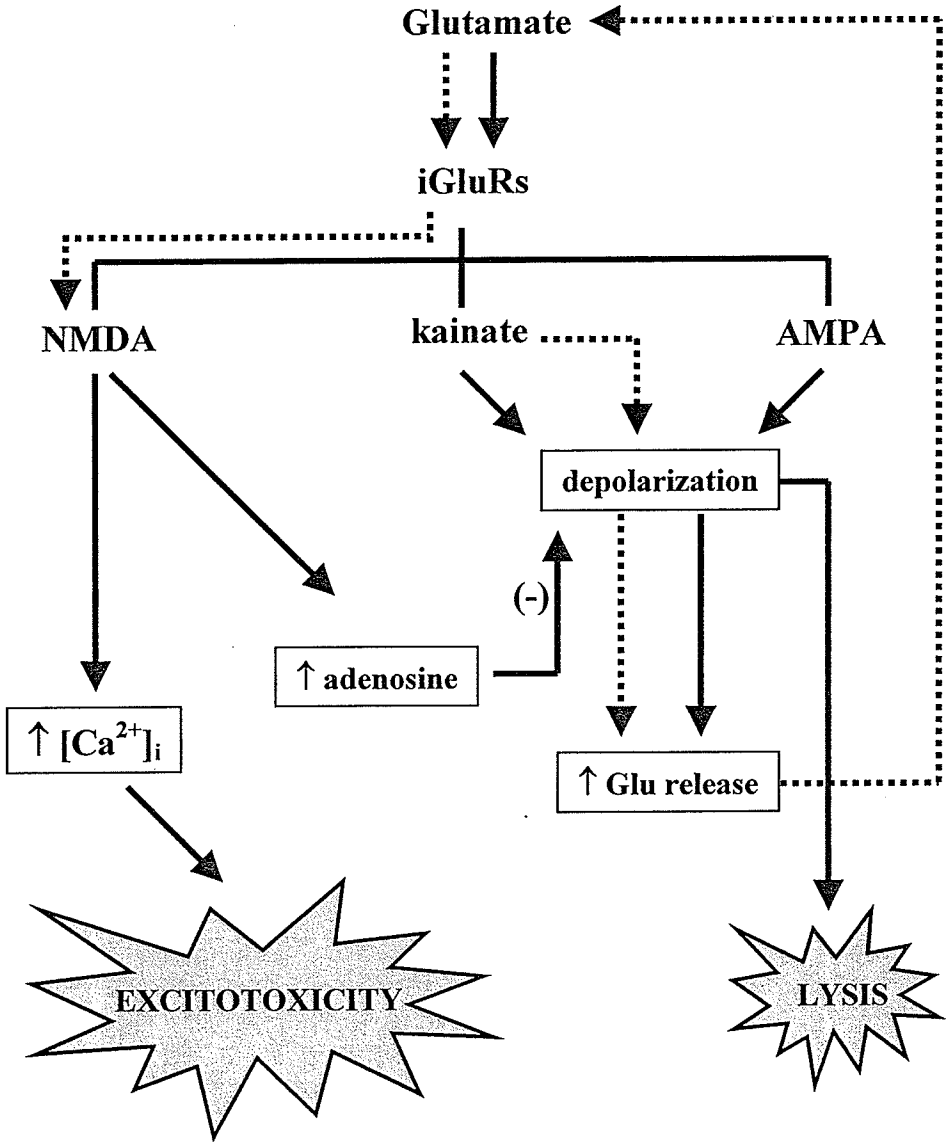

Figure G.1. The Actions of Glutamate. Extracellular glutamate acts on the pharmacologically characterized AMPA- and kainate-type ionotropic glutamate receptors (iGluRs) to initiate rapid and brief depolarization due to the influx of Na^+ current. With depolarization additional glutamate may be released to perpetuate this process. NMDA-type iGluRs are glutamate-activated only when voltage dependent Mg^{2+} block is alleviated by cellular depolarization, resulting in Ca^{2+} influx from the extracellular space and, among many other effects, production of adenosine. Adenosine, by attenuating depolarization through activation of adenosine A_1 receptors, is thought to play a potential neuroprotective role. The dotted line, starting at the kainate receptor label, outlines the path by which we propose kainate induces adenosine level increases. Aberrant activation of NMDA receptors by excessively high glutamate levels produces a large Ca^{2+} influx initiating a cascade of excitotoxic mechanisms including the formation of free radicals. Continued depolarization, producing imbalances in cellular ion homeostasis, leads to the osmotic effect of cell swelling and lysis.

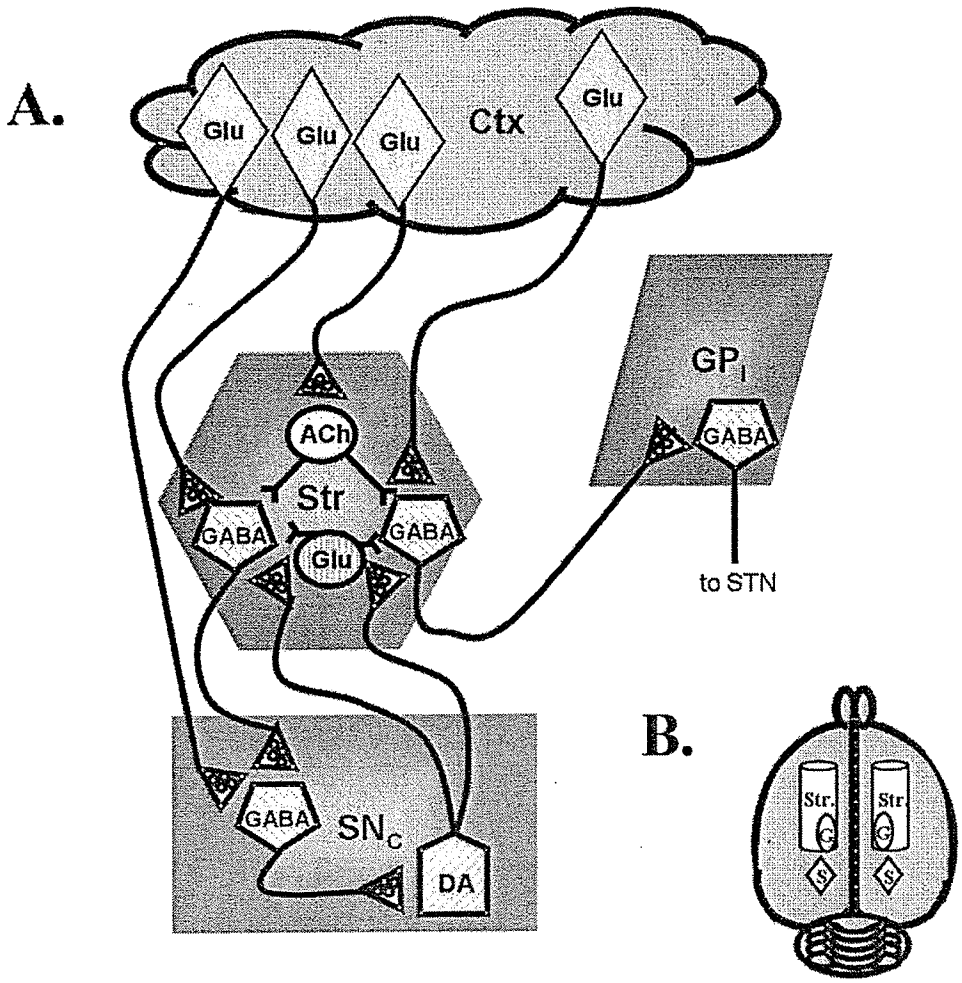

Figure G.2. Neuronal Innervation of the Striatum. A. The striatum (Str) is innervated by glutamatergic neurons that originate in the cerebral cortex (Ctx) and synapse on GABAergic medium spiny neurons in the striatum [189]. Medium spiny neurons predominate in the striatum, making up 90-95% of the neuron population. Within the striatum are intrinsic giant aspiny cholinergic interneurons [100] and the glutamatergic [128] interneurons. Medium spiny neurons leaving the striatum innervate GABA neurons in the substantia nigra (pars compacta area, SN_c), which in turn connect to dopaminergic (DA) neurons that feed back to the medium spiny neurons in the striatum. In other output pathway from the striatum, medium spiny neurons synapse with other GABAergic neurons in the globus pallidus (lateral segment, GP_l) that pass into the subthalamic nucleus (STN) [189]. This figure was adapted from [28]. B. Shown is the approximate orientation of the areas described in A in the rat brain. The cortex in this figure is peeled away revealing the underlying striatal regions. Cylindrical regions represent the tissue we acquired following dissection of the striatum (see Brain Dissections section of Chapter 2) of which the posterior ventro-medial area is primarily globus pallidus (G). Located further posterior and toward the ventral surface of the brain is the substantia nigra (S). Regions are not drawn to scale.

pathways, and efferent GABAergic projections to the globus pallidus and substantia nigra. Many types of body movements are coordinated through the striatum as indicated by the contralateral turning that can be induced by disruptions in striatal signaling following injection of glutamate agonists [190,191].

Sleep Deprivation. Sleep is a behavior familiar to all of us yet the physiological reasons for why we sleep or the mechanisms that induce and regulate sleep are largely unknown. One prominent theory is that sleep serves a restorative function to replenish energy substrates in the brain after their depletion following periods of wakefulness [14]. Because adenosine is formed as a consequence of increased metabolic activity and since adenosine can attenuate neurotransmission, it has been hypothesized that elevated adenosine levels, formed during extended periods of wakefulness, initiate the onset of sleep.

B. Glutamate – An Excitatory Amino Acid

Glutamate released from nerve terminals acts on three types of ion channel-coupled receptors that were identified initially by their relative affinities for NMDA (N-methyl-D-aspartate), kainate and AMPA (α-amino-3-hydroxy-5-methyl-4-isoxazolepropionate). AMPA and kainate receptors act predominantly to initiate synaptic depolarization, whereas in addition to contributing to depolarization, NMDA receptor activation and the resultant influx of calcium initiates a variety of complex intracellular signaling pathways. Glutamate release can also activate directly intracellular processes by binding to metabotropic glutamate receptors that are positively coupled to adenylate cyclase and phospholipase C.

Ionotropic Glutamate Receptors

AMPA Receptors. AMPA receptors play a fundamental role in the propagation of excitatory signaling between neurons. The function of these receptors to conduct glutamatergic signals is facilitated by their rapid activation and desensitization by glutamate [18,32] and the localization of AMPA receptor subunits to cell bodies, dendrites and postsynaptic sites [38,116]. The depolarizing currents mediated by AMPA receptors are predominantly due to the passage of Na^+ ions, however, several functional channel-forming combinations of AMPA receptor subunits are permeable to Ca^{2+} [85,86].

AMPA receptors are composed of four different subunits GluR1, GluR2, GluR3, and GluR4 [18,85]; all of which are present in striatum [116] on postsynaptic neurons [202]. The GluR2 subunit confers a divalent cation impermeability property to the channel [85] and neuronal populations where GluR2 expression is down-regulated are more susceptible to cell death [137]. Greater degrees of AMPA receptor diversity are obtained when receptor subunits are alternatively spliced to give two different forms for each subunit termed "flip" and "flop" variants [86]. The variants, although having similar pharmacological properties, do differ in the efficiency of activation by glutamate [86].

Pharmacological agonists at AMPA receptors, in addition to AMPA, include domoate, a neurotoxin found in some types of marine algae, and kainate [18]. Kainate binds with much lower affinity than AMPA and causes non-desensitizing currents [142]. Agonist potency at AMPA receptors is: domoate = AMPA >

glutamate > kainate [18]. Antagonists at AMPA receptors are the quinoxalinedione compounds [87] CNQX and NBQX [185].

Kainate Receptors. Like AMPA receptors, kainate receptors are generally regarded to be fast-signalling glutamate receptors because their constituent ion channels allow the passage of depolarizing Na^+ currents and the receptors rapidly desensitize to glutamate [18,32]. Kainate receptors are composed of low affinity GluR5, GluR6, and GluR7 subunits (K_D for kainate = 50-100 nM) [18] and high affinity KA1 and KA2 (K_D for kainate = 5 nM) [18] subunits [32]. GluR-5, 6, and 7 subunits can form homomeric receptors, whereas the high affinity subunits KA-1 and KA-2 only form functional receptor complexes when coupled with a low affinity subunit [32]. Homomeric receptor complexes of GluR5 are sensitive to AMPA whereas those of GluR-6 and GluR-7 are not [32]. In the striatum, *in situ* hybridization studies have revealed the presence of GluR-6, GluR-7 and KA-2 subunit mRNA and only traces from that of GluR-5 and KA-1 [226].

The role of kainate receptors in neurotransmission is somewhat ambiguous given the findings of some recent studies. Activation of kainate receptors has been shown to both facilitate [179] and inhibit [33] transmitter release in hippocampus depending on the subregion studied. Kainate receptors in cerebral cortex facilitate glutamate release by a presynaptic mechanism [152] and in hippocampus they modulate GABA release [169]. In striatum, kainate receptors have been demonstrated on intrinsic postsynaptic neurons [202], however, their presence on presynaptic terminals of afferent neurons in the striatum, such as the corticostriatal

glutamatergic neurons, is controversial. Receptor localization studies are largely inconclusive in showing a presynaptic presence of kainate receptors in the striatum. However, studies showing that destruction of corticostriatal nerves entering striatum significantly decreases kainate-evoked glutamate release [192,234] and reduces the toxic effects of intrastriatal kainate injection [121], and that kainate increases glutamate release from excitatory terminals in striatum [62,234] support the idea of presynaptic kainate receptors.

Agonists at kainate receptors include kainate and domoate. The antagonist classically used to block kainate receptor responses is CNQX which is about one fifth as effective blocking the kainate receptor as it is blocking AMPA receptors [87].

NMDA Receptors. The NMDA-type glutamate receptor, compared to AMPA and kainate receptors, is a more slowly gated ion channel (Fig. G.3.). This glutamate receptor subtype has been extensively studied for its involvement in calcium-mediated cellular mechanisms, the complexity with which its activation is modulated, and its role in synaptic plasticity and glutamate excitotoxicity.

NMDA receptors are composed of five different subunits: NMDAR1 [130], NMDAR2A, NMDAR2B, NMDAR2C and NMDAR2D [103,124]. For NMDAR1, eight splice variants have been identified [86,129]. NMDAR1 homomeric complexes and heteromeric NMDAR1/NMDAR2 combinations form functional NMDA receptors, however, NMDAR2 subunits alone do not form functional homomeric channels [86,129]. Studies of NMDAR subunit mRNA abundance have revealed high levels of NMDAR1 and NMDAR2B and moderate levels of NMDAR2A in

striatum [221]. Within striatum, the majority of NMDA receptors are located postsynaptically, however, some evidence suggests a presynaptic localization where they are thought to serve as excitatory autoreceptors [202]. General characteristics of NMDA receptors are illustrated in Figure G.3. Here, we will not address the

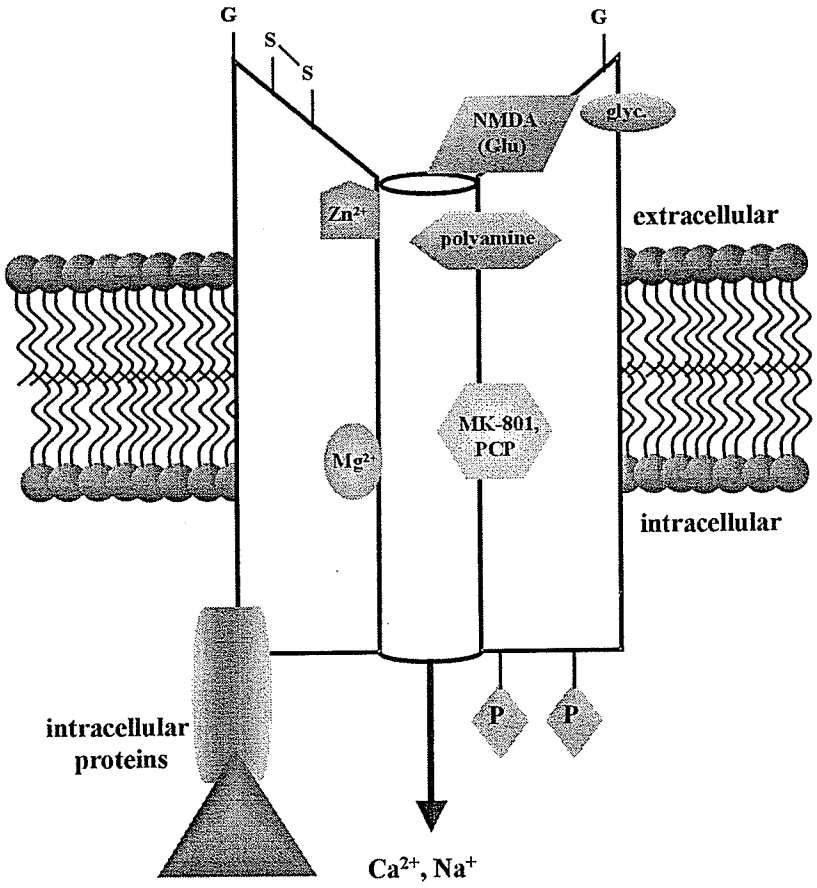

Figure G.3. The NMDA Receptor. The NMDA receptor is subject to modulaton by several different types of compounds. Activation of the receptor allows the influx of predominantly Ca^{2+} and some Na^{+} ions. Not only does receptor activation require the interaction of glutamate (Glu) at the receptor's ligand binding site, but also the interaction of glycine (glyc) at a separate site [96]. Under basal conditions, the receptor is subject to voltage-dependent block by Mg^{2+} [8,135]. Non-competitive antagonists, acting away from the receptor's ligand binding site, include MK-801, phencyclidine (PCP), and Zn^{2+} [86]. In addition to polyamine compounds (spermine, spermidine), which are known to potentiate the receptor's activity [123], reduction of disulfide bonds on the receptor also increases responses [6]. Other allosteric modification to the receptor includes glycosylation (G) [61] and phosphorylation (P) [168]. Yet another method of altering the function of NMDA receptors is achieved through direct interaction with associated intracellular proteins [235].

individual variations in characteristics between NMDA receptor complexes containing different subunit combinations as they have been reviewed extensively elsewhere [86,129].

Although NMDA receptors are referred to as ionotropic, advances in protein analysis techniques have revealed that NMDA receptors are associated with proteins in the post-synaptic density that are in turn coupled to other proteins which mediate intracellular signaling pathways such as nitric oxide production [177]. In addition, for comparable quantities of Ca^{2+} influx, the flow through NMDA receptors proves to be toxic whereas that through voltage gated Ca^{2+} channels is not [176,207]. Taken together, these studies suggest that the actions of activated NMDA receptors result not only from the influx of extracellular Ca^{2+}, but also from activation of intracellular proteins directly associated with NMDA receptor complexes.

Metabotropic Glutamate Receptors

In addition to its role in propagating excitatory neurotransmission through actions on ionotropic receptors, extracellular glutamate can directly alter intracellular signaling pathways by activating cell-surface metabotropic glutamate receptors (mGluRs). Early studies showed that glutamate increased inositol trisphosphate (IP_3) accumulation [188] and later cloning-and functional characterization studies confirmed the existence of glutamate receptors that could directly activate intracellular signal transduction mechanisms [89,117]. Structurally, mGluRs are G-protein coupled (GPC), contain the seven transmembrane spanning domain common

to other GPC receptors, but share little sequence similarity with other members of the G-protein family [102,153]. Based on sequence similarity, mGluR subtypes are divided into groups I, II, and III [132]; the numeric designation arising from the order in which they were cloned. In general, group I mGluRs (mGluR1, mGluR5) increase phospholipase C (PLC) activity whereas receptor subtypes in groups II (mGluR2, mGluR3) and III (mGluR4, mGluR6, mGluR7, and mGluR8) are negatively coupled to adenylate cyclase [102,153]. Shown by *in situ* hybridization analysis, mGluRs 1-5 are all present in the striatum with mGluR5 being in highest abundance [203]. Whereas mGluRs are localized to the periphery of the synaptic region, iGluRs appear fairly uniformly throughout the synapse [136]. This spatial organization is said to contribute to the selectivity of GluR activation during episodes of glutamate release. At the corticostriatal synapse, stimulation of group III mGluRs results in the attenuation of glutamatergic transmission by presynaptic mechanisms [155].

Glutamate Transporters

The transmitter actions of glutamate are terminated by its removal from extracellular spaces by glutamate transporters (GLTs) located on both neuronal and glial cells. The three GLTs identified in rat brain are GLAST (L-glutamate/L-aspartate transporter) [197], GLT-1 [154], and EAAC-1 [99]. EAAC1 transporters are located on neurons [99,171] whereas GLT-1 controls glutamate uptake into glial cells [154,171]. GLAST transporters are found on glial cells [171,197]. In striatum, the predominant types of GLTs are EAAC1 and GLT-1 [171]. Glutamate uptake is Na^+-dependent [99,154,197] and this electrogenic transport process is somewhat

offset by the extrusion of a K^+ ion with every Na^+/glutamate pair absorbed [154]. Under depolarizing conditions as occur with ischemia, glutamate transport may be reversed and thereby contribute to increased extracellular glutamate levels [184,199,216]. Free radicals, another product of ischemic damage, have also been found to inhibit glutamate transport [204].

C. Adenosine: A Neuromodulator

Adenosine Receptors

Adenosine receptors are GPC receptors that are generally classified according to either stimulatory or inhibitory effects on adenylate cyclase activity. Of the four adenosine receptor subtypes present in brain, A_1 and A_3 receptors when activated decrease cyclic AMP (cAMP) production while the two A_2 receptor subtypes, A_{2A} and A_{2B}, when activated have the opposite effect [71]. All adenosine receptor subtypes except for the A_3 receptors are sensitive to antagonism by methylxanthines (eg. caffeine, theophylline) [71].

A_1 Receptors. Activation of adenosine A_1 receptors (A_1Rs) decreases adenylate cyclase activity due to receptor-mediated activation of an inhibitory G-protein (G_i). Of the four adenosine receptor subtypes, A_1Rs have the highest affinity for adenosine (K_i = 10 nM) [215]. A_1Rs inhibit neurotransmission through mechanisms such as increasing K^+ conductance [205] and inhibiting voltage-dependent Ca^{2+} influx [180] and these properties contribute to the endogenous neuroprotective actions of adenosine. In brain, A_1Rs are most abundant in cortex and hippocampus [71] and are

also present in the striatum on intrinsic neurons and corticostriatal nerve terminals [229] where they suppress glutamatergic neurotransmission [66].

A_2 Receptors. Adenosine A_2 receptors (A_2Rs) are coupled to stimulatory G-proteins (G_s), and when activated, increase intracellular levels of cAMP. The A_2R family is subdivided into high affinity A_{2A} (1-20 nM) and low affinity A_{2B} (5-20 μM) receptors [71]. In brain, A_{2A}Rs are highly abundant in striatum, globus pallidus and nucleus accumbens [92]. In striatum, activation of A_{2A}Rs suppresses GABAergic synaptic transmission onto medium spiny neurons [127], increases acetylcholine release [79] and can desensitize A_1Rs [52] in a protein kinase C-dependent manner. In addition, A_{2A}R activation in striatum increases glutamate release [158]. Further evidence for the endogenous neuroprotective role of adenosine is provided by studies showing that activation of A_{2A}Rs can initiate anti-inflammatory mechanisms [42] that include inhibiting the production of pro-inflammatory cytokines [108,119]. Because of their relatively low abundance in brain, low affinity for adenosine and the lack of specific pharmacological agents for A_{2B}Rs, relatively less is known about the significance of adenosine signaling through A_{2B}Rs.

A_3 Receptors. Adenosine A_3 receptors (A_3Rs) were the last subtype of adenosine receptors to be identified [239]. Because of the very low affinity of A_3Rs for adenosine (>1 μM) [71], this receptor subtype is thought to be involved in signaling during events such as ischemia, when adenosine levels are relatively high [215]. Expression studies of A_3 mRNA abundance have revealed only low levels of this

receptor in brain [239]. However, in striatum A_3R activation stimulates phospholipase C-mediated phosphoinositide hydrolysis [1]. Because A_3R activation desensitizes A_1Rs [56] and can induce apoptosis in astrocytes [3,4], A_3R activation may play a role in mediating events in the focus zone of an ischemic infarct where adenosine levels are very high and recovery of tissue is unlikely.

Adenosine Enzymes

Several enzymes are involved in controlling levels of endogenous adenosine (Fig. G.4). Inhibition of adenosine-catabolizing enzymes, adenosine kinase and adenosine deaminase, increases endogenous adenosine levels and may thus provide a potential therapeutic intervention point in strategies intended to sustain increased levels of adenosine.

Adenosine Kinase. Adenosine kinase (AK) catalyzes the phosphorylation of adenosine to AMP. AK inhibition appears to have a greater effect on basal tissue levels of adenosine than on adenosine levels following stimulation by, for example, NMDA receptor activation [49]. Because AK has a relatively high affinity for adenosine and is subject to substrate inhibition by adenosine, AK activity may function predominantly to regulate adenosine levels under unstimulated conditions when adenosine levels are relatively low. Recent studies have shown that AK activity can also be inhibited in a PKC-dependent fashion following adenosine A_1R activation [187].

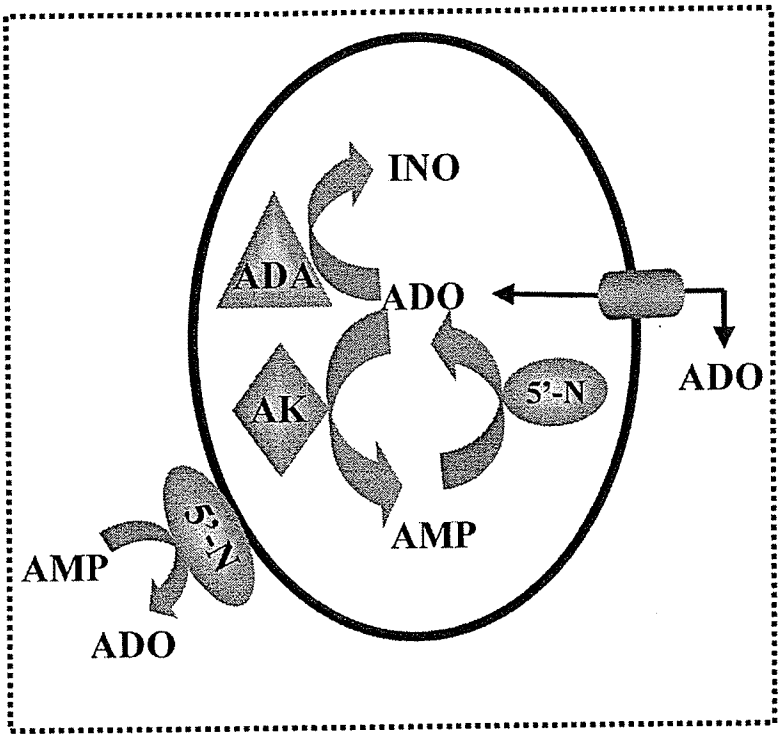

Figure G.4. Regulation of Tissue Adenosine Levels. The diagram above shows several of the major mechanisms of adenosine formation and depletion. Intracellular mechanisms include adenosine formation from AMP by cytosolic 5′-nucleotidase (5′-N) and adenosine depletion with the phosphorylation of adenosine to AMP by adenosine kinase (AK) and deamination of adenosine to inosine by adenosine deaminase (ADA). Adenosine is moved into and out of the cell through equilibrative and concentrative nucleoside transporters. In the extracellular space, AMP can also be converted to adenosine by the action of ecto-5′nucleotidases. The dotted line encompasses the intra- and extracellular spaces that we study simultaneously when analyzing tissues fixed by microwave irradiation. Not represented in the diagram is the effect of circulation, which sweeps away adenosine from the extracellular space or the S-adenosylhomocysteine system. Also not outlined in the figure is the pathway of adenosine formation from cAMP via ecto- and endo-phosphodiesterases that convert cAMP to AMP.

Adenosine Deaminase. Adenosine deaminase (ADA) catalyzes the conversion of adenosine to inosine. Despite its low abundance in brain compared with other organs, studies with ADA inhibitors indicate that ADA plays a significant role in controlling brain adenosine levels [112,131,134]. In contrast to AK, ADA appears to play a lesser role in controlling basal levels of endogenous adenosine than it does under stimulated conditions like, for example, NMDA receptor activation [47].

5′-Nucleotidase. The conversion of AMP to adenosine is catalyzed by both intracellular [139] and extracellular [45] forms of 5′-nucleotidase (5′-N). In contrast to ADA and AK, inhibition of 5′-N activity decreases adenosine levels under both basal and excitatory conditions [49].

Adenosine Transporters.

The movement of adenosine across the cell membrane is facilitated by both equilibrative, and Na^+-dependent concentrative nucleoside transporters. Equilibrative transporters are classified based on their sensitivity to the transport inhibitor nitrobenzylthioinosine (NBTI); the inhibitor-sensitive ones being referred to as "es" and the insensitive ones "ei". Recent studies have implicated adenosine transport function in regulating extracellular adenosine levels in hypothermia, suggesting that adenosine may contribute in the neuroprotective mechanisms of hypothermia [55]. Under both basal and NMDA-stimulated conditions, inhibition of adenosine transport increases tissue levels of adenosine [49].

Chapter 1

Measurement of Adenosine and Adenine-Based Nucleotide Levels in Rat Brain Tissue Fixed by Microwave Irradiation.

Abstract

Adenosine is formed in large part from the breakdown of ATP, particularly under stimulated conditions when tissue metabolic rate is elevated. The extent to which changes in the energy state of a tissue, particularly depletion of ATP levels, results in adenosine formation is largely unquantified probably due to the inherent challenges in obtaining accurate and precise levels of adenine-based nucleotides and adenosine from tissues. Such challenges include the extreme sensitivity of purinergic compounds to post-mortem metabolism, the nearly 1000-fold difference in the basal concentrations of ATP and adenosine, and simultaneously measuring the levels of these compounds in small discrete tissue samples without exceeding the detection limits of any one. Previous studies from our research group have demonstrated that microwave irradiation is an effective method of fixing tissues to eliminate post-mortem metabolism of purines. In this chapter, we describe analytical techniques for measuring simultaneously adenine-based nucleotides and adenosine in small discrete tissue samples. We propose a tissue homogenization model that describes tissue processing parameters, based on sample weight, that yield analytical results within linear detection limits for both tissue purine and total protein measurements. This methodology allows for quantitative assessment of shifts in tissue levels of ATP and adenosine in discrete brain regions under both endogenous and experimental conditions.

Introduction

A large volume of excitotoxicity studies have shown that brain adenosine levels, measured directly in tissues [47,49,50] or in microdialysis samples [83,93,145,146,151], are increased in the presence of iGluR agonists, namely NMDA. Given the neuroprotective properties of adenosine [70], interpretation of these studies has often led to the hypothesis that EAA-induced adenosine level increases serve as a protective response to acute excitotoxic insult. A critical factor not well characterized from this research is the magnitude of ATP level decrease associated with each adenosine level increase. Because tissue death is a potent stimulus for adenosine production, adenosine level increases after excitotoxic insult might only be physiologically protective if a tissue has not been irreparably damaged by excessive ATP (energy charge) depletion. For this reason, it is important to study adenosine level changes in terms of the concurrent changes in ATP levels.

Because of the complexity of the brain's cytoarchitecture, studies investigating specific signalling mechanisms in discrete brain regions must be targeted to those regions alone because the inclusion of uninvolved, surrounding tissue may dilute or mask a legitimate effect. Analytical techniques to facilitate these studies must therefore be effective even on a very small-scale. Adenosine is said to act in a site- and event-specific manner and therefore its concentration in the immediate vicinity of a stimulus should be high and then dissipate in an outward direction. The extent to which this hypothesis is valid can only be tested by analyzing small tissue regions extending concentrically from the injection site.

Simultaneous measurement of adenosine and nucleotide levels can be somewhat challenging given the reciprocal nature with which ATP and adenosine levels fluctuate and the near 1000-fold difference in their concentrations. In addition, care must be taken in measuring basal adenosine levels given their very low concentration in unstimulated tissues. In this chapter we describe a method for simultaneously determining tissue levels of adenosine and adenosine-based nucleotides in small samples (>3 mg) that was adapted from various techniques reported by others [48,227,228,238]. This method allowed us to characterize the effect of glutamate receptor stimulation not only on tissue adenosine levels but also on the levels of high-energy nucleotides as well. We could therefore characterize, for the first time, the relationship between adenosine level increases and concurrent changes in the energy state of a tissue.

Methods

Animals. Adult male Sprague-Dawley rats obtained from the University of Manitoba Central Animal Care breeding facility weighing 200 ± 20 g were used in these studies. Rats were allowed at least five days to acclimatize before procedures were carried out. All protocols were performed in accordance with University of Manitoba Animal Care Ethics Committee guidelines.

Surgical Procedures. Rats were anaesthetized with sodium pentobarbital (74 mg/kg ip) and placed in a stereotaxic frame. All drug injections were directed to the middle of the right striatum. From the intersection of the midline and bregma on the surface of the skull, the injection needle was moved 3.0 mm laterally and then lowered, through a small burr hole drilled into the skull, 4.5 mm ventrally [143]. Drug injections were delivered through a 30-gauge needle in either 0.5 or 1.0 µl volumes. The 1.0 µl injections were administered over two minutes and an additional two minutes were allowed for drug diffusion before needle removal. For 0.5 µl injections, injection and diffusion times were one minute each. Following drug injection, animals were placed on a heating pad to maintain normal body temperature and were then sacrificed by microwave irradiation 15 min from the time that drug injection was completed (unless otherwise stated).

Microwave Irradiation. Following intrastriatal injection or any other experimental treatment, animals were sacrificed by focused microwave irradiation (Cober Electronics). Microwave power settings were always set at 10 kW and time was

varied according to animal size and brain region chosen for recovery. Heavier animals required slightly longer times and for the recovery of ventrally-located regions, times were shortened compared to those when more dorsal ones were selected for analysis. For intrastriatal injection studies, the microwave time was set at 1.5 sec. In the sleep deprivation studies described in Chapter 3, microwave times were set 1.1-1.2 sec when basal regions were to be recovered. Times of 1.5-1.6 sec were used when dorsal regions were to be recovered. The above microwave times are quoted for animals weighing approximately 200 ± 20 g.

To verify the degree of thermal fixation in the brain tissue (85°C desired), temperature readings were taken at the base of the pineal gland during dissection immediately after opening the skull. Given the extreme posterior location of these measurements, we took them to be conservative estimates of anterior brain temperature.

Brain Dissections. Immediately following microwaving, brains were removed and individual brain regions were dissected on an ice-cold tray and immediately frozen on a dry ice-chilled metal plate. After freezing, samples were transferred to individual pre-frozen microcentrifuge tubes and stored at -80°C until taken for analysis by high performance liquid chromatography (HPLC). A detailed description of striatal brain region dissection is shown in Figure 1.1.

Tissue Preparation. Frozen tissue samples were weighed in plastic centrifuge tubes (80Ti type, Beckman) containing 750 µl of cold 2% trichloroacetic acid (TCA). For

accurate weighing of tissue samples, centrifuge tubes containing TCA were placed on an analytical balance and the scale was zeroed prior to transfer of the frozen

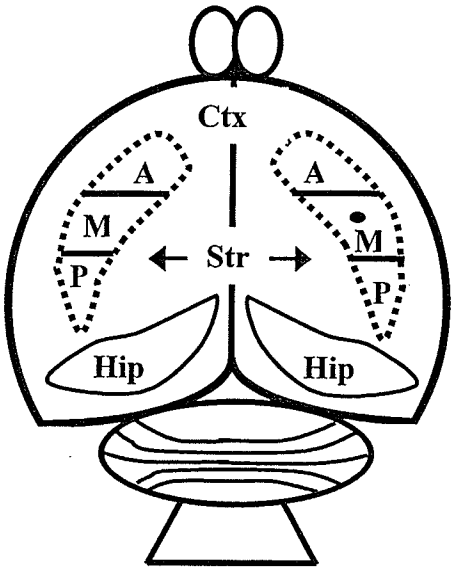

Figure 1.1. Striatal Subregions. Shown in the rat brain schematic diagram above are the dorsal brain regions that lie immediately beneath the cerebral cortex (Ctx), including the hippocampal (Hip) and the striatum (Str,) regions (indicated within the dotted lines). The dot within the right striatal region represents the targeted injection site. For closer analysis of spatial effects, each striatal region was dissected into three subregions designated anterior (A), middle (M), and posterior (P).

samples[A]. Once weighed, centrifuge tubes containing samples were placed on ice and where necessary, additional 2% TCA was added to tubes (see Fig. 1.6). Tissues were homogenized with a Polytron homogenizer (Brinkmann) at setting #6. For samples up to approximately 15 mg in weight and suspended in up to 1.0 ml, tissues were homogenized for 13 s. For samples over 20 mg and in volumes greater than 1.0 ml, homogenization was carried out for 20 s. Afterwards, samples were mixed by vortex and 50 µl aliquots of each homogenate were removed and stored on ice for subsequent protein analysis. Remaining homogenates were centrifuged at 4°C for 15 min at 25,000 x g and 500 µl of each resulting supernatant were neutralized with an

equal volume of tri-n-octylamine/freon (45:155) in 1.5 ml microcentrifuge tubes. Samples were mixed by vortex for 7 s followed by centrifugation at room temperature for 2 min at 13,000 x g to facilitate separation of organic and aqueous phases and then stored on ice. The top aqueous layer of each sample was taken for analysis of nucleotide and adenosine content by HPLC.

HPLC Analysis of Adenosine. All tissue samples were analyzed in duplicate. For each sample, 100 µl of neutralized aqueous layer was combined with 100 µl of 0.3 M $ZnSO_4$ to induce precipitation of charged nucleotides. Following $ZnSO_4$ addition, 100 µl of 0.3 M $Ba(OH)_2$ was added to each tube resulting in the formation of a white precipitate. Samples were centrifuged for 5 min at room temperature at 13,000 x g[B] and 150 µl of supernatant from each tube were combined with 25 µl of 5% chloroacetaldehyde. Incubating the chloroacetaldehyde/analyte mixture at 80°C for 60 min produced the fluorescent derivatives of adenosine and cAMP. Following incubation, samples were centrifuged at room temperature for 2 min at 13,000 x g and 130 µl of each sample were loaded into HPLC sample vials. HPLC analysis was carried out isocratically using a mobile phase consisting of 0.04 M KH_2PO_4[C] containing 12% methanol adjusted to pH 5.0 with potassium hydroxide (KOH). Mobile phase flow rate was set at 1.5 ml/min and separation of 75 µl injections was carried out using a C_{18} µBondapak analytical column (3.9 x 150 mm, Waters). Fluorescent detection was carried out at excitation and emission wavelengths of 275 and 408 nm, respectively. For a detailed summary of HPLC reagents, instrumentation, and chromatograms see Appendix I.A.

HPLC Analysis of Nucleotides. All tissue samples were analysed in duplicate. For each sample, 80 µl of neutralized aqueous phase were added directly into HPLC sample vials. An injected volume of 10 µl was separated using a C_{18} µBondapak analytical column (3.9 x 150 mm, Waters) and a mobile phase consisting of 0.1 M KH_2PO_4 with 1% methanol and adjusted to pH 6.0 with KOH. Flow rate was set at 1.0 ml/min. Separated components were identified by UV detection at 267 nm.

Protein Analysis. Total protein was measured by the Bradford method [21] using a commercial kit (BioRad). The 50 µl portions of TCA homogenate stored on ice after homogenization were centrifuged at 4°C for 15 min at 13,000 x g. Supernatants were removed completely and remaining protein pellets were resuspended in 0.1 M NaOH. The quantity of NaOH used was dependent on the mass of the original tissue sample and the original TCA homogenization volume. The tissue homogenization model presented in this chapter can be used to estimate the appropriate NaOH volume to maintain the protein analysis in a linear range. Protein pellets suspended in NaOH were incubated for 15 min at 80°C. During incubation, samples were mixed by vortex periodically in order to ensure that all pellets were completely dissolved. Following incubation, samples were centrifuged at room temperature for 2 min at 13,000 x g to collect any condensation formed within the tubes and remove any interfering particulate matter. Supernatants were analyzed in triplicate by adding 10 µl aliquots to wells of 96-well microplates followed by addition of 200 µl of diluted (1:5 with water) BioRad protein reagent. Microplates, after equilibration for five

minutes, were read at 620 nm using a microplate reader (Bio-Tek Instruments). Included in the analysis of each plate were 0.5, 1.0, 2.0, 3.0, 4.0, and 5.0 μg/10 μl bovine serum albumin (BSA) standards.

Identification and Quantification of Compounds. For adenosine and adenine nucleotides, analyte peaks were identified by comparison to standards. One single standard was prepared for use in both analyses by diluting 10 mM ATP, ADP and AMP standards and 1 mM adenosine and cAMP standards[D] with 2% TCA to give a single mixture containing 30 μM ATP, 10 μM ADP, 5 μM AMP, 0.1 μM adenosine and 0.1 μM cAMP. Standards were treated with the exact same preparation procedure that was used for tissue samples. For nucleotide analysis, a 10 μl injection of standard mixture gave 300, 100 and 50 pmol peaks for ATP, ADP and AMP, respectively. For adenosine analysis, a 75 μl injection of standard yielded 10 pmol peaks of cAMP and adenosine (the concentration of each compound in the 100 μl aliquot subject to $ZnSO_4/Ba(OH)_2$ treatment was 0.1 μM). Analyte peaks were quantified by area using Millennium version 3.05 software (Waters).

Pooling of Striatal Subregion Data. In analyses where striatal subregions were analysed as opposed to whole striatum, as carried out in earlier work, the following calculations were used to determine purine levels in whole striatum:

$$[ATP]_{str} = \left[\frac{M_{ant}}{M_{str}} \times [ATP]_{ant}\right] + \left[\frac{M_{mid}}{M_{str}} \times [ATP]_{mid}\right] + \left[\frac{M_{post}}{M_{str}} \times [ATP]_{post}\right]$$

The equation above shows how levels of ATP measured in individual striatal subregions ($[ATP]_{ant}$, $[ATP]_{mid}$, $[ATP]_{post}$) were converted to represent ATP levels in a whole striatal region ($[ATP]_{str}$) from one side of the brain. The contribution of each subregional purine level to the value representing the entire striatal region was dependent on the ratio of the mass of the individual subregion (M_{ant}, M_{mid}, or M_{post}) to the mass of the whole striatal region (M_{str}) where $M_{str} = (M_{ant} + M_{mid} + M_{post})$. The above equation is shown for ATP, however, the same technique was used in calculation of total striatum levels of ADP, AMP and adenosine.

A. Samples were transferred quickly from the frozen microcentrifuge tubes to the tubes on the balance to prevent melting of the sample during transfer.

B. This centrifugation was carried out to collect condensed water drops and sediment and solid interferences.

C. In earlier work reported from this lab, a 0.01 M KH_2PO_4 mobile phase with the same pH and methanol content as listed was used. It was found, however, that with analysis of very low basal levels of adenosine that a higher salt concentration (0.04 M) was required to completely resolve interfering cAMP peaks from small adenosine peaks. With relatively large adenosine peaks, the small interfering cAMP peaks contribute insignificantly to peak quantitation.

D. All standards were prepared in water and then immediately frozen in individual aliquots and stored at -80°C.

Results

Analysis of Nucleotides. HPLC analyses of ATP and ADP yielded linear peak area results for injected nucleotide quantities between 2.5 and 500 pmol as indicated by the correlation coefficients (r^2) of 0.994 and 0.995, respectively (Fig. 1.2) For AMP, the upper limit of analysis was 300 pmol yielding an r^2 value of 0.996. To verify that our tissue analyses were routinely carried out within these linear ranges, we pooled the data collected from 260 arbitrarily chosen rat brain striatal samples, spanning several different treatments, and calculated the mean and 95% confidence limits of the pmol values of nucleotides detected from 10 µl sample injections. Values for mean and 95% confidence limits (in parentheses) for ATP, ADP and AMP were 305.73 – (290.99, 320.47), 127.13 (121.05, 133.21) and 47.64 (42.73, 52.55), respectively. These representative data, superimposed

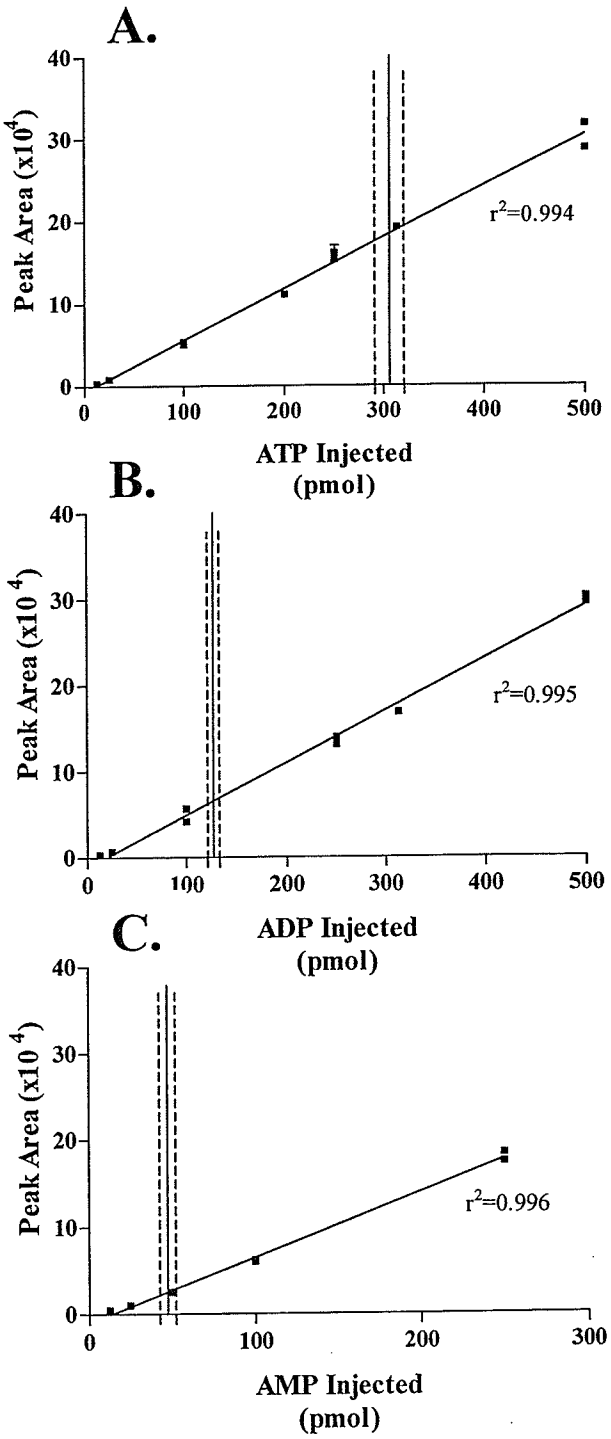

Figure 1.2. Nucleotide Standard Curves. Data shown are mean ± SD (n=3) of peak areas measured from HPLC analysis of ATP (A), ADP (B), and AMP (C) standards. The data points shown come from 3 separate analyses carried out over a 10 month period and correlation coefficients for each curve are annotated. The vertical solid and dashed lines represent the mean and 95% confidence intervals of pmol values measured from 260 representative rat brain striatal tissue samples.

on the plots in Figure 1.2, indicate that our HPLC analyses of nucleotides were carried out well within detectable linear ranges.

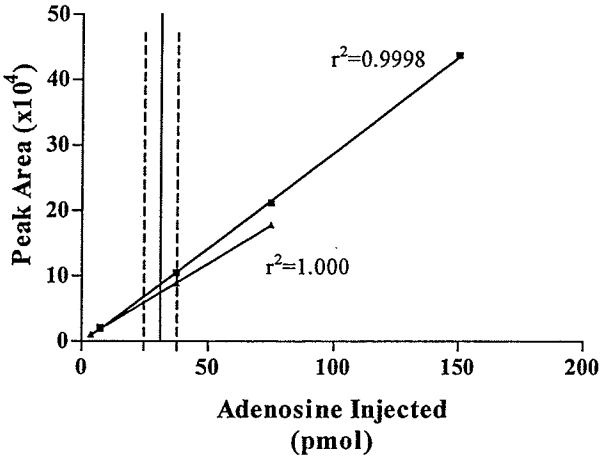

Figure 1.3. Adenosine Standard Curve. Data shown are mean ± SD (n=3) of peak areas measured from HPLC analysis of adenosine standards. The two separate curves (■,▲) represent analyses carried out 2 months apart. Also annotated are correlation coefficients for each curve. The vertical solid and dashed lines represent mean and 95% confidence intervals of pmol values measured from the 260 tissue samples described in Figure 1.2.

Analysis of Adenosine.

Detection of adenosine was linear for injected quantities from 0.75 to 1500 pmol (Fig. 1.3, entire range not shown here). Unlike the data from nucleotide standards, the adenosine data were reported in two separate relationships according to time of analysis. Although the standard analyses carried out on the separate occasions were both linear, the slopes from each of the data groups differed and so the data were reported on separate curves. To verify that our HPLC analyses for adenosine were indeed carried out within linear range, we pooled the pmol values of adenosine measured from analysis of the same 260 representative tissue samples described above and calculated a mean value of 31.2 pmol with 95% confidence limits of 24.9 and 37.7 pmol (Fig. 1.3). Although not shown here, similar analyses with cAMP standards revealed a linear detection range between 2.5 and 1500 pmol. Standard curves in both adenosine and nucleotide analyses were generated by injecting a constant volume of each standard, of appropriate concentration, to give the indicated pmol/injection quantities.

Protein Analysis. Protein analyses were validated in a fashion similar to that conducted for nucleotides and adenosine. Analysis of BSA protein standards was linear up to 4.0 μg/10 μl (aliquots taken for protein analysis were 10 μl). Averaging the raw data collected from the 260 representative samples described above, we determined a mean value of 1.85 μg/10 μl and 95% confidence limits of 1.79 and 1.91 μg/10 μl. These data verify that our protein analyses were carried out well within the boundaries of linear detection (Fig.1.4).

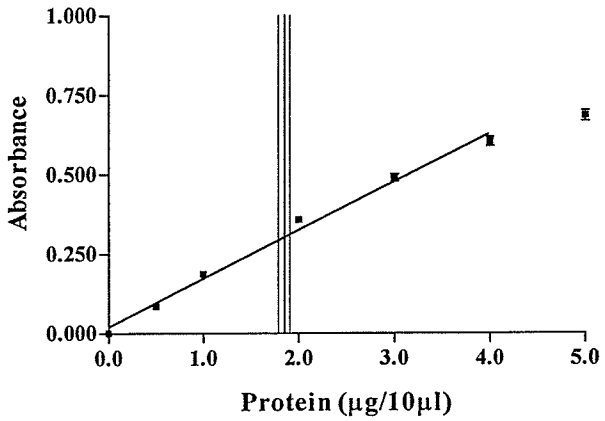

Figure 1.4. Protein Analysis Linear Range. Bovine serum albumin (BSA) protein standards were used to prepare all standard curves. Data shown are means ± SD from 10 separate analyses, each carried out in triplicate. Protein measurements were found to be most linear ($r^2 = 0.991$) up to the 4.0 μg/10 μl level. The thick vertical and thinner lines represent the mean (1.85) and 95% confidence limits (1.79, 1.91), respectively, of protein measurements from the 260 tissue samples described in Figure 1.2.

In addition to verifying that our protein readings were determined within the linear range of detection, it was also critical to ensure that our determination of protein in tissue samples was both efficient and consistent over the range of protein concentrations to be expected in the tissue homogenates. Using BSA protein, we prepared a series of standards and subjected them to treatment with 2% TCA and protein measurement in a fashion identical to how tissue samples were handled (a more detailed description of the experiment is presented in Appendix I.B.). The analysis revealed that from 1.0 to 3.0 mg/ml protein we were able to consistently recover and detect 95% of the theoretical yield (Fig. 1.5). Pooling the data from the 260 tissue samples described above, we calculated a mean value of 1.60 mg/ml and

95% confidence limits of 1.54 and 1.66 mg/ml. These data show that our protein isolation and measurement procedures were 95% efficient and were consistent, in terms of yield, within the range of protein concentration used.

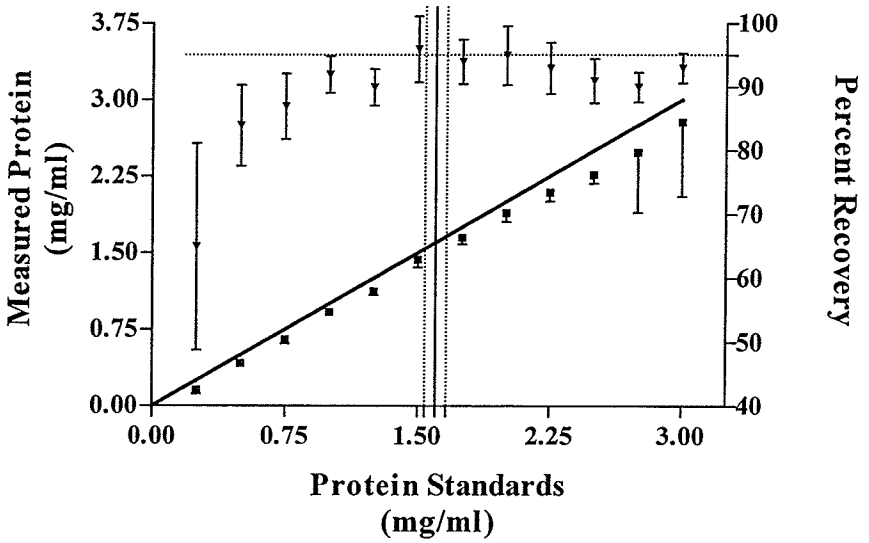

Figure 1.5. Determination of Protein Detection Efficiency. Shown above are the means ± SD of levels of protein detected (■) and percent protein detected experimentally (▲) from three protein analyses carried out as outlined in Table I.B.1. The diagonal line represents 100% protein detection. The horizontal dotted line shows the 95% detection level. The solid vertical line and the associated two vertical dotted lines mark the mean (1.60) and 95% confidence limits (1.54,1.66), respectively, of the TCA homogenate protein concentrations (mg/ml) in the 260 tissue samples reported in the tissue homogenization model.

Tissue Homogenization Model. Throughout this section we reported on experiments that determined our linear detection limits and using the raw data from a representative set of tissues we verified that our analyses indeed fell with in these linear detection ranges. It was important, however, to create a protocol with which a user could easily identify, according to the wet mass of a tissue sample, the quantities of 2% TCA and 0.1 M NaOH to use during sample preparation to ensure that both purine and protein readings fell into linear ranges. Using raw data from the 260 rat brain striatal samples we created a user-friendly model that would predict, based on

the wet mass of a sample, the volumes of TCA and NaOH that should be used in the sample preparation procedure (Fig.1.6). The fundamental assumption used in calculating the model was that the sum of pmol quantities of ATP, ADP and AMP (Σ_{nuc}) for each tissue sample should be approximately the same and for our purposes, we based our calculations in the model on a target value of $\Sigma_{nuc} = 300$ pmol. Using dilution factor corrections, we predicted the nucleotide, adenosine and protein data that would have resulted had the 260 samples in the model been processed according the procedural specifications that were ultimately proposed. The means and 95% confidence limits for projected nucleotide, adenosine, and protein measurements fell well within linear ranges for each set of samples within a designated TCA volume. A detailed description of the tissue homogenization model and associated calculations used are shown in Appendix I.C.

Mass (mg)	TCA Vol. (µL)	NaOH (µL)		ATP pmol	ADP pmol	AMP pmol	Ado pmol	Protein µg/10 µL	Σ_{Nuc} pmol
4.0 5.0 6.0 7.0 8.0	575	200	Mean 95% CI	177.3 156.9,197.6	59.1 51.1,67.1	17.0 13.8,20.3	9.77 5.43,14.10	1.66 1.55,1.78	253.4
9.0 10.0	700	350	Mean 95% CI	198.2 176.2,220.2	75.2 68.9,81.6	27.2 17.8,36.5	17.22 6.96,27.48	1.58 1.49,1.68	300.6
11.0 12.0	800		Mean 95% CI	214.4 198.8,230.0	85.4 78.1,92.7	30.1 21.9,38.2	20.98 8.81,33.15	1.67 1.60,1.74	329.8
13.0 14.0 15.0	1000		Mean 95% CI	224.5 211.4,237.7	89.4 83.7,95.1	30.5 24.2,36.9	17.17 11.25,23.10	1.72 1.66,1.78	344.4
16.0 17.0	1300	300	Mean 95% CI	206.8 189.6,224.0	82.1 76.0,88.1	24.1 18.5,29.7	10.76 6.04,15.49	1.73 1.62,1.85	313.0
18.0 19.0 20.0	1500		Mean 95% CI	196.1 174.5,217.6	86.4 78.0,94.7	37.1 24.9,49.4	23.72 8.38,38.46	1.75 1.67,1.83	319.5
21.0 22.0 23.0	1800		Mean 95% CI	190.3 172.9,207.8	94.7 88.3,101.1	41.9 32.2,51.5	26.09 12.57,39.60	1.75 1.69,1.82	326.9
24.0 25.0 26.0 27.0 28.0 29.0 30.0	2000		Mean 95% CI	211.2 191.7,230.8	91.8 86.4,97.3	40.0 29.6,50.3	35.88 16.72,55.04	1.83 1.75,1.90	343.0
31.0 32.0 33.0 34.0 35.0	2500	250	Mean 95% CI	200.8 157.9,243.8	82.3 74.1,90.4	21.7 11.4,32.1	20.57 6.50,34.63	2.02 1.66,2.39	304.8
~									
45.0 to 55.0	4500	300	Mean 95% CI	173.3 147.5,199.1	90.1 74.4,105.7	39.9 24.7,55.2	21.39 7.98,34.80	1.50 1.28,1.72	303.3

Figure 1.6. Tissue Homogenization Model. The first three columns predict the volumes of 2% TCA and 0.1 M NaOH, given a sample's wet tissue mass, for use in the tissue preparation and protein analysis procedures to ensure that purine and protein measurements fall within linear detection range. The data on the right side of the figure correspond to statistical analysis of projected data obtained by applying the regimen in the first three columns, using appropriate dilution factors, to the empirical data collected from the 260 representative striatal tissue samples.

Discussion

For the simultaneous determination of adenine-based nucleotide or adenosine levels in discrete brain regions, several challenges needed to be addressed. First, due to the extremely labile nature of these purinergic compounds, particularly in a post-mortem environment, tissue enzymes had to be rapidly inactivated in order to preserve true endogenous levels. Second, when only specific brain regions were to be analyzed, the method of tissue inactivation needed to leave intact the physical features of the brain to allow accurate and precise dissection of brain regions. Finally, due to the reciprocal nature of ATP and adenosine level fluctuations and the nearly 1000-fold difference in the endogenous levels of these two compounds, measuring the concentrations of both from a single sample could often result in adenosine levels too low or ATP levels too high for accurate determination. Perhaps because of these challenges, no quantitative characterizations of the relationship between ATP depletion and concurrent adenosine formation in brain tissue have been made.

Previously, we established that microwave irradiation was an effective method of rapidly inactivating brain tissue and eliminated post-mortem changes in purine levels by endogenous enzymes [48]. In addition, this technique when used optimally leaves brain structures completely intact to allow for accurate and precise dissection of very small brain regions.

In this chapter we described an analytical procedure deigned to facilitate the simultaneous determination of adenosine and adenine-based nucleotides in brain tissues fixed by microwave irradiation. By homogenizing tissues in trichloroacetic

acid (TCA) cellular debris was eliminated leaving a mixture of aqueous, acid-soluble compounds. Neutralizing this mixture with a tri-n-octylamine/freon solution yielded an extract that could be directly analysed for ATP, ADP, and AMP or subject to $ZnSO_4/Ba(OH)_2$ treatment (to remove charged nucleotides) and then analyzed for adenosine and cAMP content. The added sensitivity of detecting the fluorescent analogs of adenosine and cAMP was found to compensate for additional sample dilution steps introduced by the $ZnSO_4/Ba(OH)_2$ and derivitization treatments. To compensate for any loss of analyte in the preparation procedures, the standard mixture used to quantify compounds was subject to the same conditions as tissue samples were.

Due to interference by TCA in the Bradford method of protein analysis we introduced a homogenate centrifugation step followed by resuspension and digestion of the resulting protein pellet in NaOH, a medium compatible with the Bradford analysis. To verify that this analytical procedure was indeed sound, we tested a range of protein standards in concentrations that we could expect in our tissue analyses and found that this method yielded a consistently high level of efficiency (95%) for protein determination.

The tissue homogenization model described in this chapter served two purposes. First, by pooling a large population of data from our injection experiments we were able to verify statistically that our raw data measurements consistently fell well within linear detection ranges in both purine and protein analyses. This verification was critical because of the wide fluctuation of purine levels that resulted

with different drug treatments and the inherent reciprocal relationship between adenosine and ATP levels.

The main purpose of the tissue homogenization model was to generate a guideline by which brain tissues fixed by microwave irradiation could be processed, based only on wet weight, to yield purine and protein levels that would fall within linear detection ranges. By setting target values for raw sum of nucleotides (Σ_{nuc}) and protein concentration data we worked backwards to determine TCA volume and protein dilution factors to accommodate all ranges of wet tissue weight. The final model, being easy to use, greatly enhances the time efficiency of this work at the benchtop.

The ability to measure the relationship between levels of purinergic compounds in a single tissue sample will help broaden our knowledge of the relationship between adenosine and ATP levels under both stimulated and basal conditions. With this information, we can more effectively address the questions of whether adenosine serves as an endogenous neuroprotectant and how the individual protective properties of this purine nucleoside could be exploited using therapeutic interventions.

Chapter 2

Effects of Glutamate Receptor Stimulation on Adenosine and Energy Charge Levels in Rat Brain.

Abstract

Given the endogenous neuroprotective properties of adenosine, its formation and release following glutamate receptor stimulation is thought to represent an early resistance mechanism against the damaging processes resulting from glutamate excitotoxicity. In contrast, however, high adenosine levels are also known to occur in permanently damaged tissue, merely reflecting the results of obstructed energy metabolism. In this chapter, we addressed the hypothesis that glutamate receptor activation increases adenosine levels by characterizing the adenosine level increases induced by activation of different glutamate receptors using L-glutamate and/or specific glutamate receptor agonists and antagonists. Using the methodology developed in Chapter 1, we determined the effects of glutamate receptor induced adenosine level increases in terms of tissue energy charge (EC) depletion and verified that these effects occurred largely in a site- and event-specific manner. In some cases, however, where strongly-depolarizing stimuli were administered unilaterally, we did observe small changes in purine levels in corresponding contralateral regions which are known to be connected by neuronal pathways to the treated ipsilateral regions. From a quantitative perspective, our data suggest that adenosine level increases are twice as responsive to changes in tissue EC under excitatory conditions that favour NMDA-type glutamate receptor activation compared to those conditions that are expected to induce lower levels of tissue depolarization. By quantitatively studying the relationship between EC depletion and adenosine level increases we can begin to address whether adenosine level increases, under conditions such as acute excitotoxicity, could play a physiologically protective role.

Introduction

Adenosine, an endogenous purine nucleoside, is produced and released with elevated cellular activity. Accumulating in this manner, adenosine can stimulate compensatory responses such as vasodilation [106,149] and attenuation of neurotransmission through activation of cell-surface receptors [60,66,233]. As an attenuator of neuronal activity, adenosine is known to limit the release of excitatory neurotransmitters [16,19,34,51,81,186], decrease seizure activity [5,57,69,236], and improve cell viability in models of excitotoxicity [60,65,74,150,172]. Having the potential to mediate these types of responses, adenosine has been referred to as an endogenous neuroprotectant [70,173].

A large volume of studies has been published, using several different types of brain models, showing that activating different neurotransmitter receptors or altering the activity of adenosine metabolizing enzymes and transporters can change local adenosine levels. Numerous *in vivo* studies on whole brain [47,49,50] or on *in vitro* preparations such as tissue slices [40,41,82,147], or cell cultures [181], have shown that exposure of brain tissues to glutamate receptor agonists increases adenosine production and release. A common conclusion in these studies is that glutamate receptor activation-induced adenosine release may serve a protective role during periods of excitotoxicity, when a similar degree of high intensity glutamate receptor stimulation occurs. This idea that adenosine release may be a protective response encouraged a branch of adenosine research focusing on increasing or maintaining elevated adenosine levels through altering the activity of adenosine-metabolizing enzymes or [94,107,222,236] blocking adenosine transporters [140,141,236] or a

combination of both [47,73] to maximize protective potential. With further evidence that some enzymes involved in adenosine homeostasis are selectively more active under basal conditions (when adenosine levels are generally low) compared to stimulated conditions (when adenosine levels are significantly elevated) and vice versa came the idea of REAL agents (regulators of endogenous adenosine levels) [49]. REAL agents are adenosine enzyme or transport inhibitors that may serve as therapeutic agents because they have the potential to act in a site- and event-specific manner. Because adenosine deaminase (ADA) appears to cause adenosine depletion selectively when adenosine levels are elevated, an ADA inhibitor would have minimal effect on adenosine homeostasis in normally-functioning tissue but would attenuate adenosine level depletion in those tissues affected by conditions such as excitotoxicity where adenosine levels are high.

In all of the work pertaining to characterizing and maintaining adenosine level increases, there remains very little focus on high-energy nucleotide depletion as the source for the adenosine formation. Cell death is a potent stimulus for increasing tissue adenosine levels and not knowing the extent of cellular energy depletion accompanying the adenosine level increases observed in experimental models can put into question the physiological significance of these increases. As well, particularly when levels are high, adenosine is known to mediate several harmful responses including apoptosis [215,217,218], inflammation [215], and potentiation of excitatory neurotransmission [56]. Whether adenosine exerts harmful or protective effects seems to depend on its concentration in a tissue region because higher levels through activation of adenosine A_{2A} and A_3-type receptors, can initiate some of the harmful

responses outlined above. Adenosine levels in tissues are usually highest at the point of focal stimulus (injection site or focal ischemic site) and dissipate moving away from the foci producing selective activation of adenosine receptors throughout these regions [215].

Here, we investigated the hypothesis that glutamate receptor activation increases adenosine levels by measuring the relationship between glutamate receptor-induced adenosine level increases and concomitant reductions in levels of high-energy nucleotides, namely ATP, ADP, AMP. Our results suggested that adenosine level increases and concurrent energy charge depletion occur in a two-tiered fashion depending on the depolarizing strength of an event and whether significant NMDA receptor activation had occurred as a result. In addition, by analyzing small tissue regions at or surrounding intrastriatal drug injection sites, we demonstrated that changes in energy and tissue adenosine levels appear to occur in a site- and event-specific fashion. Finally, we report a novel finding that strongly-depolarizing excitatory amino acid stimuli, injected unilaterally into the striatum, induce changes in purine levels in striatum on the contralateral side.

Methods

Animals. See description in Chapter 1.

Surgical Procedures. Described in Chapter 1.

Chemicals. L-Glutamate (monosodium salt), kainic acid, N-methyl-D-aspartate (NMDA) and tri-n-octylamine (TOA) were purchased from Sigma Chemical Company (St. Louis, MO). Chloroacetaldehyde was obtained from Fluka (Ronkonkoma, NY). 5-Methyl-10,11-dihydro-5H-dibenzocyclohepten-5,10-imine maleate (MK-801), 6-cyano-7-nitroquinoxaline-2,3-dione (CNQX), 2,3-dihydroxy-6-nitro-7-sulphamoylbenzo(F)-quinoxaline (NBQX), L-(-)-threo-3-hydroxyaspartic acid (HAsp), and (1S,3R)-1-aminocyclopentane-1,3-dicarboxylic acid (ACPD) were purchased from Tocris Cookson (Ballwin, MO). All HPLC reagents were ordered from Fisher Scientific (Nepean, Ont).

Intrastriatal Injections. Injection procedures were outlined in Chapter 1 and the drug doses used in each experiment have been described in Figure legends. Tris injection vehicle was composed of 50 mM Tris adjusted to pH 7.4 with HCl. Artificial CSF (aCSF) vehicle contained 124 mM NaCl, 5 mM KCl, 0.1 mM $CaCl_2$, 1.2 mM $MgCl_2$, 26 mM $NaHCO_3$, 10 mM glucose with final pH adjusted to 7.4 with HCl. Salt solution was composed of 140 mM NaCl, 4.7 mM KCl, 1.2 mM $MgSO_4$, 2.5 mM $CaCl_2$, 10 mM glucose, 1.4 mM KH_2PO_4, and 4.3 mM Na_2HPO_4 with final pH adjusted to 7.4 using NaOH. All vehicle and drug solutions were prepared on the day

of use and pH levels were always adjusted to 7.4. MK-801 was administered i.p. (4 mg/kg) in a 0.9 % NaCl solution 30 min before drug injections were carried out intrastriatally.

Brain Dissections. Dissections were carried out as described in Chapter 1. Striata were dissected whole or were cut coronally into three subregions designated anterior (Ant), middle (Mid) and posterior (Post) of equal rostro-caudal length (Fig. 1.1). When dissecting microwaved tissue, brain regions separated by white matter tracts pull apart easily. From rat brain atlas diagrams [143], we concluded that anterior subregions were predominantly caudate-putamen (striatum) with a small portion of nucleus accumbens near the ventral surface; middle subregions were all striatum tissue, and posterior regions contained predominantly striatum with some globus pallidus near the medial-ventral surface.

Purine and Protein Analyses. Outlined in Chapter 1.

Data Analysis and Statistics. All data were reported as mean ± S.E.M. Statistical comparisons between two groups (contralateral vs ipsilateral) were carried out using unpaired, two-tailed t-tests and statistically significant differences were annotated by asterisk (*). For comparisons between more than two data groups an ANOVA was carried out followed by a Student-Neuman-Keuls multiple comparisons test. Statistically significant differences found from multiple comparisons tests were indicated by a dagger (†). In order to compare results from subregional analysis to

whole striatum data, and historical results, we devised a method of pooling the subregional data based on the mass of each subregion, allowing us to predict purine levels in whole striata from subregional data. The data pooling technique is described in the Methods section of Chapter 1. The equation used to calculate energy charge is:

$$EC = ([ATP] + \tfrac{1}{2}[ADP]) / ([ATP] + [ADP] + [AMP]).$$

where the maximum EC level approaches 1.0.

Results

Intrastriatal L-Glutamate Injection. In previous work from this group [47,49,50], EAA-induced increases in brain tissue adenosine levels were characterized using specific pharmacological glutamate receptor agonists, namely AMPA, kainate, and NMDA. Here, we tested the effects of the endogenous EAA receptor agonist L-glutamate (Fig. 2.1). L-Glutamate at doses of 111 and 333 nmol increased tissue adenosine levels to an extent not significantly different from injection of the Mg^{2+}-free Tris buffer vehicle. However, adenosine levels in striata injected with vehicle or glutamate at 111 or 333 nmol doses were significantly greater than those measured in

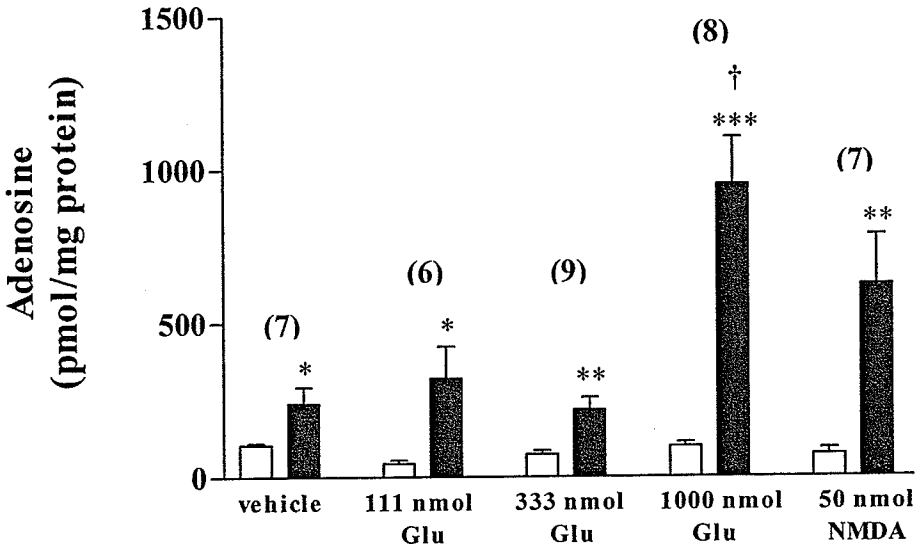

Figure 2.1. L-Glutamate Injections. Shown are tissue adenosine levels (mean ± S.E.M.) measured in injected (black bars) and corresponding contralateral striata (white bars) following administration of L-glutamate or NMDA (doses shown). The vehicle used in these experiments was Mg^{2+}-free 50 mM Tris buffer at pH 7.4. The number of rats used in each treatment group is shown in parentheses.
*,**,*** - different ($p<0.05$, 0.01, 0.001) from corresponding contralateral region.
† - different ($p<0.05$) from all other bars representing injected striata.

the corresponding contralateral regions. L-glutamate at doses of 1.0 μmol produced large, statistically significant ($p<0.05$) increases in tissue adenosine levels when compared to levels from the lower glutamate doses ($p<0.05$) or the 50 nmol NMDA injections. Although the 50 nmol NMDA injection increased tissue adenosine levels to an extent greater than the two lower doses of glutamate, the differences did not reach a level of statistical significance.

Antagonism of L-Glutamate Effects. Because glutamate-induced adenosine level increases could have arisen from a variety of mechanisms, given the several different types of glutamate receptors that might be activated with the injection of exogenous glutamate, we tested the ability of different glutamate receptor antagonists to block the effects of glutamate on adenosine responses (Fig. 2.2). With vehicle injection alone (Mg^{2+}-free Tris), we found that the NMDA-type glutamate receptor antagonist MK-801, and to a greater extent the non-NMDA glutamate receptor antagonists CNQX and NBQX not only reduced the adenosine levels stimulated by vehicle injection, but also significantly ($p<0.001$) lowered tissue adenosine levels in corresponding contralateral striatal regions. Consistently, CNQX and NBQX attenuated the adenosine level increases caused by 111 nmol glutamate injection (Fig. 2.2B). Higher glutamate doses could not be tested with CNQX and NBQX due to solubility limitations with the co-injection of the antagonist drugs. MK-801 blocked the adenosine level increases by 333 nmol (Fig. 2.2B) and 1.0 μmol (Fig. 2.5) glutamate injections.

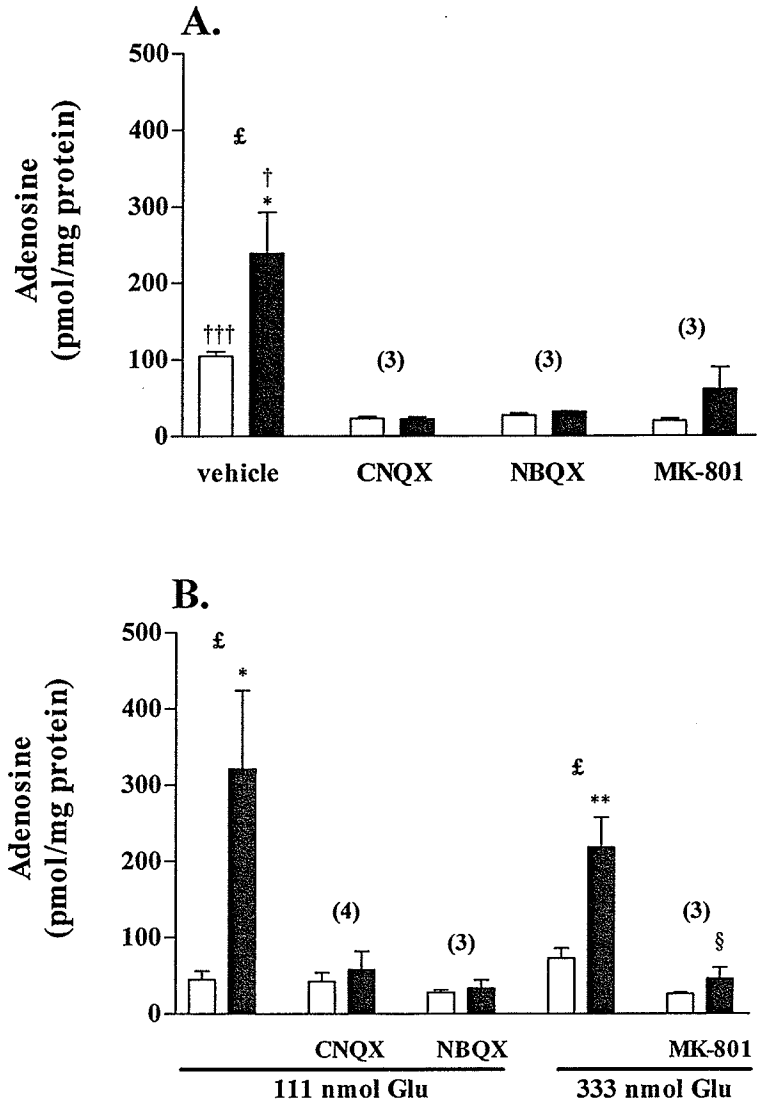

Figure 2.2. Glutamate Receptor Anatgonist Injections. Shown are tissue adenosine levels (mean ± S.E.M.) in injected (black bars) and contralateral (white bars) striata following injection of non-NMDA glutamate receptor antagonists CNQX (5 nmol) and NBQX (15 nmol) alone (A) or in combination with L-glutamate (B). MK-801 (4 mg/kg ip) was given 30 min prior to intrastriatal injection of either Tris vehicle (A) or L-glutamate (B). The number of rats used in each treatment is shown in parentheses.
*,** - different ($p<0.05$, 0.01) from contralateral data set.
††† - different ($p<0.001$) from other bars of the same color.
§ - different ($p<0.05$) from 333 nmol injected striata (unpaired, 2-tailed t-test)
£ - same data set as shown in Figure 2.1.

Analysis of Adenosine and Nucleotide Levels. Measuring changes in high-energy nucleotides that occur with tissue adenosine level increases, we were able to begin studying, in a quantitative manner, the reciprocal relationship between adenosine and ATP levels (Fig. 2.3). Because we found significant increases in tissue adenosine levels following injection of Tris vehicle, we tested two other injection vehicles namely aCSF and a balanced salt solution (Fig. 2.3A and B). Intrastriatal injections

of aCSF and balanced salt solution produced small, statistically non-significant increases in adenosine levels when compared with contralateral regions and both increases were less than those measured following Tris vehicle injection (Fig. 2.3C). aCSF was used in subsequent analyses because the salt solution was found to form precipitate several hours following preparation. As expected, ATP and AMP levels changed reciprocally and the magnitude of decreases in ATP levels reflected the concomitant increases in adenosine levels although this relationship was by no means stoichiometric. Those treatments that stimulated NMDA receptors, namely Tris vehicle (the absence of Mg^{2+} reduces voltage-dependent block of NMDA receptors) and NMDA, increased levels of adenosine to an extent greater than those observed from injections of vehicle containing physiological levels of Mg^{2+} (Fig.2.4A and B). Levels of cAMP in these studies remained fairly uniform and although no statistical differences were observed when comparing injected and contralateral striata, significant differences ($p<0.05$) were found between contralateral data sets from different treatments (Fig. 2.4B). Energy charge (EC) calculations using the nucleotide data from Figure 2.3 revealed a consistent and reciprocal relationship between adenosine level increases and decreases in EC (Fig. 2.4C).

Purine Levels at the Injection Site. To determine purine levels in the immediate vicinity of an injection site (as opposed to looking at whole striata where approximately three times more tissue volume is analysed) we examined purine levels from middle injected and contralateral subregions (Fig. 2.5). Purine levels in striata of rats subjected to anaesthetic only (basal group), following insertion and placement

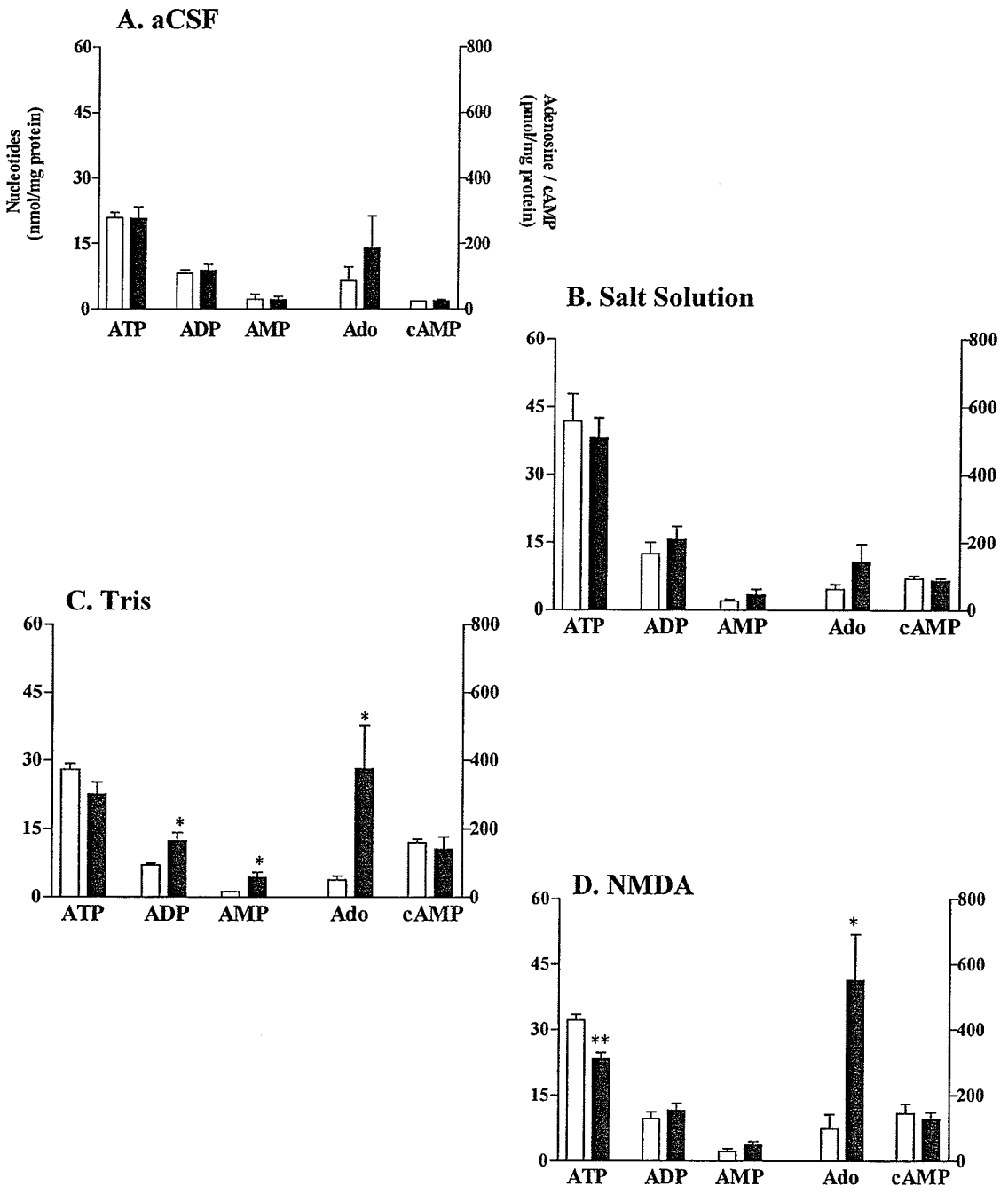

Figure 2.3. Concomitant Analysis of Nucleotide, Adenosine, and cAMP Levels. Data shown are adenosine (Ado), cAMP, and adenine-based nucleotide levels (mean ± S.E.M.) following 1.0 µl injections of aCSF (A, n=3), salt solution (B, n=6), Tris buffer (C, n=4) and NMDA (D, 50 nmol in Tris vehicle, n=5). The results shown in B, C, and D, are pooled from measurements taken from individually dissected subregions to give results representative of whole injected and contralateral striata. For details on striatal subregion dissection or the data pooling method see the Methods section of Chapter 1. A complete summary of purine levels in all individual striatal subregions is shown in Appendix II.
*,** - different ($p<0.05$, 0.01) from corresponding contralateral data set.

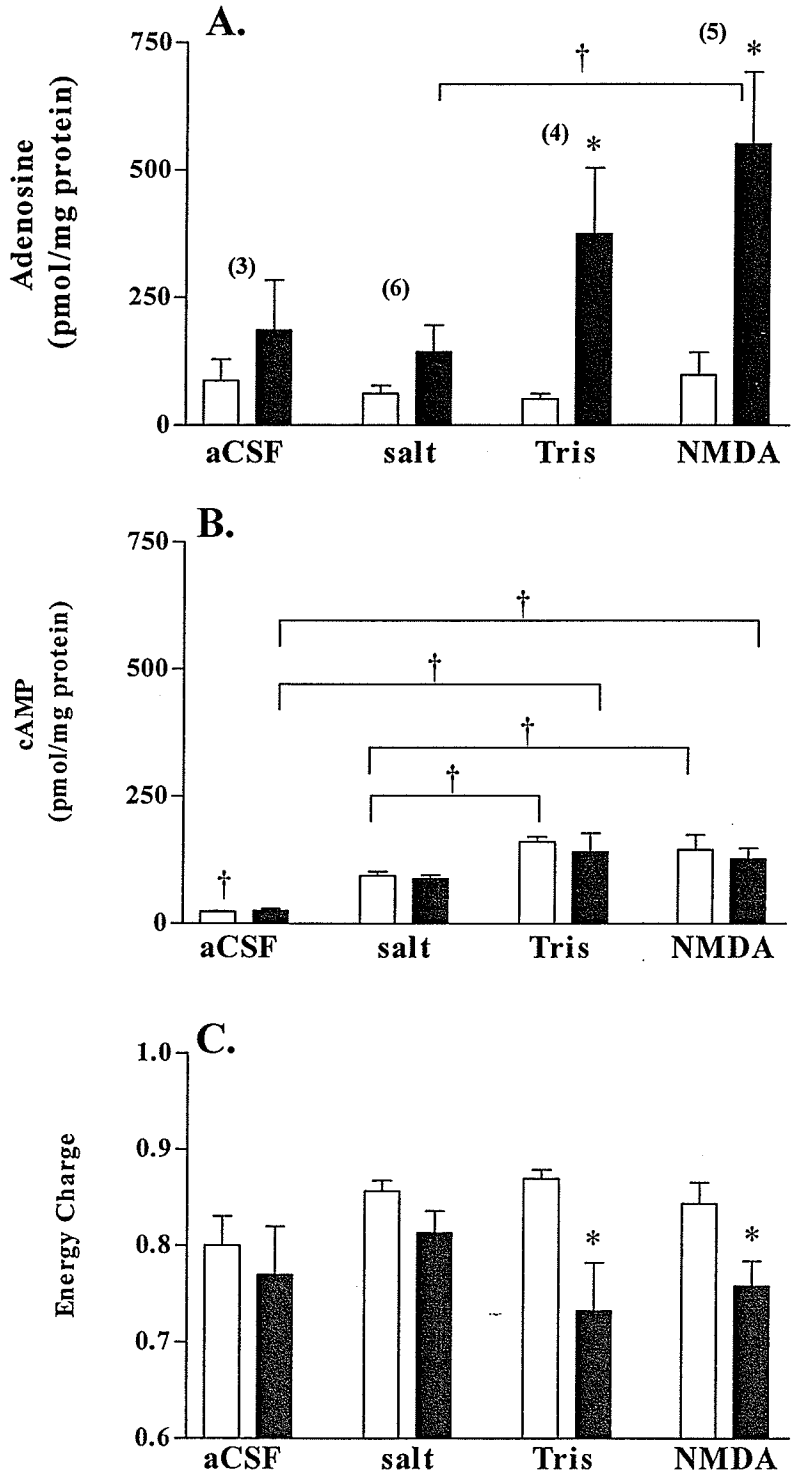

Figure 2.4. Summary of Adenosine, cAMP and Energy Charge Data. Shown together are adenosine (A), cAMP (B), and energy charge (C) data from experiments described in Figure 2.3.
* - different ($p<0.05$) from corresponding contralateral data set.
† - different ($p<0.05$) from all other bars of the same shade except as otherwise annotated.

of the injection needle (no-vol group), and aCSF injection did not differ statistically comparing injected and contralateral sides except for a decrease in energy charge ($p<0.05$) in the injected middle subregion of the no-vol group compared to the contralateral subregion.

NMDA injections delivered in aCSF vehicle gave lower ($p<0.05$) tissue adenosine levels of 309 ± 64 (Fig. 2.5A) compared to 823 ± 184 pmol/mg protein (Appendix II, Fig. II.H) for injections delivered in Tris vehicle. The amplified effect using Tris vehicle was also observed when adenosine levels following glutamate injected in aCSF (542 ± 102, pooled data from Fig. II.F) were compared to those following glutamate injected in Tris vehicle (952 ± 152 pmol/mg protein, Fig 2.1). Injection of 1.0 μmol glutamate, however, elevated adenosine levels to a greater extent ($p<0.01$) than did any of the other treatments shown (Fig 2.5A). Complimenting this effect, we observed EC values to be lowest ($p<0.01$) in the glutamate-injected regions. In the presence of the NMDA receptor antagonist MK-801, the effects of glutamate on EC depletion and adenosine accumulation were significantly attenuated ($p<0.01$).

Cortical Stimulation Studies. Unexpectedly, we observed changes in adenosine and energy charge levels in contralateral striatal regions that appeared to reflect the magnitude of changes seen in the corresponding injected regions. This was particularly evident in the glutamate injection group. Some corticostriatal glutamatergic afferent nerves are known to cross in the corpus callosum and innervate

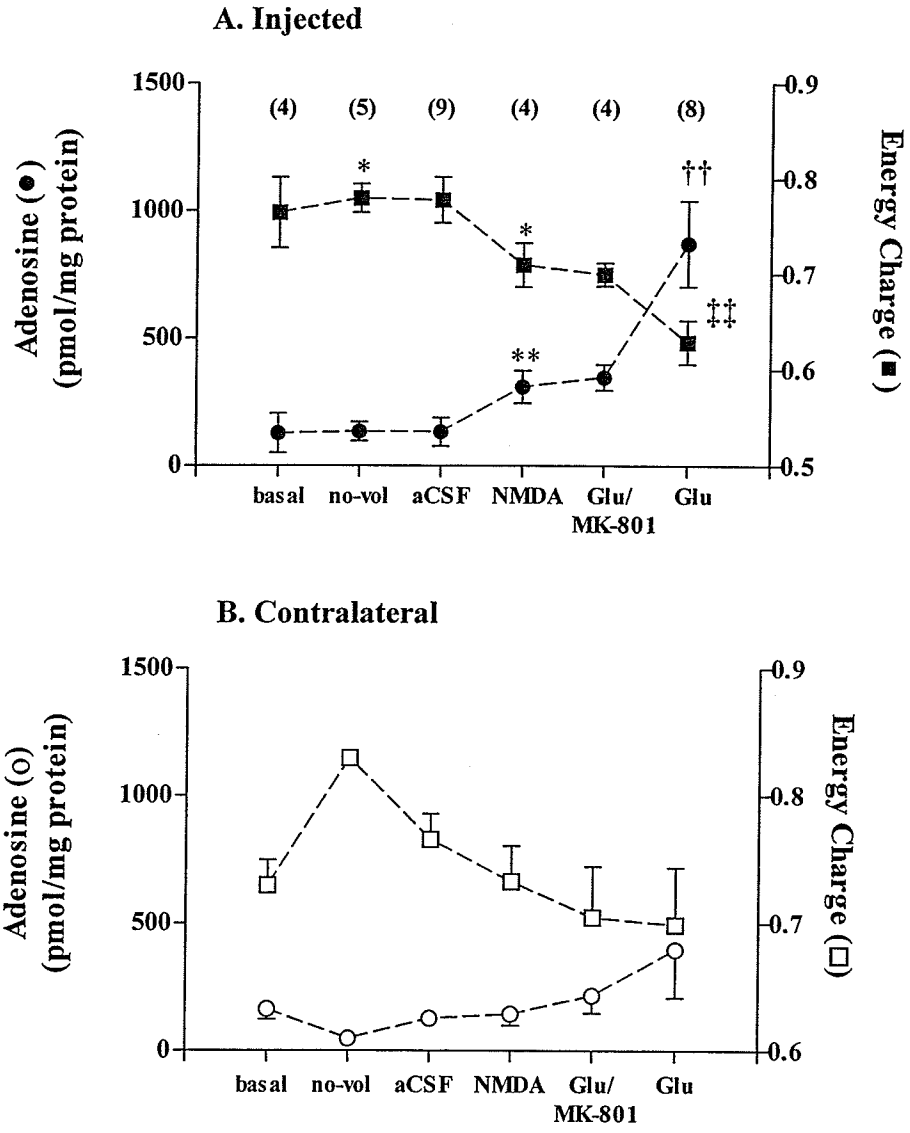

Figure 2.5. Adenosine and Energy Charge Level Changes at the Injection Site. Shown are adenosine and EC levels (mean ± S.E.M.) measured in middle injected (A, dark symbols) and middle contralateral (B, white symbols) striatal subregions following 1.0 µl injections of aCSF, NMDA (50 nmol) or glutamate (1.0 µmol) in the presence or absence of MK-801 pre-administration (4 mg/kg i.p., 30 min prior to intrastriatal injection). Shown in parentheses is the number of animals in each treatment group. The basal data group represents animals that were anesthetized and then sacrificed at the point when the surgical procedure to perform the intrastriatal injection would have been initiated. Rats in the no-vol group underwent the intrastriatal injection procedure, however, no fluid volume was delivered from the needle. For a complete summary of all subregional data from the experiments shown in this figure, refer to Appendix II.
*,** - different ($p<0.05$, 0.01) from corresponding contralateral region in B.
†† - different ($p<0.001$) from adenosine levels in all other injected middle subregions.
‡‡ - different ($p<0.01$) from energy charge values calculated for basal, no-vol and aCSF treatment groups in A.

contralateral striatal regions [17,37,225]. Accordingly, we investigated whether mechanical stimulation of the cortical surface, in the vicinity of where needle insertions into the striatum passed through the cortex, could noticeable alter purine levels in contralateral striata (Fig 2.6). Following cortical stimulation, no significant differences were observed between ipsilateral and contralateral striata, although higher adenosine levels were measured on the contralateral side. EC values in ipsilateral and contralateral striata were calculated to be 0.81 ± 0.02 and 0.78 ± 0.04, respectively.

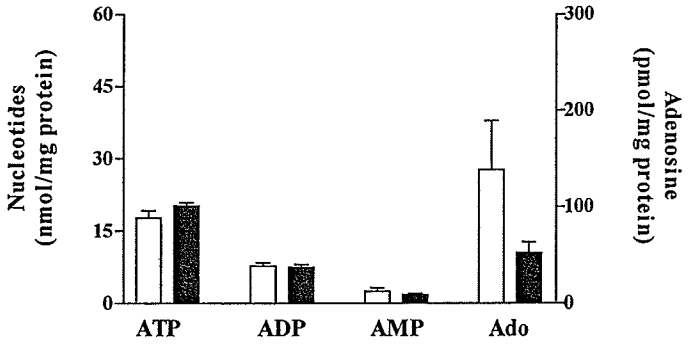

Figure 2.6. Cortex Stimulation Experiments. Shown are pooled purine data (mean ± S.E.M.) measured in contralateral (white bars) and ipsilateral (black bars) striata following unilateral mechanical stimulation of the cerebral cortex. The cortical area in the immediate vicinity of where needle injections passed through to the striatum was touched with forceps repeatedly for several seconds to simulate the manipulations that might have occurred during routine intrastriatal injections (dura was not damaged in these experiments). Following stimulation, rats were allowed to recover in the same fashion as animals undergoing drug injection. Data shown were collected from six animals and statistical evaluation detected no significant differences between purine levels in ipsilateral and contralateral striata.

Effects of Glutamate Uptake Inhibition. Activation of striatal kainate receptors results in the release of glutamate from the terminals of corticostriatal glutamatergic afferents [62,234] and our group has shown that intrastriatal injection of kainate increases tissue adenosine levels [50]. Here, we tested whether inhibiting the uptake of glutamate during kainate receptor stimulation had an additive effect on tissue adenosine level increases (Fig. 2.7). Although in the past, we observed significant increases in tissue adenosine levels in injected compared to contralateral striata following 0.25 nmol kainate injection [50], in these experiments the increases in adenosine levels did not reach a level of statistical significance. In the presence of the glutamate uptake blocker L-(-)-threo-3-hydroxyaspartic acid (HAsp) [99,154,197],

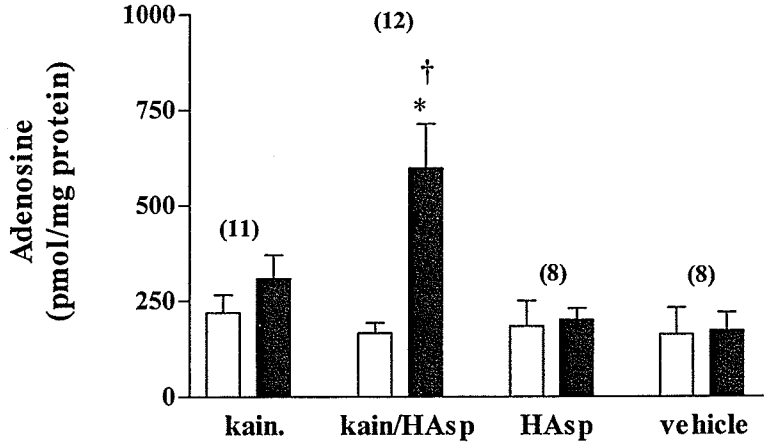

Figure 2.7. Effects of Glutamate Uptake Inhibition Kainate-Induced Adenosine Level Increases. Data shown are adenosine levels (mean ± S.E.M.) measured in contralateral (white bars) and injected (black bars) whole striata following 0.5 µl administration of Tris vehicle, kainate (0.25 nmol), L-(-)-threo-3-hydroxyaspartic acid (HAsp, 150 nmol), or a combination of both kainate (0.25 nmol) and HAsp (150 nmol). Number of animals in each treatment group is shown in parentheses. Kainate, in addition to activating glutamate receptors is also known to inhibit glutamate uptake [171].
* - different ($p<0.05$) from corresponding contralateral data set
† - different from all other dark bars

however, kainate injection resulted in large adenosine level increases that were significantly greater ($p<0.05$) than in contralateral regions and in regions injected with kainate, HAsp, or vehicle alone.

Site- and Event-Specificity of Purine Level Changes. Adenosine level changes in response to stimuli are often referred to as site- and event-specific, meaning that the adenosine level changes occur predominantly in the vicinity of the stimulus site and the magnitude of the adenosine level changes reflects the strength of the stimulus. Here, we used the same experimental treatments as shown in Figure 2.7 but upon dissection separated each striatum into three subregions of equal rostro-caudal length and measured the changes in purine levels in the immediate vicinity of the injection site, and in adjacent regions (Fig 2.8). In these experiments we found patterns in purine level changes that were seen with other EAA stimuli, namely that ATP level decreases were accompanied by reciprocal AMP level increases and the magnitude of ATP level decreases reflected the degree to which tissue adenosine levels increased. We also observed significant differences in purine levels between subregions in the same striata, which were particularly evident following treatment with the kainate/HAsp combination. These differences support the idea that adenosine responses are localized to the stimulus site. Comparing pooled and subregional data (Fig. 2.9) it was clear that analysis of the Mid subregion immediately around the injection site revealed significantly ($p<0.05$) greater changes in purine levels than were observed when striata were analysed whole.

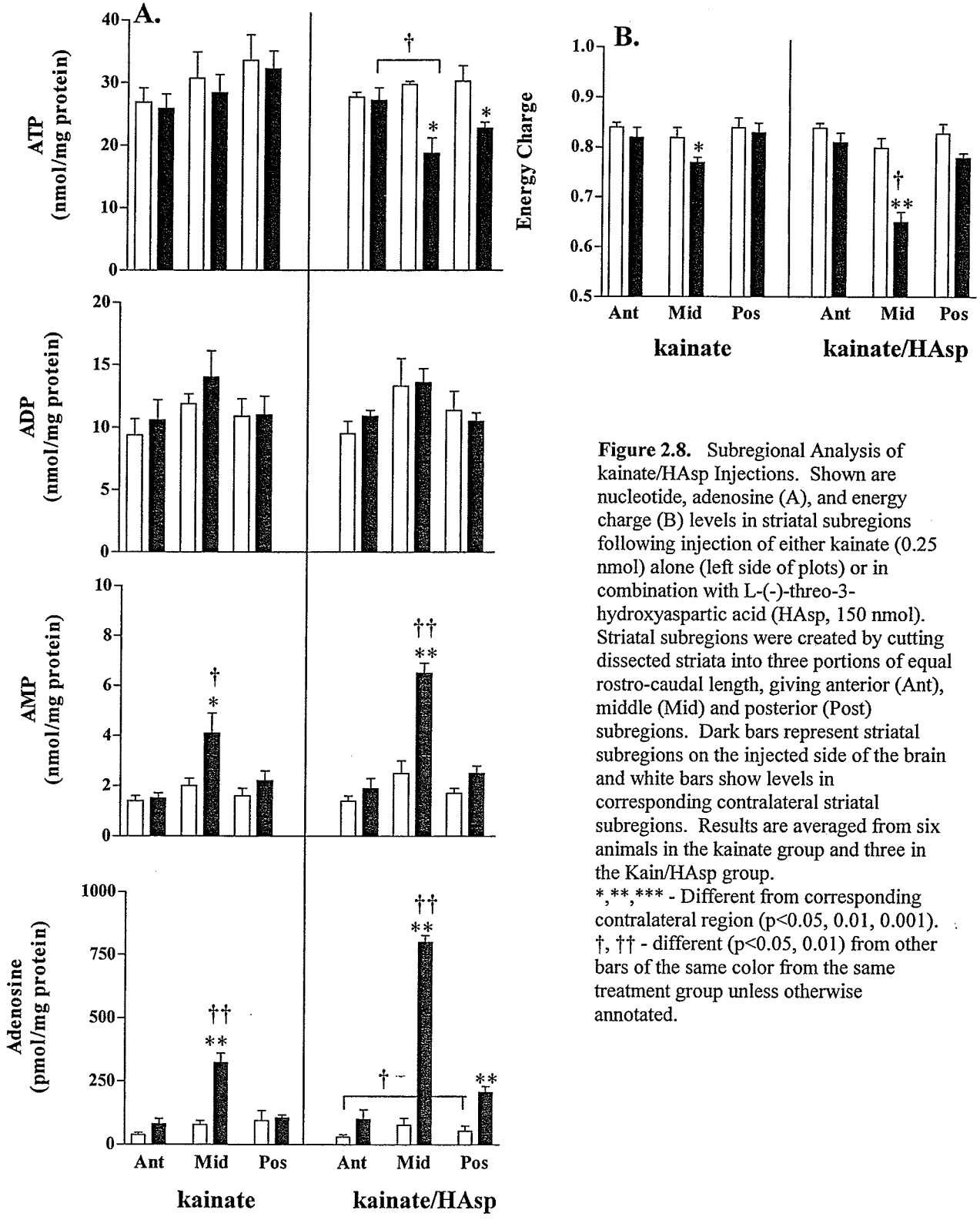

Figure 2.8. Subregional Analysis of kainate/HAsp Injections. Shown are nucleotide, adenosine (A), and energy charge (B) levels in striatal subregions following injection of either kainate (0.25 nmol) alone (left side of plots) or in combination with L-(-)-threo-3-hydroxyaspartic acid (HAsp, 150 nmol). Striatal subregions were created by cutting dissected striata into three portions of equal rostro-caudal length, giving anterior (Ant), middle (Mid) and posterior (Post) subregions. Dark bars represent striatal subregions on the injected side of the brain and white bars show levels in corresponding contralateral striatal subregions. Results are averaged from six animals in the kainate group and three in the Kain/HAsp group.
*,**,*** - Different from corresponding contralateral region ($p<0.05$, 0.01, 0.001).
†, †† - different ($p<0.05$, 0.01) from other bars of the same color from the same treatment group unless otherwise annotated.

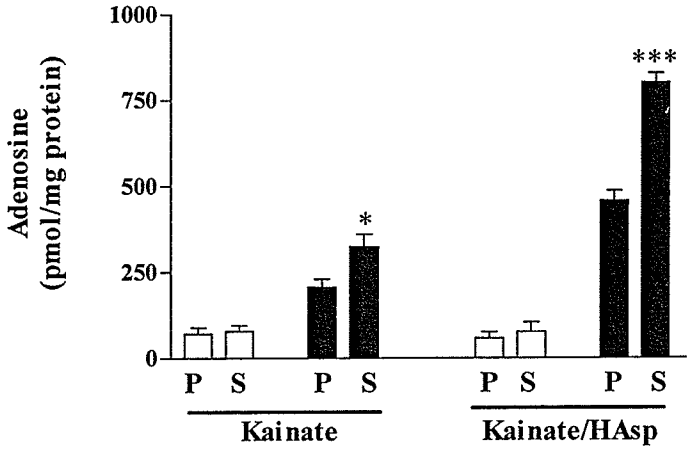

Figure 2.9. Differences Between Pooled and Subregional Purine Data. Shown are middle subregion (S) adenosine levels from Fig. 2.8 compared with mathematically-pooled (P) subregional data that represent adenosine levels had the corresponding striatal regions been analysed in whole. White and black bars represent contralateral and injected striata, respectively. *,*** - greater than pooled data ($p<0.05$, 0.001).

Effects of mGluR Activation. Activation of metabotropic glutamate receptors (mGluRs) is known to stimulate several different intracellular pathways including cAMP production and activation of phospholipase C [153]. Here we tested the hypothesis that activation of mGluRs in striatum, with the non-specific mGluR agonist (1S,3R)-1-aminocyclopentane-1,3-dicarboxylic acid (ACPD), would increase tissue adenosine levels (Fig. 2.10). At injected doses of 200 and 350 nmol we observed no statistically significant changes in adenosine levels between injected and contralateral striata. Unexpectedly, at the 350 nmol ACPD dose we observed significantly higher ($p<0.05$) levels of adenosine in the contralateral striata compared to those measured in both striatal regions in 200 nmol group.

Adenosine Levels and Energy Charge. We observed that injection of substances with varying degrees of excitotoxic potential caused different degrees of fluctuation in levels of adenosine and EC. We compiled EC and adenosine data from the various experiments described to this point and plotted, using EC as the independent variable,

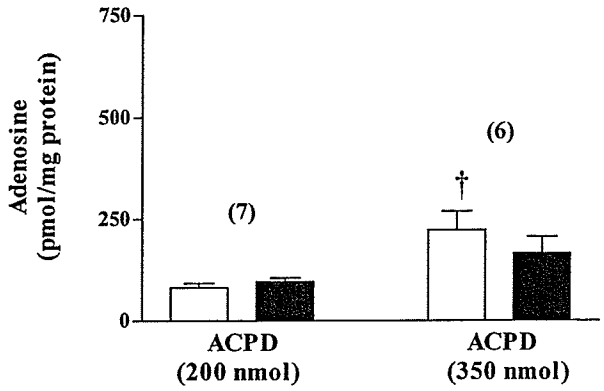

Figure 2.10. ACPD Injections. Data shown are mean ± S.E.M. of adenosine levels in injected (dark bars) and contralateral (light bars) striata. Doses of (1S,3R)-1-aminocyclopentane-1,3-dicarboxylic acid (ACPD) were delivered in a 1.0 µl injection volume using a 0.9% NaCl vehicle. Animals were sacrificed 20 min post injection in contrast to the 15 min period allowed in all other injection experiments. Number of animals in each treatment group is annotated in parentheses.
† - different ($p<0.05$) from both data sets in the 200 nmol treatment group.

adenosine values against EC levels (see Appendix III for plots) and calculated slopes. The results of this analysis are shown in Figure 2.11. In several cases we observed significant differences in slope values between injected and corresponding contralateral striata.

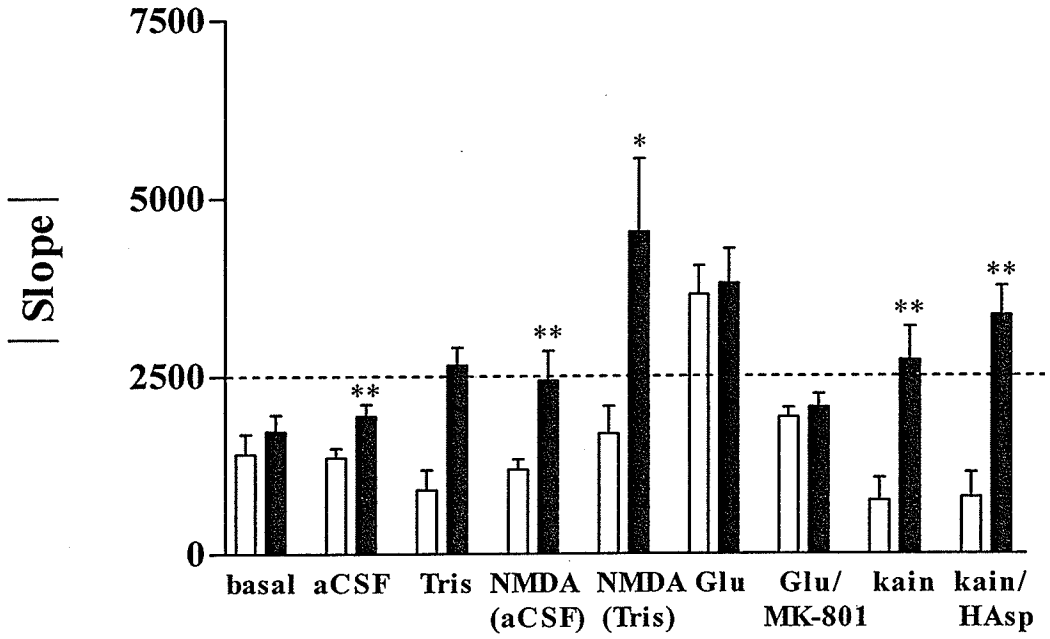

Figure 2.11. Slopes of Adenosine-EC relationships. Shown are the absolute values of slopes from linear relationships formed by plotting tissue adenosine levels against corresponding EC values. The treatments shown above and corresponding data have all been described in previous figures. See Appendix III for individual adenosine-EC graphs and correlation coefficient values. The dotted horizontal line represents a slope threshold above which NMDA receptor activation is hypothesized to initiate mechanisms that contribute to adenosine level increases. Statistical analysis also revealed that all bars represented slopes that were significantly (minimum $p<0.05$) non-zero.
*,** - slope differs ($p<0.05$, 0.01) from data set representing corresponding contralateral striatum.

Discussion

The analytical techniques described in Chapter 1 enabled us to study simultaneously high-energy nucleotide, adenosine and cAMP levels in discrete brain regions. Studying the changes in the levels of these purines allowed us to address several fundamental questions and test several hypotheses. First, we tested the hypothesis that adenosine levels rise in response to falling ATP levels as occur with glutamate excitotoxicity. Second, by analyzing very small tissue regions we tested the site- and event-specificity of changes in adenosine and nucleotide levels by measuring purine levels in tissue regions extending away from points of excitotoxicity. In addition, we tested the hypothesis that the effects of unilateral intrastriatal injection were not isolated to ipsilateral striata but were, as well, transmitted to contralateral striata. Our data suggested that different modes of adenosine level regulation exist depending on the degree of NMDA receptor stimulation.

Adenosine Levels and Energy Charge. In order to measure changes in the levels of metabolically labile purines in brain, techniques have been developed to rapidly inactivate brain enzymatic activity and eliminate post-mortem changes in nucleotide and adenosine concentrations. Procedures such as freeze-blowing [211], decapitation into liquid nitrogen and microwave irradiation [48] were all used in attempts to maintain the highest tissue EC and preserve accurate levels of purinergic compounds. Many of these studies [48,211], carried out on either whole brain or large brain regions, determined that EC values of greater than 0.80 were obtainable with

appropriate levels of metabolic deactivation (theoretical maximum approaches 1.0). Under ischemic conditions, immediately following cortical depolarization, EC values from whole brain were reported in the 0.25 – 0.30 range [212] and following 10 minutes of ischemia levels dropped further to 0.15 [138]. In studies reported here, focusing on discrete brain regions, we observed cases where tissues, upon dissection, appeared thermally fixed and conservative estimates of brain temperature immediately following microwave fixation were over 80°C, yet EC levels in some unstimulated tissues were slightly reduced (~ 0.75) and adenosine levels were elevated. In these situations, the idea that these altered levels of purines may reflect intense neuronal activity in these regions, and not merely post-mortem artefacts, is supported by several studies. During striatal perfusion experiments, animals allowed to recover from anaesthetic produced increased adenosine release (presumably due to heightened neuronal activity) compared to those maintained under anaesthetic [145]. Furthermore, tetrodotoxin (TTX), which suppresses the propagation of action potentials by blocking Na^+ flow through voltage-gated ion channels, reduced adenosine release and blocked [^{3}H]purine efflux elicited by low intensity (a simulation of actively signalling neurons) but not high intensity field stimulation of brain slices [145]. Thus, under depolarizing conditions as occur with K^+ perfusion or injection of compounds that potently activate depolarizing ionotropic receptors, tissue adenosine levels rise and EC values fall due to increases in neuronal activity and activation of adenosine-generating intracellular pathways. The extent to which decreases in ATP (and hence EC) translate into increases in adenosine levels, however, has not been well characterized.

We used a linear regression analysis of adenosine-energy charge (Ado-EC) relationships to quantitatively describe what we refer to as the two-tiered system of regulation for adenosine and purine nucleotide (represented by the EC term) levels. Doing so provided us with a way of comparing changes in the energy state of the tissue to corresponding adenosine level changes. Direct comparisons between ATP and adenosine levels are difficult because of the nearly 1000-fold difference in the endogenous concentrations of these compounds. In addition, calculation of EC takes into account the concentrations of all high-energy adenine-based nucleotides. The data in Figure 2.11, which summarizes most of the work in this chapter, supports the idea of two general states of purine level regulation. The lower level Ado-EC slope (1200-1500), observed primarily in the contralateral striatal regions, would represent adenosine level regulation under basal or slightly depolarizing conditions. We refer to this as tier-1 regulation. Above the hypothetical 2500 slope value, we propose that tissue depolarization, due to either administration of exogenous agents or endogenous conditions such as ischemia, has occurred to an extent where NMDA-receptor mediated mechanisms are activated. This more volatile adenosine-EC relationship we propose is indicative of tier-2 regulation. Pivotal changes in endogenous mechanisms that may contribute to the two-tier system we have proposed include differential regulation of adenosinergic enzymes and transporters [49,93,145] and even perhaps inhibition of glutamate uptake by peroxynitrite [204], a free radical that can be generated following NMDA receptor activation. From a slightly different perspective, studies have also shown that adenosine formed with low level NMDA receptor activation can provide an inhibitory threshold against further receptor

activation [223]. This finding may represent one of the regulatory factors defining the boundary between tier-1 and tier-2 regulation of purine levels.

Others [93,145] and we [49] have reported that different adenosinergic enzymes appear to be involved in the regulation of adenosine levels under basal and stimulated conditions, which suggests that adenosine levels under each condition are likely different. An example of apparent two-tiered adenosine level regulation was observed when our injections of Mg^{2+}-free Tris buffer had a greater effect on adenosine and EC values than did administration of aCSF. Mechanical manipulation is known to reduce voltage-dependent block of NMDA receptors by Mg^{2+} [237]. The 1.0 µl Tris injections probably provided sufficient mechanical stimulation to activate some NMDA receptors and the Mg^{2+}-free vehicle also likely diluted the endogenous Mg^{2+} concentration allowing localized relief of voltage-dependent Mg^{2+} block and thus potentiation of NMDA receptor activation causing a robust adenosine level response. For these reasons it appears that Tris vehicle injections, and drugs delivered in Tris vehicle had greater effects on purine level shifts than did aCSF or those drug treatments administered in aCSF and we therefore continued our studies using the aCSF vehicle.

Microdialysis studies in the cortex have shown that excitatory amino acids induce the release of adenosine with an order of potency of NMDA > glutamate > kainate [93,151]. At least part of this response, which is similar to results from our studies, may be explained by a two-tiered pattern of adenosine and EC level changes. With administration of glutamate and/or kainate, non-NMDA receptors are activated and result in neuronal depolarization and relief of voltage-dependent Mg^{2+} block of

NMDA receptors. Under moderate depolarization conditions, ATP levels are slightly lowered and AMP and adenosine levels are slightly elevated (tier-1 regulation). However, under high-level depolarization conditions where released endogenous glutamate [25,75] can stimulate NMDA receptors, a different combination of cellular mechanisms appears to be activated that culminate in much larger shifts of purine levels to significantly lower levels of ATP and higher levels of AMP and particularly adenosine (tier-2 regulation). The low magnitude changes in EC and adenosine levels we observed with kainate administration may represent a low level of depolarization occurring in the absence of significant NMDA receptor activation. Under these conditions we propose that purine levels are under tier-1 regulation. However, in the presence of glutamate uptake inhibitor, kainate coupled with the increase in endogenous extracellular glutamate concentration (due to uptake inhibition) apparently increased depolarization, activated NMDA receptors, and resulted in a shift to tier-2 regulation of purine levels as illustrated by the much larger changes in adenosine and EC levels. Further support for a two-tiered regulation of purine levels can be derived from studies showing that K^+-induced increases in adenosine levels were partly blocked by TTX but complete inhibition required the inclusion of an NMDA receptor antagonist [145]. Moreover, while glutamate-evoked adenosine release could be blocked partially by MK-801, complete inhibition required the inclusion of antagonists to non-NMDA receptors [83]. These findings suggest that adenosine production during periods of depolarization and/or excitotoxicity occurs in two mechanistically different phases that we have found produce different degrees of volatility in the adenosine-EC relationship. The mechanisms involved in these

phases, we proposed, are representative of either tier-1 or tier-2 purine level regulation depending on the extent of NMDA receptor activation.

Adenosine: Site- and Event-Specificity. Physiological responses of adenosine levels to stimuli are site- and event-specific in that increases in levels of adenosine occur in the immediate vicinity of a stimulus site and the magnitude of the adenosine response reflects the intensity of the stimulus and the level of adenosine receptor activation. By studying small striatal subregions at and around drug injection sites, we found that adenosine level increases were indeed much greater at the injection site and the effect rapidly dissipated in the surrounding tissues. In these cases we observed tier-1 and tier-2 purine level regulation occurring simultaneously in different tissues depending on the distance from the injection site and the intensity of the stimulus. Following events such as focal ischemia, it seems possible that tissue regions moving from tier-1 to tier-2 type purine regulation may become more prone to excitotoxic damage and at this point damaging mechanisms such as apoptosis and necrosis may be initiated. Indeed, activation of adenosine A_3 receptors, as occurs in the presence of high adenosine levels, can induce apoptosis [215]. The site- and event-specificity of the adenosine system may be taken advantage of therapeutically to minimize side effects and several groups have proposed the use of modulators of adenosine metabolism as therapeutic agents [2,68,113,214,224].

The Contralateral Effect. To determine whether the effects of unilateral drug injections into the brain are specific to the treatment, it is common practice to

compare changes between ipsilateral (treated) and contralateral (untreated) sides of the brain because the contralateral side is thought to serve as an internal control. This assumption is valid if the contralateral side is completely disconnected from the effects induced in the ipsilateral side. In our studies, we observed occasional adenosine level increases in contralateral striata following unilateral drug injection. These increases, although inconsistent, appeared most often when strong depolarizing stimuli were administered (1.0 μmol glutamate). When glutamate receptor antagonists were injected, we consistently noticed lower adenosine levels in contralateral striata. In addition, slope values of adenosine-EC relationships were much higher in the contralateral striata of glutamate-injected brains compared with any other treatment and were attenuated by MK-801. Therefore, intense depolarization of the ipsilateral striatum may stimulate neuronal activity in the contralateral striatum thereby producing small increases in adenosine levels. Indeed, unilateral mechanical stimulation of cerebral cortex increased adenosine levels somewhat in contralateral striatum, but these changes were not significantly different from ipsilateral regions. This contralateral effect can be explained neuroanatomically because corticostriatal projections originating in motor cortex [37], prefrontal cortex [17], and medial agranular cortical field [53] project bilaterally to ipsilateral [17] and contralateral striata [67] and cerebral cortex [225]. Examples of contralateral effects were observed previously in studies showing that kainic acid injection into the amygdala caused damage, of variable extent, to ipsilateral and contralateral CA1 and CA3 regions of hippocampus [105]. Moreover, following unilateral decortication, altered glutamate levels were found in contralateral striata [192]. These contralateral

effects by glutamate agonists reported by others, appear to occur with irregular frequency. According to our findings and those reported by others, it seems possible that contralateral effects are not artefacts due to problems with experimental procedures but rather are a true reflection of biological effects due to contralateral brain manipulations. Furthermore, expressing levels in terms of increases over contralateral side may lead to underestimates of the effects occurring in the ipsilateral striatum.

Although we did not see significant differences in adenosine levels between contralateral and ipsilateral striata injected with either of the mGluR agonist doses used, we did see significantly higher adenosine levels in contralateral striata at the higher dose compared to both striatum groups at the lower dose. This was interesting given that activation of group I and group III mGluRs attenuates the inhibitory effects of A_1 adenosine receptors [46]. One explanation of our results may be that elevated levels of depolarization due to relief of A_1 receptor-mediated inhibition of neurotransmission were adequate to stimulate contralateral striata thus causing the observed increases in adenosine levels in the untreated side.

Our findings support the general notion that as ATP levels drop adenosine levels rise. However, we have shown quantitatively that the flux between ATP depletion and adenosine formation occurs at different rates depending on the depolarizing strength of the stimulus involved and whether significant NMDA receptor activation occurs. We proposed that these rates are indicative of different systems of purine level regulation and have designated them tier-1 and tier-2.

Chapter 3

Effects of Sleep Deprivation on Adenosine and Energy Charge Levels in Rat Brain.

Abstract

One prominent theory addressing the physiological role of sleep states that sleep serves a restorative function in which the levels of high-energy molecules in the brain are replenished following their depletion during periods of wakefulness. In this model, adenosine has been implicated as a sleep-signaling molecule because of its production and accumulation during periods of ATP depletion and its ability to alter neuronal firing patterns primarily in an inhibitory fashion. Using male Sprague-Dawley rats in 12- and 24-hour models of sleep deprivation we measured the effect of prolonged wakefulness on adenosine and adenine nucleotide levels in specific brain regions implicated in the control of sleep including frontal cortex, basal forebrain, and hypothalamus. Our results showed that neither 12- or 24- hour periods of sleep deprivation produced a consistent pattern in adenosine level changes compared to animals allowed to rest normally. After normalizing adenine nucleotide data to remove between-experiment variability, we noticed a small but consistent depletion of ATP levels in brain regions of sleep deprived animals from both the 12- and 24-hour studies. We also carried out a preliminary study focusing on striatum, hippocampus and the parietal, temporal and occipital cortical regions. These data showed no consistent changes in adenosine or adenine nucleotide levels resulting from sleep-deprivation, however, we did observe higher adenosine levels in striatum and hippocampus compared to those measured in cortical regions. Our data suggest that sleep deprivation produces a gradual depletion of brain ATP in some brain regions and that different regulatory mechanisms control adenosine levels in cortex compared to striatum and hippocampus.

Introduction

The behavior we refer to as sleep is practiced by nearly all animals, including humans. We appreciate first hand the importance of sleep given the detrimental effects of altered sleep patterns and sleep deprivation on our ability to carry out daily tasks. Fatigue due to disrupted sleep takes a significant toll on society by reducing workplace productivity and increasing accidents both in and outside the workplace. A major limitation of today's sleep aid medications is their inability to promote restful sleep (slow-wave) as they generally only increase overall sleep time. One factor limiting the development of better sleep therapeutics is our lack of knowledge about why we sleep, the restorative functions of sleep, the neurochemical mechanisms that initiate sleep onset, and the mechanisms that regulate various sleep stages.

Sleep is divided into several stages according to characteristic patterns of electrical activity emitted by the cerebral cortex that are detected using an electroencephalograph (EEG). Sleep is classified as either non-REM or REM based on EEG readings that indicate synchronized or desynchronized neuronal activity, respectively. Non-REM sleep is further divided, based on EEG patterns, into stages 1, 2, 3, and 4 with stages 3 and 4 referred to as slow-wave sleep (SWS). When a person initially falls asleep, they begin in stage 1 of non-REM sleep and then progress through stages 2, 3, and 4 before entering REM sleep. The non-REM stages of 3 and 4, comprised of SWS, produce the deepest and most restful sleep. The pattern of separate stages that alternates during sleep is referred to as sleep architecture.

Although the appearance of a sleeping organism suggests that sleep is a fairly homogenous process, the variations in neuronal activity in the brain as it goes through the various sleep cycles are quite profound. REM sleep is referred to as paradoxical sleep because of the high, awake-like levels of brain activity that are detected during this period. Physical characteristics of this sleep stage include rapid eye movement (REM), general body paralysis that excludes ocular and respiratory muscles, and this is also the sleep stage when dreaming occurs. Because of the high levels of brain activity during REM sleep and the learning deficits that occur with REM sleep deprivation, this sleep stage is thought to play a role in memory consolidation [78].

Several regions of the brain are associated with controlling various aspects of sleep. The basal forebrain [161,162,175] and the preoptic area of the anterior hypothalamus [200] have been implicated in controlling SWS. In the posterior hypothalamus, the suprachiasmatic nucleus acts as the brain's clock, signaling the changes in the diurnal cycle [9]. Although they were not studied in this report, several other regions in the brainstem including the raphe nuclei [20,98], laterodorsal [88,101] and pedunculopontine [196] tegmental nuclei, and the mesopontine cholinergic [26,162,196] nuclei control various aspects of sleep.

The EEG patterns used to characterize different sleep stages arise from changing neuronal firing patterns in the cerebral cortex and are hypothesized to arise from altered K^+ conductance resulting from the activation of adenosine A_1 receptors by accumulated adenosine [14]. In both rat striatum and hippocampus, adenosine release was found to be elevated during active periods and in hippocampus these increases were greatest at the end of active periods [91].

Of the many compounds purported to be endogenous signaling molecules for sleep, adenosine has received considerable attention for several reasons. First, from the standpoint that sleep serves to replenish brain energy levels [14], adenosine would be a logical signal to initiate an energy restoration process given that adenosine is formed from ATP metabolism and can accumulate under conditions where the rate of cellular energy demand exceeds energy supply. Experimentally, however, very few studies [208] have demonstrated that ATP levels are depleted by sleep deprivation, although several groups have demonstrated that brain adenosine levels change according to circadian rhythm [29,91,161] and that periods of sleep deprivation result in small adenosine level increases in brain [161].

Given the changes in neuronal firing patterns associated with the onset of sleep, a second characteristic we would expect with a sleep-inducing compound is the ability to modulate neurotransmission. Indeed, adenosine is known to predominantly inhibit and in some cases potentiate neurotransmission through activation of adenosine A_1 [7,66,163,233] and A_2 receptors [183], respectively. In basal forebrain and mesopontine cholinergic neurons, two pathways involved in EEG arousal [97], adenosine exhibits tonic inhibitory control [166] and when perfused in these areas wakefulness is found to decrease and overall sleep architecture is modified [162]. In addition, stimulation of adenosine A_1 receptors by systemic [165], or intracerebroventricular administration of A_1 receptor agonists increases slow-wave activity in non-REM sleep, an effect similar to that caused by sleep deprivation [15]. In basal forebrain, activation of adenosine A_{2A} receptors increases both REM and non-REM sleep [174]. In addition to studies showing that direct adenosine receptor

activation increases sleep, the concept of adenosine as a sleep modulator is also supported by the commonly known and often abused stimulatory properties of the adenosine receptor antagonists caffeine and theophylline.

A third characteristic we would expect with a sleep-modulating compound would be diurnal regulation of its production and metabolism by endogenous enzyme systems. Indeed, studies have show that enzymes responsible for adenosine metabolism exhibit some diurnal variation in their activity levels [29].

This work focused on testing the hypothesis put forth by Bennington and Heller [14] that sleep serves a restorative function for the replenishment of brain energy reserves and that as a result of gradual energy charge depletion, adenosine levels increase during waking hours to ultimately signal the onset of sleep. To test this hypothesis we measured simultaneously ATP, ADP, AMP and adenosine levels in discrete brain regions following sleep deprivation. To date, no such studies have been carried out using methods that provide both precise and accurate measurements of purines in discrete brain regions. Studies mentioned here showing changes in adenosine levels with circadian rhythm were carried out on decapitated animals and focused on only one brain region [29] or were done on awake and freely moving animals that were implanted with microdialysis probes [91,161]. In these reported studies the adenosine level changes, although statistically significant in some cases, were relatively small and in both of the methodologies used, particularly with decapitation as a method of sacrifice, artificially high adenosine level changes can result. In the microdialysis studies, presumably sufficient time was allowed for adenosine levels to stabilize following probe implantation, however, it is not known

whether the adenosine level increases measured over the active period of the animals might have resulted from mechanical stimulation of brain tissues from even small vibrations around implanted cannuli due to animal movement. Our methods, using microwave fixation of brain tissue allow us to rapidly and efficiently halt brain metabolism [48] thus preserving the endogenous levels of high-energy nucleotides and adenosine. In addition, microwave fixation of brain tissue allows for accurate and precise dissection of small, discrete brain regions, allowing us to study changes in the levels of purinergic compounds in specific brain regions proposed to be involved in sleep. Here, we studied brain regions including basal forebrain, cortex, and hypothalamus and carried out preliminary measurements of purinergic compounds in dorsal brain regions including the frontal, parietal, temporal and occipital cortical regions as well as striatum and hippocampus. Using a sleep deprivation model, the overall hypothesis we tested was that prolonged waking resulted in depletion of brain energy stores, namely ATP, and accumulation of adenosine.

Methods

Animals. Adult male Sprague-Dawley rats obtained from the University of Manitoba Central Animal Care breeding facility weighing 200 ± 20 g were used in the present study. Following transportation, rats were allowed five to seven days to acclimatize before being used in studies. All protocols were performed in accordance with University of Manitoba Animal Care Ethics Committee guidelines.

Sleep Deprivation. In 12- and 24-hour sleep deprivation studies, animals were not allowed to sleep between 6:00 AM to 6:00 PM or between 6:00 AM to 6:00 AM, respectively. Animals were kept awake by gently handling and providing novel environmental stimuli while constant access to food and water was maintained. Control groups were placed in a quite room and were allowed to sleep normally.

Microwave Irradiation and Dissections. Following sleep deprivation, animals were sacrificed by microwave irradiation. Using a power level of 10 kW, microwave times of 1.0 - 1.1 s were used when frontal cortex, basal forebrain, anterior hypothalamus, and posterior hypothalamus were to be dissected (Fig. 3.1). Longer microwave times of 1.5 s were used when parietal cortex, striatum, temporal cortex, hippocampus, and occipital cortex were isolated (Fig. 3.2). Immediately following microwave fixation, brain temperatures were taken at the posterior limit of the cortex immediately below the pineal gland to verify that brain tissue was appropriately heated. Brain regions

were dissected on an ice-chilled metal plate and immediately frozen on dry ice.

Tissue samples were stored at -80°C until taken for HPLC analysis.

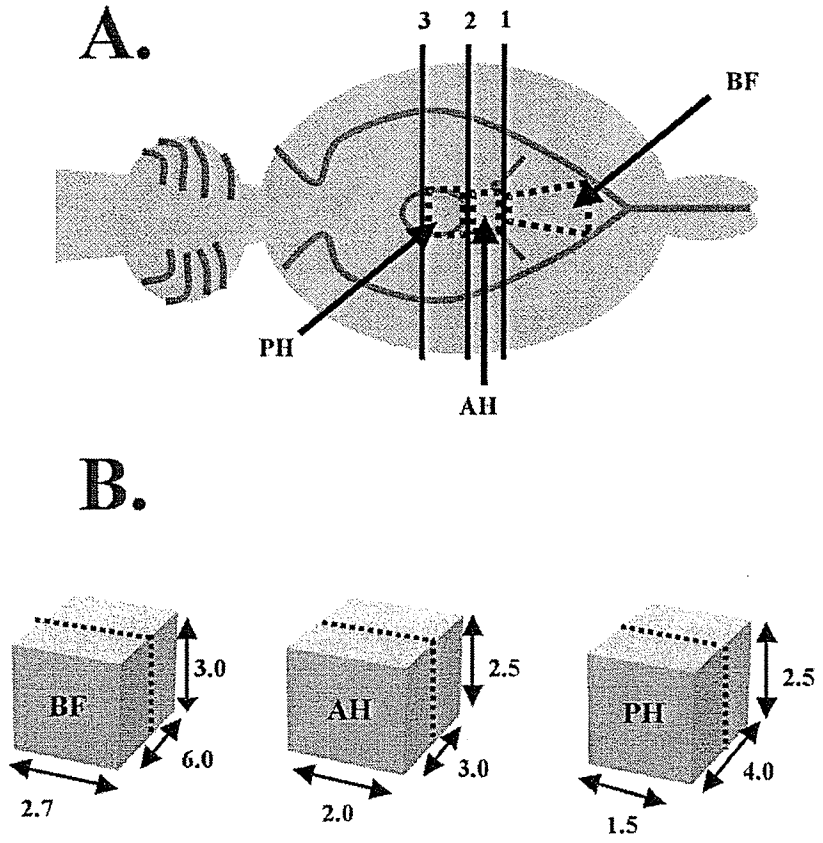

Figure 3.1 Dissection of Basal Brain Regions. A. For dissection of basal brain regions, the brain was cut coronally starting at the level of the optic nerves (≈AP 9.0 mm, cut 1). The next coronal cut was then taken 2 mm in the posterior direction (≈AP 7.0 mm, cut 2) producing a brain slice from which the anterior hypothalamus (AH) was dissected. The final cut was taken 1.5 mm further posterior (≈AP 5.5 mm, cut 3) and yielded the brain slice from which the posterior hypothalamus (PH) was dissected. The basal forebrain (BF) was dissected directly from the remaining anterior portion of the brain. Brain coordinates listed are measured from the bregma and were obtained from Paxinos and Watson [143]. B. Illustrated are the approximate measurements of the dissected basal forebrain (BF), anterior hypothalamus (AH), and posterior hypothalamus (PH) brain regions. The dotted line indicates the midline of the ventral brain surface, which is represented by the top, lightly-shaded side of each cube. Dimensions shown are in millimeter units.

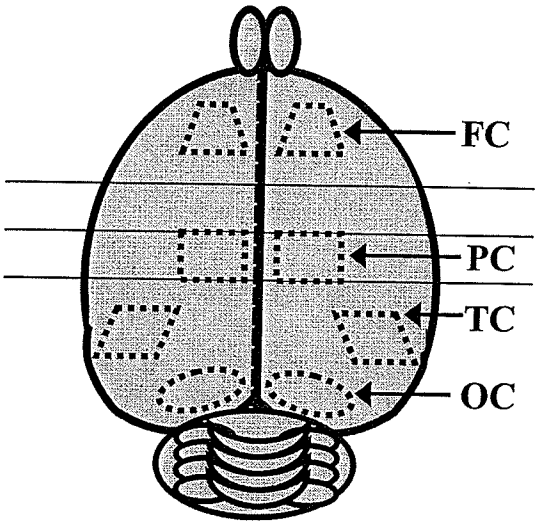

Figure 3.2. Cortical Dissections. Shown is a schematic diagram of the dorsal rat brain surface. Horizontal lines correspond to the coronal cuts described in Figure 3.1. Dotted shapes indicate where dissections of frontal (FC), parietal (PC), temporal (TC) and occipital (OC) cortex samples were carried out.

Analysis of Purinergic Compounds. See Chapter 1.

Between-Study Data Normalization.

The sleep deprivation studies outlined in this report were carried out over a two year period. In some cases, the data collected was significantly different between studies conducted at different times (Fig. 3.3). After we verified that our analytical techniques and calculations were accurate, we concluded that these differences were representative of *in vivo* conditions. These differences, however, made it impossible to pool the control or sleep deprivation data from separate studies carried out at different times. Accordingly, we developed a method to normalize the data and this allowed us to focus specifically on potential differences in purine levels between control and sleep deprived animals.

Post. Hyp. – Control Data – Study #1

	ATP	ADP	AMP	Σ Pur
	38.4	6.0	0.5	44.9
	26.5	5.6	0.3	32.4
	45.3	7.7	0.8	53.8
mean	**36.7**	**6.5**	**0.5**	**43.7**
S.E.M.	**5.5**	**0.6**	**0.2**	

Figure 3.3. Sleep Deprivation Study Sample Data. Shown are posterior hypothalamus data collected from sleep deprivation studies carried out at two different times. The number in bold, underlined text is the average Σ_{pur} value for each group.

Post. Hyp. – Control Data – Study #2

	ATP	ADP	AMP	Σ Pur
	24.2	5.8	1.1	31.1
	25.4	4.1	0.5	30.1
	22.4	3.9	0.5	26.8
	24.1	6.2	1.0	31.3
	28.1	5.9	0.9	34.9
mean	**24.9**	**5.3**	**0.8**	**30.8**
S.E.M.	**1.7**	**0.7**	**0.1**	

To normalize the between-experiments data we chose the sum of purines value (Σ_{pur}) as a constant variable to which each of the chronologically distinct data sets (control or sleep deprivation) could be normalized. Previous data from our intrastriatal injections work supported the validity of this assumption. We therefore normalized the data according to the following equation:

$$ATP_{norm1} = ATP_1 \times \left[\frac{\frac{(\Sigma_{pur1} + \Sigma_{pur2})}{2}}{\Sigma_{pur1}} \right]$$

Equation #1

$$ATP_{norm2} = ATP_2 \times \left[\frac{\frac{(\Sigma_{pur1} + \Sigma_{pur2})}{2}}{\Sigma_{pur2}} \right]$$

Equation #2

In the equation above, the subscript 1 indicates control data from one study and the subscript 2 represents control data from a second study carried out at a different time. Normalization was carried out only between data sets of the same type, either control or sleep deprivation. The term $[(\Sigma_{pur1} + \Sigma_{pur2})/2]$ calculated an average value for Σ_{pur} to which each data set could be normalized. This value was then divided by the average Σ_{pur} for that data set (Σ_{pur1}) to create a factor that was then used to correct each data point (ATP_1) in Study #1 (Eqn. #1). The same procedure was used to normalize the data from Study #2 (Eqn. #2). The term in square brackets is greater than 1.0 in one equation and less than 1.0 in the other resulting in a uniform increase in the nucleotide data from one study and a uniform decrease in the data from the other study. Both data sets were normalized to the $[(\Sigma_{pur1} + \Sigma_{pur2})/2]$ value. Shown in Figure 3.4 are the normalized data converted from the values shown in Figure 3.3.

Post. Hyp. – Control Data – Study #1

	ATP	ADP	AMP	Σ Pur
	32.7	5.1	0.4	38.3
	22.6	4.8	0.2	27.6
	38.6	6.6	0.7	45.9
mean	**31.3**	**5.5**	**0.4**	**37.3**
S.E.M.	**4.7**	**0.5**	**0.1**	

Post. Hyp. – Control Data – Study #2

	ATP	ADP	AMP	Σ Pur
	29.3	7.0	1.3	37.5
	30.7	4.9	0.7	36.3
	27.0	4.7	0.6	32.4
	29.2	7.5	1.2	37.8
	34.0	7.1	1.1	42.2
mean	**30.1**	**6.2**	**1.0**	**37.3**
S.E.M.	**1.2**	**0.6**	**0.1**	

Figure 3.4. Normalized Sleep Deprivation Study Sample Data. Shown are the normalized posterior hypothalamus data calculated from the data in Figure 3.3.

Results

24-Hour Sleep Deprivation Studies. After normalizing (nucleotide data only) and pooling the data from three separate experiments (Fig.3.5), we found that 24-hour sleep deprivation produced no significant changes in nucleotide levels in the basal regions of sleep-deprived rats compared to control animals. The data do, however, show consistent trends toward decreased levels of ATP in the brain regions of sleep-deprived animals. Results from individual studies are shown in Appendix IV (A, B, and C). Interestingly, the variation in sum of nucleotide values observed between our individual sleep deprivation studies was similar to variation seen in some of our intrastriatal injection experiments (compare results in Appendix II.D with II.C, F or J). In both control and sleep deprivation treatment groups, energy charge (EC) levels were significantly lower ($p<0.001$) in the frontal cortex region compared to the other three basal regions studied (Fig.3.5). As indicated by the data in Appendix IV, our analytical methods were unable to consistently detect the very low endogenous adenosine levels present in the basal brain regions in Studies 1 and 2 but by Study 3, however, we rectified this problem. Therefore, the adenosine data in Figure 3.5 was taken directly from Study 3. Although it was not the direct focus of these studies, we also carried out purine analysis on portions of dorsal brain regions following one 24-hour sleep deprivation study (Fig. 3.6), which were originally dissected for the purpose of glycogen analysis (not discussed here). The results from this single study revealed generally lower ATP levels in control and 24-hour sleep deprived rats and higher levels of adenosine in striatum and hippocampus. In cerebral cortex, even

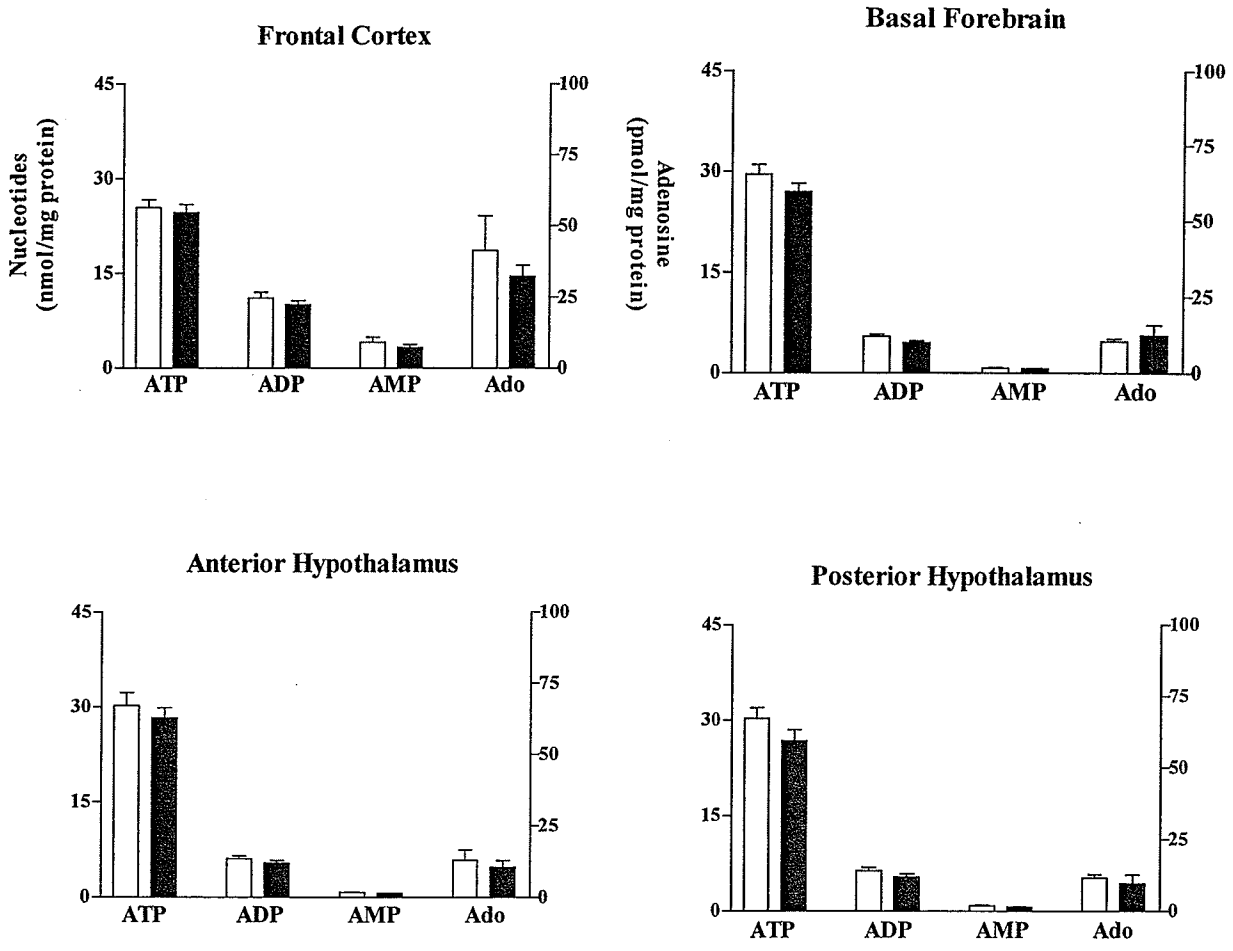

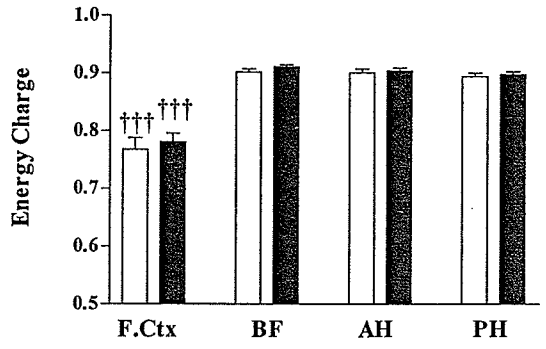

Figure 3.5. 24-Hour Sleep Deprivation. Shown are pooled data from control (n=17, light bars) and sleep deprived (n=16, dark bars) animals collected from three separate sleep deprivation studies. Data from the three studies were normalized and pooled according to the method outlined in the Methods section. All axes are presented in the same units as shown in the frontal cortex graph. Data from the individual studies are shown in Appendix IV.A, B, and C. ††† - different ($p<0.001$) from all other bars of the same shade.

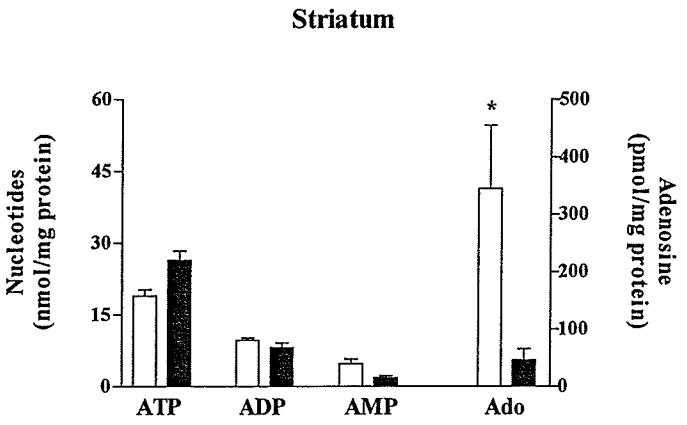

Figure 3.6. 24-Hour Sleep Deprivation – Dorsal Regions. Shown are purine levels (mean ± S.E.M.) from control (n=5, light bars) and sleep deprived (n=4, dark bars) rats. All axes are presented in the same units as annotated in the striatum graph. Results shown are from one study. * - different ($p<0.05$) from corresponding sleep deprivation data set.

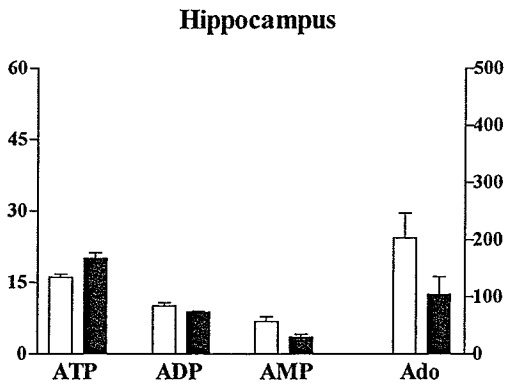

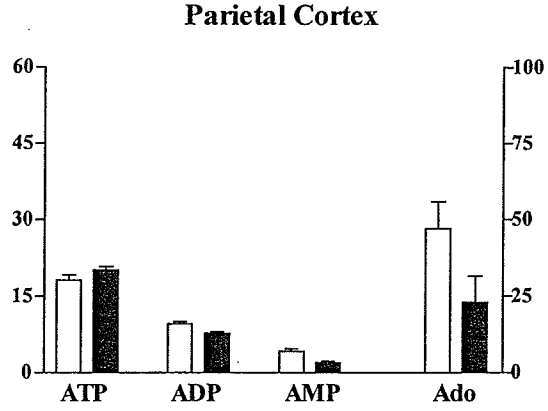

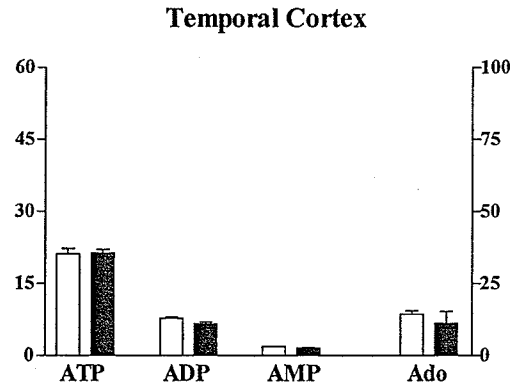

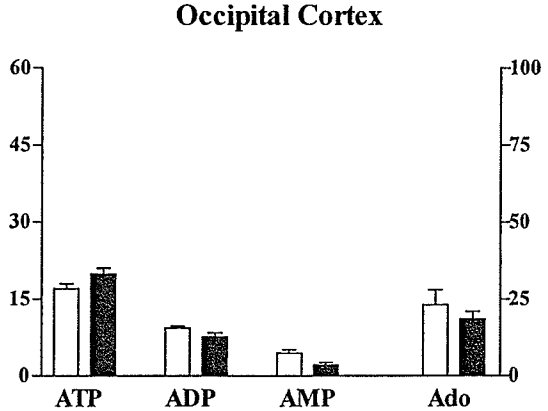

though ATP levels were lower when compared to levels in basal regions, adenosine levels were not elevated to the same extent as in hippocampus and striatum.

12-Hour Sleep Deprivation Studies. Consistent with the 24-hour sleep deprivation experiments, 12-hour periods of sleep deprivation produced no statistically significant purine level changes in basal brain regions, however, we did observe consistent and small decreases in the levels of ATP in frontal cortex, basal forebrain, and anterior hypothalamus regions (Fig.3.7). EC values in frontal cortex from control and 12-hour sleep deprived rats were significantly lower than those measured in the other basal regions studied. Purine analysis of dorsal brain regions following 12 hours of sleep deprivation (Fig. 3.8) revealed similar results to those from the 24-hour study except for lower adenosine levels in the striatal and hippocampal regions and a significant ($p<0.05$) increase in adenosine levels in the occipital cortex of the sleep deprived treatment group compared to controls (Fig. 3.8).

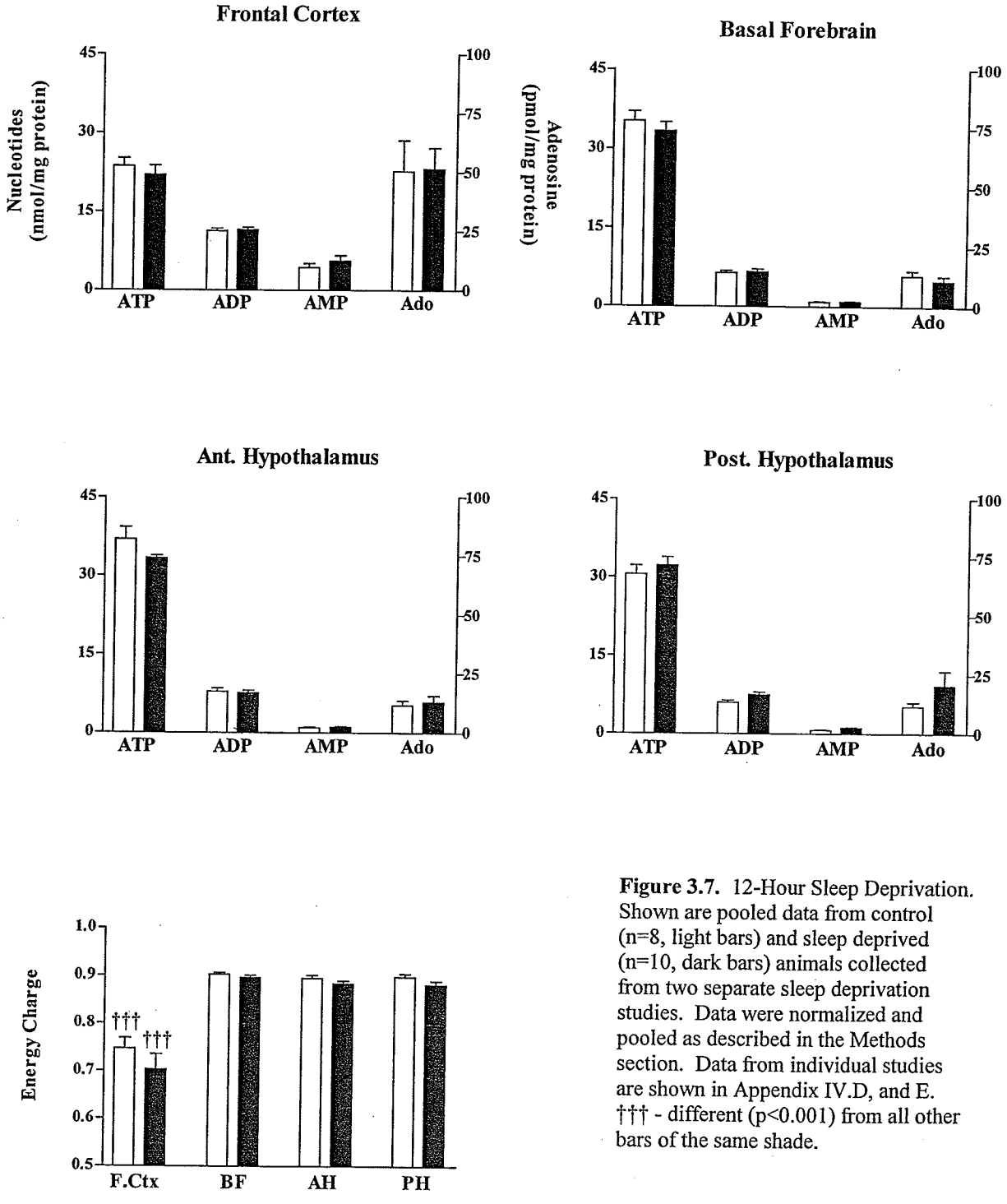

Figure 3.7. 12-Hour Sleep Deprivation. Shown are pooled data from control (n=8, light bars) and sleep deprived (n=10, dark bars) animals collected from two separate sleep deprivation studies. Data were normalized and pooled as described in the Methods section. Data from individual studies are shown in Appendix IV.D, and E. ††† - different ($p<0.001$) from all other bars of the same shade.

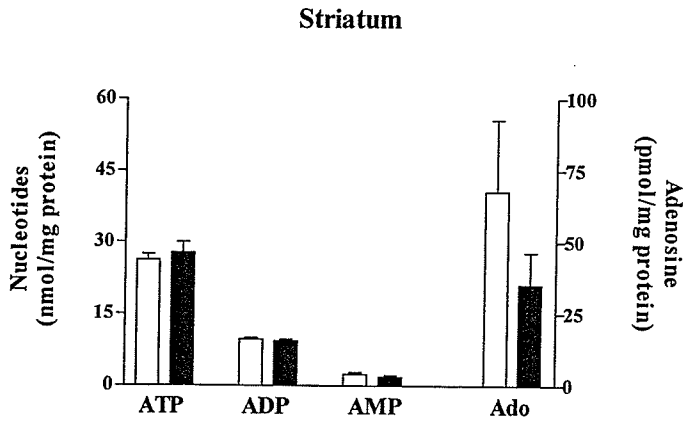

Figure 3.8. 12-Hour Sleep Deprivation – Dorsal Brain Regions. Shown are purine levels (mean ± S.E.M.) from control (n=5, light bars) and sleep deprived (n=5, dark bars) rats. Results shown are from one study.
* - different ($p<0.05$) from corresponding sleep deprivation data set.

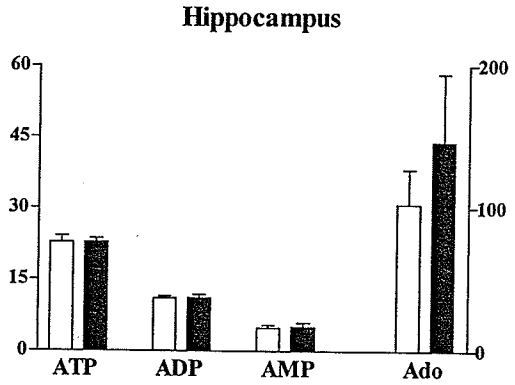

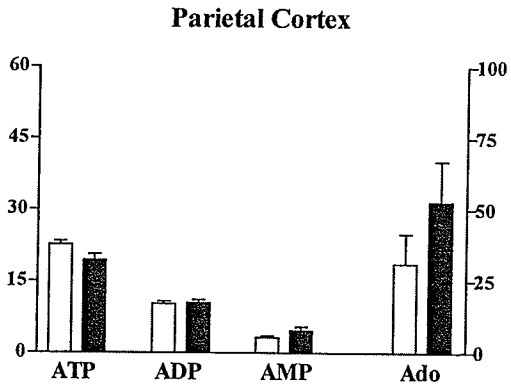

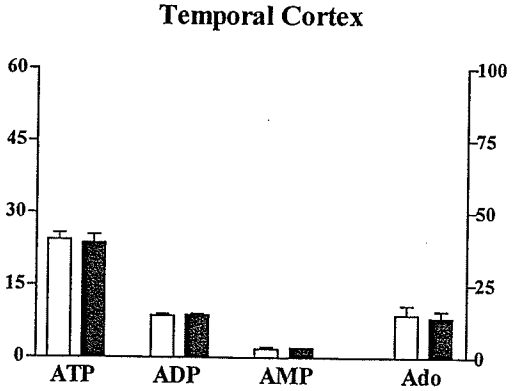

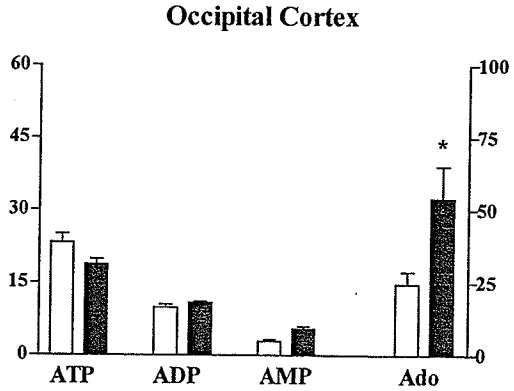

Discussion

The hypothesis that sleep serves a restorative function in the brain [14] to replenish depleted glycogen and high-energy phosphate stores predicts two general phenomena. First, that wakefulness results in a gradual depletion of brain energy stores and a consequential increase in adenosine levels. Second, the increase in brain adenosine levels with continued wakefulness induces changes in the firing patterns in brain areas associated with the onset and control of sleep. The few studies carried out to address the first phenomena have shown decreases in creatine phosphate and ATP levels in whole brain [208] and small increases in extracellular adenosine levels in basal forebrain [160,161] and cortex [160] following periods of sleep deprivation. No studies, however, have monitored changes in levels of high-energy purine nucleotides and adenosine simultaneously using methods shown to measure accurate levels of endogenous purines, in multiple brain regions associated with sleep, following extended periods of wakefulness. Here, we carried out such studies using the techniques developed in Chapter 1.

Data from individual sleep deprivation studies reported here were found to differ in terms of sum of purine nucleotides (Σ_{pur} = ATP + ADP + AMP) levels. Although this variation existed between studies, data from control and sleep deprivation groups within individual studies were predominantly not statistically different, and trends were largely toward slightly lower Σ_{pur} levels in sleep deprived animals. In order to detect changes in nucleotide levels that might be masked by between-experiment variability in Σ_{pur} values, we combined data from individual sleep deprivation studies of the same duration and then separately normalized control

and sleep deprivation data groups for each individual brain region to an average Σ_{pur} value calculated for each group. This method allowed us to remove between-experiment variability in both data sets without numerically altering the magnitude of changes in purine nucleotide levels in each region. This was of obvious importance in testing our hypothesis that tissue energy level would decrease with sleep deprivation. For normalization purposes we made the assumption that Σ_{pur} levels in the same treatment group should be essentially constant between individual experiments. Data from our experiments with excitatory amino acid injections supported this assumption. It should be emphasized that data normalization carried out on combined control group data did not take into account Σ_{pur} values from corresponding sleep deprivation data groups because we could not be sure, from a theoretical standpoint, that sleep deprivation did not alter Σ_{pur} values. Under the premise that high-energy purine nucleotides are gradually depleted with prolonged wakefulness, it is possible that the Σ_{pur} level could drop if accumulated purines such as AMP, that are gradually formed during energy depletion, are converted to IMP or adenosine.

Our data showing between-experiment discrepancies in Σ_{pur} values may have resulted for several reasons. First, individual sleep deprivation experiments were carried out several months apart at different times of the year and animals in each of the studies were likely obtained from different breeding groups. Second, there is literature reporting mechanisms in disease that can lead to alterations in nucleotide levels [22,148]. We are not implying that some of our experiments were carried out

on diseased animals, but are offering evidence for biological mechanisms that may alter purine nucleotide levels.

In these studies we set out to test the hypothesis that brain tissue adenosine levels increased with sleep deprivation due to gradual wakefulness-induced depletion of high-energy nucleotides. With sleep deprivation carried out over the time periods chosen in these studies we did not expect ATP level decreases of the magnitude reported in our excitotoxicity work given that there has been no previous record of animals undergoing ischemic depolarization under these conditions. Indeed, in our studies we observed only very small yet consistent decreases in ATP levels in the basal brain regions of sleep-deprived rats. In the same fashion, we did not expect adenosine levels to rise indefinitely with prolonged sleep deprivation because if they did, the adenosine A_1 receptors, which mediate most of the adenosine effects with sleep, might desensitize and the sleep promoting effects following continuous adenosine accumulation would be lost. From a behavioral standpoint, we observed that animals went through alternating active and sleepiness periods over the duration of each sleep deprivation study with the drive to sleep during each sleepy period increasing with study duration. Assuming that adenosine acts as a signal for the onset of sleep, these behavioral characteristics and our inability to detect consistent adenosine level increases with sleep deprivation suggested that adenosine levels over periods of sleep deprivation may actually fluctuate over time as opposed to steadily accumulate (Fig. 3.9). In the models proposed in Figure 3.9, adenosine levels are predicted to oscillate during periods of sleep deprivation to reflect the sleep-active cycles that we observed from the animals. In the same fashion we predict that ATP

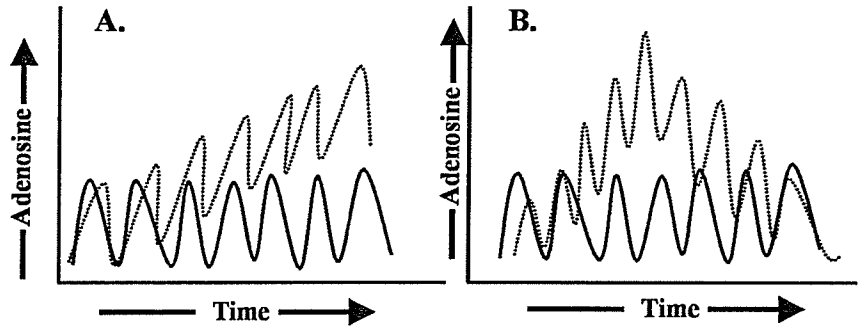

Figure 3.9. Proposed Adenosine Level Fluctuations During Sleep Deprivation. Shown are patterns of adenosine level fluctuations proposed to occur with normal circadian rhythm (solid lines) and with sleep deprivation (dotted lines). Assuming that adenosine is a sleep moderator, we can associate peaks in adenosine concentration with maximum sleepiness and troughs with awake, alert activity. In all cases, adenosine levels are predicted to fluctuate to reflect the alternating sleepy-active episodes observed over the duration of a sleep deprivation study. In panel A, it is hypothesized that with sleep deprivation, the adenosine levels follow a fluctuating pattern as with control, however, with increasing sleeplessness, the adenosine level fluctuations climb continually to higher levels. The increasing "average" can then account for the increased desire to sleep with continuing sleep deprivation. In panel B, a slightly more complex pattern is proposed. As in A, average adenosine levels increase in a stepwise fashion, however, a maximum is reached where adenosine levels and desire to sleep are the highest. Afterwards, sleep desire begins decrease with decreasing adenosine levels. In the pattern proposed in B, with continued sleep deprivation, we would predict a repeat of the wave pattern with an increased amplitude that may occur over a longer duration. From a behavioral standpoint, the pattern in B is representative of animals that initially follow the pattern in A, but then go through a long period of active behavior showing little desire to sleep.

levels would fluctuate, except with a lesser amplitude and longer period between wave peaks. When ATP levels approach wave troughs and AMP levels simultaneously rise, we predict that energy levels would then be replenished by the activation of glycogen mobilizing pathways. At ATP wave peaks these mobilizing pathways would then be inhibited. Indeed, in separate studies we have observed significant glycogen depletion in certain brain regions following sleep deprivation (unpublished observations). According to this model it would be difficult to detect consistent increases in ATP, and particularly adenosine, when sampling tissue at a designated clock time. Consistent increases in adenosine levels in this case would be detected only by chance or if sampling happened to occur at the same time in each

rat's sleep-active behavior cycle. Detecting these increases might be possible with careful monitoring of the rat's behavior and activity levels following sleep deprivation to determine the appropriate time for tissue sampling. We propose that consistent collection of tissue samples from sleep deprived animals in the middle of a sleepy period would reveal significant increases in tissue adenosine levels compared to control animals sampled at the start of an active cycle.

The decreased EC values we observed in frontal cortex regions were of particular interest given that the associated adenosine levels, although compared to other basal regions seemed high, were actually quite low compared to adenosine level increases from the same drop in EC in striatal tissues. Our studies of dorsal brain regions with sleep deprivation are also consistent with these findings given the high adenosine levels in striatal and hippocampal tissues, compared to those in the three cortical regions sampled. These findings and the study by Wojcik and Neff (1982), showing the adenosine levels in striatum were almost five times higher following decapitation that in frontal cortex [228], suggest that the potential for adenosine production in the striatum is much greater than in cortex. In addition, recent studies have also shown that 5′-nucleotidase, an enzyme that converts AMP to adenosine, has relatively low activity in cortical tissues compared to other brain regions [111]. These studies might help explain the difference in volatility of the adenosine-EC relationships we observed in cortical compared to striatal tissues and would imply different modes of adenosine level regulation in the two brain regions. This notion is analogous to the two-tiered model for adenosine and nucleotide regulation we proposed in Chapter 2. Perhaps the glutamatergic/adenosinergic systems in place in

the striatum that give rise to the volatile adenosine-EC relationships characteristic of tier-two type purine regulation are absent or are under different control in the cortex.

Chapter 4

Expression Profiling of Adenosine-Related Genes in Rat Brain: Changes With Diurnal Rhythm and Age – Preliminary Studies.

Abstract

Adenosine, because it can accumulate during periods of ATP depletion and due to its ability to alter neuronal firing patterns primarily in an inhibitory fashion, has been implicated as a sleep-signaling molecule in models that propose sleep as a process to restore levels of high-energy phosphates that are depleted during wakefulness. Here, we attempted to measure changes in adenosine-related gene expression that might occur over the diurnal cycle or with aging to determine which regulatory elements of adenosine homeostasis might give rise to the changes in sleep that occur in these two paradigms. Three different gene expression studies in their preliminary stages are described in this chapter. In the first study, we adapted a linear mRNA amplification technique in order to intensify the gene expression message when studying very small tissue samples given the relatively low natural abundance of mRNA in tissues and the non-linear amplification of different sized mRNA molecules in a given population when traditional PCR-based methods are used. Using this technique we attempted to compare differences in gene expression between day and night. In the second study, we compared adenosine-related gene expression between 2- and 24-month old rats using larger tissue samples and our own cDNA mini arrays. In the final project we attempted to compare gene expression changes between young and aged rats using a commercially prepared cDNA array containing 588 genes. These were preliminary studies and limited conclusions about changes in gene expression were reached. However, the methods that were developed will facilitate rapid continuation of these projects.

Introduction

In the human population, aging is often associated with altered sleep patterns that result in increased time to sleep onset, higher incidence of wakefulness periods during the night and increased daytime sleepiness [24]. These changes, said to be associated with a less robust circadian rhythm, are exaggerated in those suffering from age-related dementias [24]. With aging, similar alterations in sleep patterns occur in rats including a reduction in circadian rhythm amplitude and increased sleep fragmentation [201,210]. Several have proposed that neurobiological deficits in specific brain regions that alter the balance of specific neurotransmitter systems give rise to age-related impairments in both sleep and learning and memory [114,198].

Changes in adenosine metabolism and signaling in the aged rat brain alter neurotransmission and may give rise to age-related changes in sleep. With aging, the levels of adenosine A_1 receptors (A_1Rs) are decreased in hippocampal and cortical regions [31,43,44,193] while A_{2A} receptor (A_{2A}R) abundance in these same regions increases [43]. In the striatum, A_1R abundance does not appear to change with aging, however, levels of A_{2A}R decrease [43,178]. In terms of adenosinergic enzymes, the activity of 5′-nucleotidase was increased [72] while that of adenosine deaminase was found to decrease [144] in brains of aged compared to young rats. Age-related changes in adenosine signaling and regulation are known to alter neurotransmission in several brain regions including hippocampus [95,182,193], cortex [110] and striatum [35,36,159,193]. In some cases, these changes in adenosine receptor abundance and subsequent alteration of neurotransmission can be linked to changes in the expression of adenosine-related genes [31,178].

Changes in neuronal signaling in the brain over the diurnal cycle can initiate the onset of sleep, control the various stages of sleep (sleep architecture) and induce wakefulness. Evidence that adenosine plays a role in these changes comes from studies showing that levels of adenosine [29,91,161], adenosine receptors [170,213] and adenosine-metabolizing enzymes [29] exhibit diurnal patterns of variation. As outlined in Chapter 3, in brain regions implicated in sleep, adenosine can alter the onset and regulation of sleep stages. To date, no studies have shown whether adenosinergic genes are differentially expressed over the diurnal cycle. In contrast, many studies have shown diurnal variation in the expression of immediate early genes (IEGs) such as c-fos [10,11,76,77,156] and jun-B [125] and in those genes involved in regulating the circadian clock including per1 and per2 [118,230].

The brain is an extremely complex organ in terms of its highly intricate cytoarchitecture and heterogeneity of cell types. Studies carried out on large brain regions (ie: entire cerebral cortex), investigating specific neurological mechanisms such as sleep, can produce ambiguous findings when a legitimate effect in a specific nucleus of cells is masked or diluted by the concurrent analysis of a relatively large surrounding and uninvolved tissue volume. For this reason gene expression studies have been incrementally reduced in scale down to the single cell level [58,59].

Messenger RNA (mRNA), the cellular indicator of gene expression, represents only 1-5% of total cellular RNA. Reducing the size of a tissue sample to increase the regional specificity of an analysis produces greater challenges in measuring the relative abundance of individual mRNA species because levels of isolated mRNA are too low for routine methods of analysis. For this reason, methods

have been developed to amplify mRNA populations isolated from samples as small as a single cell while maintaining the original proportions of individual endogenous mRNA species and thus preserving the gene expression profile in the sample. The drawback to using traditional PCR-based methods results from the tendency of DNA polymerase to disproportionately reduce the amplification of longer cDNA molecules resulting from large mRNA transcripts [209]. Starting with an mRNA population containing only a few copies of each transcript, this type of disproportionate amplification of the gene expression signal produces ambiguous results when mRNA expression patterns are compared. To address this problem, methods have been developed to amplify the mRNA message using RNA polymerase, which facilitates the linear amplification of even large mRNA transcripts resulting in an anti-sense mRNA (aRNA) product in the same proportions as the original mRNA sample [209]. Here, we adapted the RNA polymerase-based mRNA amplification methods to study the changes in gene expression patterns that occur with aging and over the diurnal cycle in small (1-2 mg) discrete brain regions. Our intention was to identify genes, particularly ones involved in adenosine metabolism that may be involved in the regulation, or in the case of the aging model, dysregulation of sleep.

Methods

The preliminary experiments described in this Chapter were carried out at the University of Pennsylvania in the Department of Sleep and Respiratory Neurobiology under the supervision of Drs. Allan Pack and Mirek Mackiewicz.

Animals. Young (2 month) or old (24 month) male Fisher rats obtained from Charles River breeding facilities (Boston, MA) were used in these studies.

Tissue Dissections. Rats were sacrificed by decapitation and brain regions were immediately dissected on a cold surface. When required, small tissue punch samples were obtained from 2 mm thick coronal brain slices. The cortical samples used in these studies were taken from the parietal region.

Experiments. Three different gene expression studies are described in this chapter. In the first study, we adapted RNA polymerase-based mRNA amplification methods to studying gene expression in small tissue punch samples of parietal cortex. In the second study, we created small-scale cDNA arrays by spotting cDNA from several different adenosine transporters, receptors, and adenosine metabolizing enzymes onto blotting membranes. By hybridizing these membranes with radiolabeled single-stranded cDNA derived from mRNA from either young or old rats we attempted to characterize gene expression changes between young and old animals. In the third study, we used a commercial rat brain cDNA array kit to measure changes in gene expression between young and old animals to gain a wider perspective on

age-related changes in gene expression. The commercial array contained cDNA spots for 588 different genes from 16 different categories. In a fourth study, we demonstrated that high integrity mRNA could be isolated from small tissue punch samples fixed by microwave irradiation. The specific methods developed here have not been described elsewhere, therefore a detailed methods section is presented at the end of the chapter which outlines all reactions, reagents and conditions that were used or developed in carrying out this work. Supplemental information has also been provided in Appendix V.

Results and Discussion

Diurnal Changes in Gene Expression. We used a novel method of amplifying mRNA to test for changes in the expression of adenosine-related genes across the diurnal cycle. This mRNA amplification procedure (Fig. 4.1), described in detail elsewhere [58], amplifies mRNA from very small tissue samples (~ 2 mg) or single cells, and yields an accurate measure of relative mRNA abundance. High-activity T7-RNA polymerase was used in the amplification step of this procedure because it generates high integrity copies of RNA without bias to size of the original DNA template. Traditional PCR methods to amplify gene expression patterns were not used because of the tendency of DNA polymerase to disproportionately reduce the amplification of longer cDNA molecules [209].

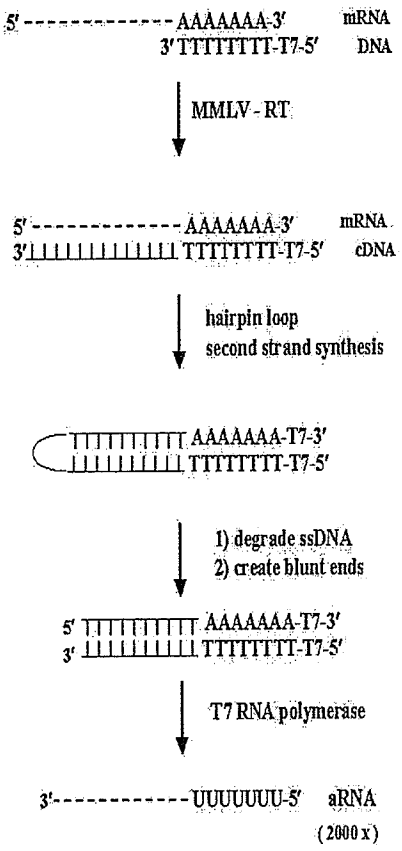

Figure 4.1. Reaction Scheme for Amplification of mRNA. The original mRNA sequence is preserved in the construction of a double-stranded cDNA molecule fitted with a T7-RNA polymerase promoter region. Once fully constructed, the cDNA molecule is transcribed using a high activity T7-RNA polymerase to produce an RNA molecule anti-sense with respect to the sequence of the original mRNA.

As outlined in Figure 4.1, the reverse transcription of mRNA was primed with an oligo

(dT)-T7 primer [58] and a double-stranded DNA (dsDNA) molecule containing both a T7-RNA polymerase promoter and the information from the mRNA transcript coded in the form of cDNA was produced. The primer used above annealed to the poly-A tail of eukaryotic mRNA and at the same time incorporated the T7 promoter region into the dsDNA molecule; a step necessary for the subsequent amplification step with T7-RNA polymerase. Following the second strand cDNA synthesis, several reactions were carried out to prepare the cDNA for reaction with RNA polymerase. The product of the T7-RNA polymerase reaction was a single-strand radiolabeled RNA molecule that was antisense (aRNA) with respect to the original mRNA molecule. The sequence of reactions in Figure 4.1 is estimated to yield a 2000-fold amplification of mRNA message [209]. The amplified aRNA product was then used for hybridization to cDNA arrays or further amplified approximately an additional 500-fold in a second series of reactions similar to those outlined in Figure 4.1 [58].

Starting with a rat brain parietal cortex sample isolated from a young Fisher rat sacrificed at either 2 AM or 2 PM, we used the procedure outlined in Figure 4.1 to synthesize high molecular weight radiolabeled aRNA as illustrated by the autoradiograph shown in Figure 4.2. This result, however, came after considerable work in optimizing the conditions for each individual reaction and verifying its success. One such verification step involved incorporating [^{35}S]dATP in the second-strand synthesis reaction. Overall, the entire procedure was very challenging due to the very small quantity of mRNA starting material coupled with the numerous cDNA precipitation (purification) steps required throughout the procedure.

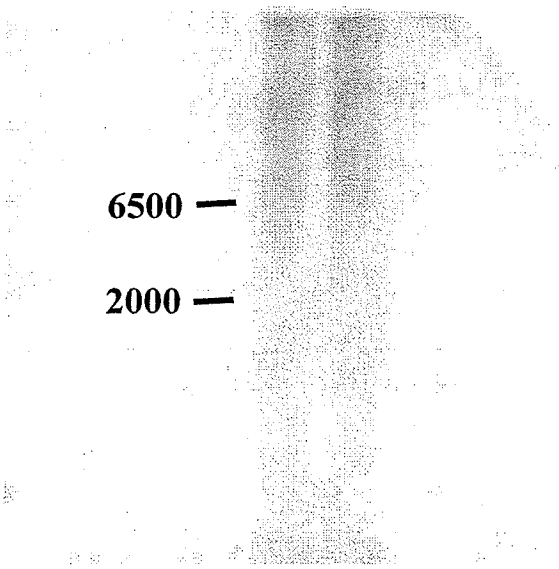

Figure 4.2. Amplified aRNA. Shown is an autoradiograph of amplified aRNA synthesized from parietal cortex mRNA isolated from young Fisher rats. Samples were taken after sacrifice at either 2 AM (left lane) or 2 PM (right lane). The above separation was carried out on a 1.5% non-denaturing agarose gel. Molecular weight markers are annotated.

An attempt to hybridize the aRNA probes to cDNA dot blots (Detailed Methods section A.11) proved unsuccessful, as no hybridized probe was detectable from either of the two blots. Most likely, too little labeled aRNA was present and a second round of amplification would be necessary to obtain an aRNA signal that would enable accurate and precise measurement.

Age-Related Changes in Gene Expression. Miniature cDNA arrays containing genes related to adenosine metabolism were created in order to determine differences in gene expression in parietal cortex of young and old rats. Included on the mini-array were adenosine receptors and transporters as well as adenosine-metabolizing enzymes and several constitutively expressed genes for normalization purposes (Detailed Methods section B.2). The array was probed with radiolabeled single-strand cDNA generated using mRNA isolated from a large sample of parietal cortex from either a young or old rat. The relative levels of gene expression were determined without any prior amplification of the mRNA message. A detailed description of this project is given in Detailed Methods section B.

As shown in Figure 4.3, there appeared to be no significant changes in adenosine-related gene expression between young and old rats. Adenosine deaminase mRNA was not detectable given its low abundance in cortex compared to other brain regions such as the tuberomammillary nucleus [112]. Additional experiments on smaller more discrete brain samples coupled with an amplification procedure may have yielded detectable signals for ADA and may also reveal gene expression differences between young and old rats.

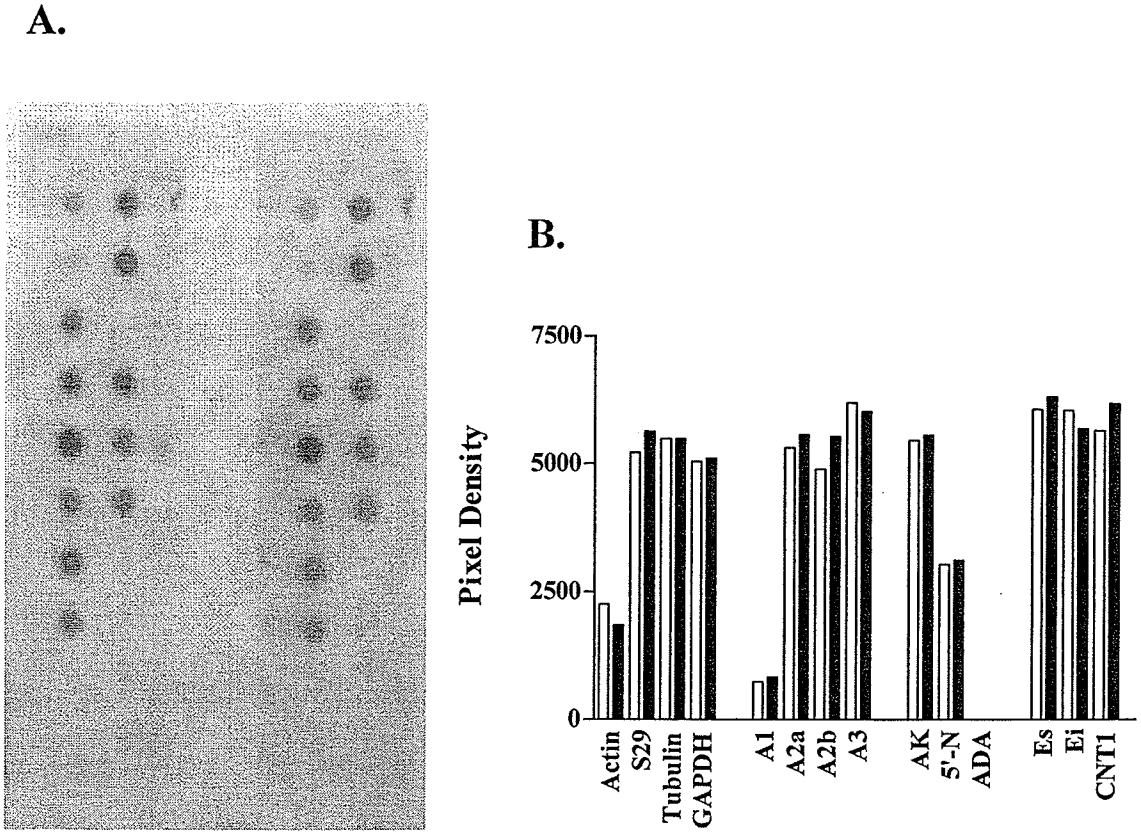

Figure 4.3. cDNA Mini Arrays. A. Comparison of adenosine-related gene expression in parietal cortex of a young (left array) or an old (right array) Fisher rat. The orientation of genes on the two identical arrays is described in Detailed Methods section B.2. The primer sets used to synthesize the array cDNAs are listed in Appendix V.A. B. Quantitative analysis of both arrays, by densitometric methods, yielded the figure on the right showing relative gene expression levels in the young (white bars) and the old (dark bars) rat. Values in the bar graph are shown after normalizing both data sets to expression level of the tubulin gene.

We also investigated changes in gene expression between young and old rats using a commercially-available Atlas™ rat cDNA expression array (Clontech) containing 588 different cDNAs. With these arrays we measured expression profiles using radiolabeled cDNA probes constructed from first-strand cDNA synthesis

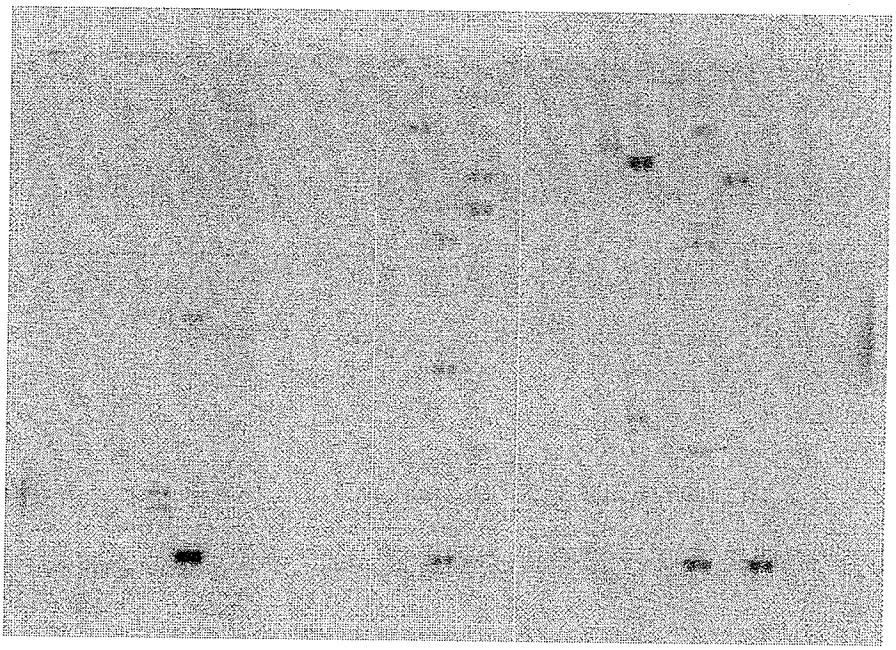

Figure 4.4. An Atlas™ rat brain cDNA array (Clontech) containing 588 genes spotted in duplicate from 16 separate classes. After hybridizing with a cDNA probe synthesized from parietal cortex mRNA from an old rat, 45 genes were detectable. The identity of these genes and their relative intensity are listed in Appendix V.B. The autoradiograph above was developed after an exposure time of approximately 1 week at -80°C.

(Detailed Methods section C). Initially, we hybridized one Atlas™ array with a cDNA probe constructed from mRNA extracted from parietal cortex of an old rat (Fig. 4.4.). A complete list of the 45 detected genes along with relative intensity estimates is listed in Appendix V.B. However, due to the high level of background signal emitting from one of the blots that was previously used to obtain the results

shown in Figure 4.4, comparisons were not possible between parietal cortex gene expression levels in young and old rats. Additional studies are required implementing an amplification step on the original mRNA population to produce more intense autoradiographs allowing for the detection of a greater number of genes.

mRNA Isolation From Small Microwaved Tissue Samples. To extend our analysis of gene expression to our studies of excitatory amino acid regulation of adenosine levels we isolated mRNA from very small tissue punches (~ 2 mg) from microwave-fixed tissue and performed first-strand DNA synthesis. We showed previously that intact mRNA could be isolated from tissues fixed by microwave irradiation [120]. Isolation of mRNA was carried out as outlined in Detailed Methods section A.1. As shown in Figure 4.5 (top lanes 2 and 3) we were able to amplify the glyceraldehyde-3-phosphate dehydrogenase (GAPDH) mRNA message from small microwaved tissue punches. Because ribosomal RNA (rRNA) is degraded in microwaved brain [120] we were unable to detect rRNA in the two mRNA samples from microwaved brain (bottom lanes 2 and 3 in Fig 4.5) compared to the strong rRNA signals in decapitated brain (bottom lane 1 in Fig. 4.5). Light smears of high molecular weight mRNA were observed in bottom lanes 2 and 3 of Figure 4.5.

The ability to isolate intact mRNA from very small tissue samples fixed by microwave irradiation allows us to measure simultaneously metabolite and gene expression levels in discrete brain areas following stimuli such as NMDA receptor activation [84]. Changes in early gene expression following injection of glutamate receptor agonists into striatum occur as early as 30 min [219,220] or in other cases

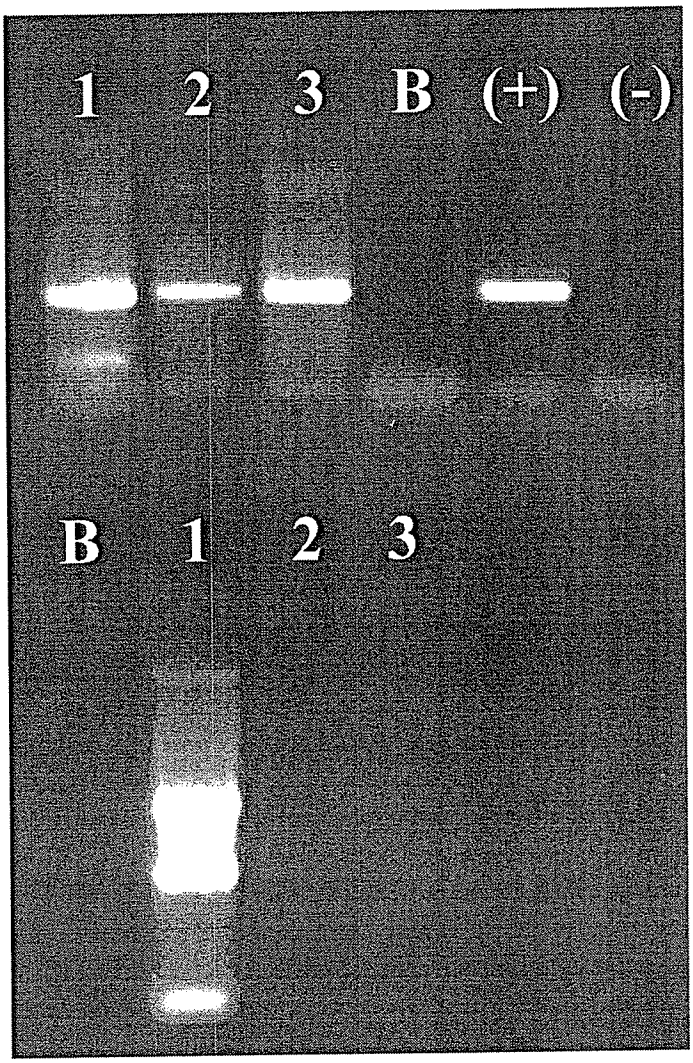

Figure 4.5. mRNA Isolation and First Strand cDNA Synthesis. Top Half: RT-PCR (26 cycles) products, using rat glyceralde-3-phosphate dehydrogenase (GAPDH) primers, from reactions carried out on mRNA isolated from decapitated brain tisssue (1), a tissue punch (~ 2 mg) from microwaved striatum (2), and a tissue punch from microwaved cortex (3). Shown in lane B is a no-mRNA control and lanes designated by (+) and (-) show results from positive and negative controls, respectively. Bottom Half: Non-denaturing agarose gel separation of the mRNA samples used in the RT-PCR reactions shown in the top half of the figure. See the Detailed Methods section for procedural details on RNA isolation and RT-PCR.

two hours [84,164]. Matching the levels of metabolite markers with concurrent gene expression changes may finally allow us to begin evaluating the degree to which EC must be depleted in order for destructive processes such as apoptosis and necrosis to be initiated. This will help us determine the extent to which adenosine level increases

due to ATP metabolism, under conditions such as glutamate receptor stimulation, are neuroprotective.

Detailed Methods

A. Measuring Gene Expression Using Antisense RNA Amplification

A.1. Isolation of Total RNA

For total RNA isolation, small (~ 3 mm^3) tissue portions were cut from frozen parietal cortex samples without thawing. In 500 µl microcentrifuge tubes, tissues for total RNA isolation were combined with 100 µl of Ultraspec™ RNA reagent[a] and homogenization was carried out by passing the tissue through a 25 Ga needle attached to a 1.0 ml syringe. After storing homogenates on ice for 5 min, 100 µl of chloroform was added to each tube and mixing was carried out by vortex at medium speed for 20 s. Samples were stored on ice for 5 min and then centrifuged at maximum speed for 15 min at 4°C. Top aqueous phases (~40 µl) were carefully[b] removed and transferred to new 500 µl microcentrifuge tubes. After adding an equal volume of isopropanol, tubes were placed on ice for 10 min and then centrifuged at maximum speed for 25 min at 4°C. Resulting supernatants were discarded, pellets[c] were washed with 75% ethanol, and samples were centrifuged once more at maximum speed for 25 min at 4°C. Supernatants were removed and pellets were dried under vacuum for 5-8 min[d]. Total RNA was suspended in 20 µl of DEPC-treated water and stored at -20°C. RNA quality was determined by agarose gel (1-1.5%) electrophoresis under non-denaturing

conditions with subsequent ethidium bromide staining. Molecular weights were estimated using 1.0 μg of ϕX174 DNA/*Hae* III size markers.

a - Total RNA was isolated using the Ultraspec™ RNA isolation system (Biotecx bulletin #27, 1992) with some modifications to the suggested protocol.

b - Removal of any interface will result in DNA contamination.

c - Pellets are not easily visible at this point and may appear only as a small colorless smear at the bottom of the tube. The location of the pellet can be estimated according to the orientation of the microcentrifuge tube in the centrifuge.

d - Pellets should be dried to remove excess ethanol which may interfere in subsequent steps, however, drying RNA pellets too long will result in difficulties with subsequent suspension.

A.2. DNase Treatment of total RNA[a]

For each reaction, the following components were combined in a 500 µl microcentrifuge tube to give a final volume of 50 µl:

2.5 µl 0.1 M Tris-Cl (pH 8.3)

0.5 µl ribonuclease inhibitor (40 U/µl)

2.5 µl 0.5 M KCl

2.5 µl 15 mM $MgCl_2$

5.0 µl DNase (RQ1, RNase-Free, 1 U/µl)

16 µl total RNA

21 µl DEPC-treated water

Mixtures were incubated at 37 °C for 15 min. Reactions were stopped by addition of 50 µl of 3:1 buffered phenol/chloroform. Phases were mixed thoroughly by vortex and separated by centrifugation at maximum speed for 2 min at 4°C. Top, aqueous phases (~ 35 µl) were transferred to 1.5 ml microcentrifuge tubes and mixed with 5 µl of sodium acetate (pH 5.2) and then 200 µl of 100% ethanol. RNA precipitation was facilitated by incubation in a dry ice/ethanol bath for 90 min. Following precipitation, RNA was collected by centrifugation at maximum speed for 30 min at 4°C. Upon removal of supernatants, RNA pellets were washed with cold 80% ethanol and centrifuged for 30 min at 4°C. Supernatants were removed and pellets were dried briefly[b] under vacuum and then suspended in 15 µl of DEPC-treated water.

a – Procedure adapted from a previous report [109].

b – See note d in the Isolation of Total RNA section.

A.3. First Strand cDNA Synthesis

The following reagents were used in each reaction:

5.0 µl 5x first strand buffer

2.5 µl 100 mM DTT

1.0 µl oligo (dT)-T7 primer (0.5 µg/µl)[a]

0.5 µl ribonuclease inhibitor (40 U/µl)

5.0 µl DEPC-treated water

6.0 µl total RNA

Components were mixed and then incubated at 100°C for 2 min. After cooling on ice, the following components were added:

0.5 µl ribonuclease inhibitor (40 U/µl)

4.0 µl dNTP mixture (2.5 mM dATP, dGTP, dCTP, dTTP)

1.0 µl MMLV reverse transcriptase (2 U/µl)

First strand synthesis was carried out for 60 min at 37°C. Reactions were stopped by incubating samples for 7 min at 100°C. Samples were then cooled on ice and stored at –20°C until later use.

a – Sequence of oligo (dT)-T7 primer: 5′-AAA CGA CGG CCA GTG AAT TGT AAT ACG ACT CAC TAT AGG CGC $(T)_{24}$-3′ [58]

A.4. Polymerase Chain Reaction (PCR)

For each reaction the following reagents were combined[a]:

5.0 µl 10x PCR buffer

1.0 µl 3′ end primer (0.1µg/µl)

1.0 µl 5′ end primer (0.1 µg/µl)

4.0 µl dNTP mix (2.5 mM dATP, dGTP, dTTP, and dCTP)

5.0 µl 100 % glycerol

0.5 µl AmpliTaq® DNA Polymerase (5 U/µl)

30.5 µl DEPC-treated water

3.0 µl DNA sample

After combining all reagents, 50 µl of mineral oil was layered over the aqueous reaction mixture. To qualitatively verify the success of first cDNA strand synthesis, 29 reaction cycles of PCR were carried out using the following temperature parameters and actin primers[b]:

denaturation:	94°C for 30 sec
annealing:	55°C for 1 min
polymerization:	72°C for 30 sec

a - For three or more reactions, a master mix was prepared containing all components except sample DNA. Reaction mixture was then added to individual reaction vessels followed by sample DNA.

b – See primer list in Appendix V.A. for sequences.

A.5. Second Strand cDNA Synthesis

Samples from first strand synthesis reactions were heated for 3 min at 95°C to denature DNA-RNA hybrids. After cooling, the following reagents were added to each reaction:

10 µl	DEPC treated water[a]
4.0 µl	10x second strand buffer
4.0 µl	dNTP mixture (2.5 mM dATP, dGTP, dCTP, dTTP)[b]
1.0 µl	T4 DNA polymerase (1U/µl)[c]
1.0 µl	Klenow fragment (1U/µl)[c]

Reactions were mixed gently by vortex and incubated for 2.5 hours at 14°C. S1 nuclease digestions of single-stranded DNA were carried out immediately after the second strand synthesis step.

a – For [^{35}S] labeling of second strand synthesis, 10 µl of [^{35}S]dATP (500 Ci/mmol) was substituted for 10 µl of DEPC-treated water.

b – In labeling reactions with [^{35}S]dATP the following nucleotide mixture was used; 2.5 mM dCTP, dGTP dTTP and 25 µM dATP.

c – Enzyme was diluted with 1x reaction buffer (supplied with enzyme).

A.6. S1 Nuclease Degradation of Single-Stranded cDNA

The following reagents were added to second strand synthesis reactions:

319 µl DEPC-treated water

40 µl 10x S1 buffer

1.0 µl S1 nuclease (1U/µl)

Reactions were incubated for 5 min at 37°C and stopped with the addition of 400 µl of 1:1 phenol/chloroform. Phases were mixed by vortex for 30 sec and separated by centrifugation at maximum speed for 60 s. Top aqueous phases were transferred carefully to new 1.5 ml microcentrifuge tubes. DNA was precipitated by adding 1 ml of 100% ethanol to samples and incubating them in a dry ice/ethanol bath for 2 hours. For collection of DNA, samples were centrifuged at maximum speed for 15 min at 4°C. Supernatants were discarded and pellets[a] were dried briefly (5-8 min) under vacuum and then suspended in 20 µl of DEPC-treated water. For reactions containing [^{35}S]dATP labeling, 3.0 µl of sample were taken for agarose gel electrophoreisis.

a - Protocols state that a large salt pellet can result at this point. Should this occur it is suggested that the ethanol precipitation step be repeated with no added salt. This problem can also be minimized by using smaller volumes during the S1 reaction.

A.7. Creation of Blunt-Ended cDNA

The following reagents were added to the suspended DNA from S1 nuclease reactions:

2.5 µl 10x KFI buffer

2.0 µl dNTP mixture (2.5 mM dATP, dCTP, dGTP and dTTP)

0.5 µl Klenow fragment (1U/µl)

After mixing, reactions were incubated for 15 min at 37°C and then stopped by addition of 1:1 phenol/chloroform. Phases were mixed by vortex for 30 s and then separated by centrifugation at maximum speed for 1 min. Top aqueous phases were transferred to new 1.5 ml microcentrifuge tubes and combined with 2.5 µl of 5 M NaCl and 75 µl 100% ethanol. DNA was precipitated by incubating samples in a dry ice/ethanol bath for 2 hours followed by centrifugation at maximum speed for 15 min at 4°C. Supernatants were discarded and pellets were dried for 5-8 min under vacuum and then suspended in 20 µl of TE buffer.

A.8. Drop Dialysis of Double-Stranded cDNA

Drop dialysis of each double-stranded DNA sample was performed in duplicate. Each drop (10 µl) was carefully placed in the middle of a 0.025 µm filter (Millipore) floating on the surface of TE buffer. Dialysis was carried out in a 24-well culture plate with approximately 3 ml of TE buffer in each well. All wells were filled with buffer to reduce evaporation of the DNA drops. Dialysis was carried out at room temperature for 5 hours and the TE buffer in wells used for dialysis was refreshed four times during this period. After dialysis, drop volume was decreased considerably for some samples. Remaining drop volume was removed and filter spots[a] were rinsed[b] twice with 7 µl of TE buffer and once more with an additional 3 – 4 µl to give a final collected volume of approximately 18 µl.

a – The area on the filter where the drop was originally placed appeared dull whereas the surrounding region of the filter had a glossy appearance.

b – Rinsing was carried out carefully by repeatedly (10-15 times) pipetting TE buffer onto the filter paper.

A.9. Synthesis of aRNA

For aRNA synthesis reactions, the following reagents were combined in a 500 µl microcentrifuge tube:

4.0 µl 5x RNA amplification buffer

1.0 µl 100 mM DTT

2.0 µl 3 NTP mix (2.5 mM ATP, GTP and UTP)

2.5 µl 0.1 mM CTP

0.5 µl ribonuclease inhibitor

1.0 µl T7 RNA polymerase (1000 U/µl) µl

2.0 µl drop dialyzed DNA

5.5 µl DEPC-treated water

1.5 µl [α^{32}P] CTP (800 Ci/mmol)

The above components were mixed by pipet and incubated[a] for 4 hours at 37°C. Reactions were stopped by the addition of 20 µl of 1:1 phenol/chloroform and 2.0 µl of 3 M sodium acetate (pH 6.5). Samples were mixed by vortex for 30 s and phases were separated by centrifugation at maximum speed for 1 min. Top aqueous phases were transferred to 1.5 ml microcentrifuge tubes and aRNA was precipitated by adding 70 µl of 100% ethanol, mixing, and then incubating in a dry ice/ethanol bath for 2 hours. aRNA was collected by centrifugation at maximum speed for 15 min at 4°C. Supernatants were discarded and pellets were dried[b] under vacuum for approximately 5 min and then suspended in 20 µl of DEPC-treated water. To verify

the aRNA product, 2.0 µl were taken for agarose gel electrophoreisis with lambda DNA/*Hind* III markers.

a – This incubation can be carried out conveniently in a PCR thermocycler maintained at 37 °C.

b – Remember note d in the Isolation of Total RNA section.

A.10. Purification of aRNA

Before use as a probe, aRNA was precipitated to remove residual unincorporated nucleotides. To each 18 µl aRNA sample the following reagents were added:

1.5 µl tRNA (1.0 µg/µl)

2.0 µl 3 M sodium acetate (pH 5.2)

60 µl 100 % ethanol

Samples were mixed and incubated on dry ice for 30 min. RNA was recovered by centrifugation at maximum speed for 30 min at 4°C. Supernatants were discarded and pellets were washed once with 60 µl of cold 75% ethanol. Residual ethanol was removed by air drying. Pellets were suspended in 20 µl of DEPC treated water. aRNA probes derived from parietal cortex total RNA of rats sacrificed at 2 AM and 2 PM contained 9724 and 13,096 cpm/µl, respectively

A.11. Hybridization with aRNA

aRNA was incubated at 84°C for 5 min and then cooled on ice. Hybridization was carried out as outlined in Detailed Methods section B.3. Each aRNA sample was added to approximately 2-3 ml of hybridization solution and hybridization was carried out overnight. Washing steps were as outlined in Detailed Methods section B.3.

B. Mini-Array Analysis of Adenosine-Related Genes

B.1. ^{32}P-Labeled cDNA Probe Synthesis

The following reagents were combined in a 1.5 ml microcentrifuge tube:

5.0 µl 5x first strand buffer

2.5 µl 100 mM DTT

1.0 µl 3′ primer mixture[a]

0.5 µl ribonuclease inhibitor

5.0 µl total RNA (1 µg/µl)

Components were mixed and incubated at 100°C for 2 min. After cooling on ice, the following were added:

0.5 µl ribonuclease inhibitor (40 U/µl)

2.0 µl dNTP mixture[b]

2.0 µl MMLV reverse transcriptase (2U/µl)

10.0 µl [α^{32}P] dATP (800 Ci/mmol)

Reactions were incubated for 60 min at 37°C followed by 7 min at 100°C. After incubations, reactions were cooled on ice and then stored at –20°C until future use. Purification of ^{32}P-labeled cDNA probes was carried out using Qiagen's QIAquick PCR purification kit and protocol[c]. After purification, approximately 48 µl of sample was left for hybridization experiments.

a – The primer mix was obtained by combining 1.0 µl of each of the 14, 3′-primers (each 10 µg/µl stock conc.).

b – For labeling with [α^{32}P] dATP the following dNTP mixture was used (5.0 mM dTTP, dGTP, dCTP, and 50 µM dATP).

c – For removing primers, nucleotides, polymerases and salts from single- or double-stranded PCR products ranging from 100 bp to 10 kb.

B.2. Preparation of cDNA Mini-Arrays

cDNA used for preparation of dot blot membranes was synthesized using first strand synthesis reactions (Detailed Methods section A.3) carried out using total RNA from whole rat brain homogenates. The resulting single-stranded cDNA was then used in 14 individual PCR reactions (Detailed Methods section A.4) each containing a set of PCR primers for one gene of interest. All PCR primers were designed to amplify 3′-end regions of their respective genes to ensure that DNA products would have a high probability of hybridizing with single-stranded cDNA probes synthesized from total RNA using an oligo (dT) primer. For PCR amplifications involving ADA, A_1, CNT1, and A_3 (see complete list of genes below) second rounds of PCR amplification were necessary to generate sufficient cDNA for blot preparation. After PCR amplification, products were analyzed by agarose gel electrophoresis (2.5 %)

with ethidium bromide staining. PCR products were purified using Qiagen's QIAquick PCR purification kit and protocol (see Detailed Methods section B.1) and once more verified by agarose gel electrophoreisis. Band intensity of each amplified DNA sample was determined and aliquots of approximately 0.1 – 0.5 μg DNA were placed on the final blot.

Dot blots were constructed on Zeta-Probe® blotting membrane (Bio-Rad) using a Bio-Dot™ apparatus (Bio-Rad) to guide dot orientation. DNA was prepared according to protocols supplied with the membrane. Briefly, DNA was prepared in a final volume of 500 μl containing 0.4 M NaOH and 10 mM EDTA and denatured by heating at 100°C for 10 min. Membranes were immersed in distilled water and then inserted into the Bio-Dot™ apparatus. Apparatus wells were rinsed with distilled water and then emptied by vacuum suction without allowing the membrane to become dry. After boiling and subsequent cooling on ice, DNA samples were applied to the wells of the Bio-Dot™ apparatus. After aspirating the samples through the membrane, wells were washed once with 500 μl of 0.4 M NaOH. Vacuum was continued until all wells were essentially dry. The membrane, once removed from the Bio-Dot™ apparatus was rinsed briefly in 2x SSC and then crosslinking of the DNA to the membrane was carried out in a Bio-Rad Gene Linker™ UV chamber on a 30 mJ setting.

Three categories of adenosine-related genes were placed on each blot: receptors (3, 5, 7, 9), enzymes (6, 8, 10) and transporters (4, 13, 15). Also included were housekeeping genes (1, 2, 11, 12) and a negative control (14). Each dot blot was designed with the following layout:

1. actin
2. S29 (ribosomal protein)
3. A_1 receptor
4. concentrative nucleoside transporter 1 (CNT1)
5. A_{2A} receptor
6. adenosine deamanise (ADA)
7. A_{2B} receptor
8. adenosine kinase (AK)
9. A_3 receptor
10. 5′-nucleotidase (5′-N)
11. α-tubulin
12. glyceraldehyde-3-phosphate dehydrogenase (GAPDH)
13. equilibrative, NBTI-sensitive nucleoside transporter (es)
14. ϕX174 DNA/*Hae* III
15. equilibrative, NBTI-insensitive nucleoside transporter (ei)

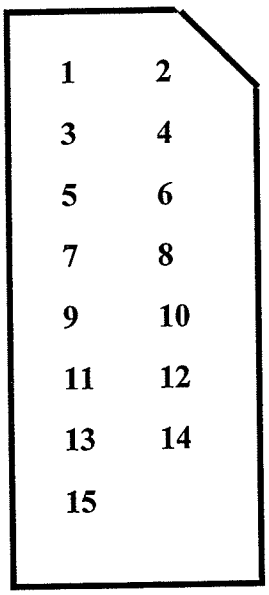

B.3. Mini-Array Hybridization

For mini-array hybridization, a solution composed of 50% formamide, 5x SSPE, 0.5% SDS, 0.5% Blotto[a], 0.2 mg/ml single-stranded salmon sperm DNA and 5% dextran sulfate was prepared from the reagents below:

15 ml 100% formamide

7.5 ml 20x SSPE

1.5 ml 10 % SDS

1.5 ml 10% Blotto

1.5 ml 4 mg/ml single-stranded salmon sperm DNA

3.0 ml 50% dextran sulfate

Arrays were pre-hybridized using 12 ml of the solution outlined above in 15 ml conical tubes at 42°C for 4 hours. Purified cDNA probes were denatured at 95°C for 5 min and then added to the hybridization tubes containing the solution outlined above to give a final hybridization volume of 2.0 ml. Hybridization was run overnight at 42°C.

Arrays were washed initially with a solution of 2x SSC and 0.5% SDS. A second set of washes was carried out with 0.1x SSC and 0.5% SDS. Membranes were exposed to BioMax Film for times ranging from 1-3 hours at room temperature. Films were analyzed by densitometry using Scion Image version 1.60 software.

a – Blocker, non-fat dry milk (BioRad, cat #: 170-6404)

C. Measurement of Gene Expression using a Commercial cDNA Array

Atlas™ rat cDNA expression arrays were obtained from Clontech. Kits included 2 identical arrays on nylon membranes each containing 588 rat cDNAs, 9 housekeeping control cDNAs as well as negative controls; each cDNA was immobilized in duplicate dots (10 ng cDNA/dot). Sufficient reagents were supplied for 10 cDNA probe synthesis reactions.

C.1. ^{32}P-Labeled cDNA Probe Synthesis[a]

For each cDNA probe synthesis, 5.0 µl of total RNA was combined with 1.0 µl of 10x CDS primer mix* in a 500 µl microcentrifuge tube. Mixtures were incubated in a PCR thermal cycler for 2 min at 70°C and then 2 min at 50°C. Immediately afterwards, 14 µl of the mixture below was added to each tube:

4.0 µl 5x reaction buffer*

2.0 µl 10x dNTP mix*

5.0 µl [α^{32}P]dATP (3000 Ci/mmol)

1.0 µl 100 mM DTT*

2.0 µl MMLV reverse transcriptase*

Reactions were mixed and incubated for 25 min at 50°C. Each reaction was terminated by adding 2.0 µl of 10x termination mix*. cDNA probes were purified using Qiagen's QIAquick PCR purification kit and protocol. Spin columns provided with the Atlas kit were not used.

* - Reagent provided with Atlas membrane kit.

a - Carried out according to protocols provided by Clontech.

C.2. Array Hybridization[a]

Atlas arrays were moistened in distilled water, placed onto a mesh backing and inserted into hybridization bottles. Pre-hybridization was carried out for approximately 2 hours in 10 ml of pre-warmed (68°C) hybridization medium (1.5 mg of sheared salmon sperm DNA[b] added to 15 ml Expresshyb* solution).

After purification using the Qiagen kit, cDNA probes were suspended in a volume of approximately 50 µl. To each purified probe sample, 5 µl of 10x denaturing solution (1 M NaOH, 10 mM EDTA) was added and mixtures were incubated at 68°C for 20 min. After incubation, 1.3 µl of C_0t-1 DNA* followed by 55 µl of 2x neutralizing solution (1 M NaH_2PO_4, pH 7.0) were added to each sample and incubation at 68°C was continued for an additional 10 min. cDNA probe samples were then combined with 5.0 ml of pre-warmed hybridization medium and added to hybridization bottles after pre-hybridization medium was discarded. Hybridization was carried out with continuous agitation (5-7 rpm) overnight at 68°C.

After discarding hybridization mixtures, membranes were washed four times (each 30 min, 100 ml) with wash solution #1 (2x SSC, 1% SDS) and twice (each 30 min, 100 ml) with wash solution #2 (0.1x SSC, 0.5% SDS). Membranes were carefully removed from hybridization bottles, peeled from mesh supports and wrapped in plastic film. Mounted on Whatman paper (3 MM Chr), membranes were exposed to BioMax x-ray film with intensifying screen for approximately 1 week at –80°C.

* - Reagent provided with Atlas membrane kit.

a - Carried out according to protocols provided by Clontech.

b – Heat denatured for 5 min at 95 – 100°C and then rapidly cooled on ice.

Final Conclusions
And
Future Directions

Conclusions and Future Directions

In this work we studied how levels of adenosine and adenine-based nucleotides in brain tissue are regulated during episodes of acute insult and in the regulation of the normal homeostatic process of sleep. Under both paradigms, we identified not only adenosine level changes but also the fluctuations in tissue energy state that gave rise to these changes. From models of acute excitotoxicity, we determined that the decline in tissue energy state and more specifically ATP levels was translated into adenosine level increases at two different rates depending on the depolarizing strength of the excitotoxic stimulus and degree of endogenous NMDA receptor activation. In our sleep deprivation studies we found that adenosine does not steadily accumulate with prolonged wakefulness, however, we did see some evidence of a small, yet consistent, depletion of ATP in several brain regions. In addition, our measurements of purine levels in different sleep-related brain regions revealed what appeared to be different tissue-specific regulatory mechanisms for controlling the balance between endogenous levels of ATP and adenosine. These tissue-specific mechanisms were especially evident when comparing the volatile shifts in the adenosine-EC relationship seen in tissues such as striatum and hippocampus with the much less responsive adenosine-EC shifts observed in cortical tissues. From these findings we concluded that "tier-1" purine regulation appeared to predominate in cortical tissues whereas in striatum and hippocampus there appeared to be the additional potential for "tier-2" purine regulation as well.

Concurrent analysis of ATP and adenosine levels begins to provide clear insight into validating the extent to which adenosine can act as an endogenous

neuroprotecticve molecule. Along with being able to accurately determine purine levels and tissue energy state, however, it is necessary to link the changes in energy state to the functional changes in the tissue induced by energy depletion. By incorporating the gene expression methods outlined in Chapter 4 into the acute excitotoxicity research described in Chapter 2, it might be possible to identify the cellular regulatory mechanisms that are activated when tissues undergo various degrees of EC depletion. This type of analysis might reveal EC threshold(s) below which destructive processes such as apoptosis and necrosis are initiated. In models of acute excitotoxicity, which represent the early onset events in stroke, EC depletion might be the initial stimulus that sets into motion the damaging cascade of events that include intracellular Ca^{2+} influx, loss of mitochondria potentials and free radical formation. If such a "destructive" EC threshold could be identified, it would provide a target to which therapeutic interventions could be directed, including those involving adenosine metabolism, which would help attenuate EC depletion under pathological conditions. Perhaps the defining factor in determining if endogenous adenosine plays a neuroprotective role is whether it can act significantly to resist the decline in EC levels during episodes of acute trauma.

Results from our sleep deprivation studies suggested that adenosine does not accumulate steadily with prolonged wakefulness. In our view, this finding does not exclude adenosine as an important regulatory molecule in sleep because adenosine levels may actually fluctuate with prolonged waking as discussed in Chapter 3. We did, however, find that ATP levels appeared to be slightly depleted with sleep deprivation in some of the brain regions studied, which is consistent with the sleep

regulatory hypotheses put forth by Bennington and Heller [14]. In future studies, it will be important to investigate purine levels in sleep deprived animals that are sacrificed when in a common behavioral state, either active or sleepy, as opposed to using a designated clock time as the study endpoint. This procedural modification would more effectively address whether a correlation exists between adenosine level changes in sleep-related regions and behavioral state. In addition, because these sleep-related studies are essentially behavioral in nature, it will be critical to continue minimizing physical stress on the animals during studies and keep animal handling as consistent as possible between investigators. In Chapter 2 we proposed that large increases in basal neuronal signaling can increase local adenosine levels, therefore, stress-inducing animal handling, particularly before tissue sampling may significantly alter the distribution of tissue purine levels established over the sleep deprivation period.

Depletion of tissue EC is arguably the first definitive step in the harmful cascade of events that follow acute brain insult. Because events such as focal ischemia result in tissue damage of varying degrees, it seems possible that the magnitude of EC depletion with a given trauma may determine the extent to which downstream, harmful mechanisms are activated. The research described in this thesis helps to set the groundwork for studies to investigate ways of helping to preserve normal balances of purinergic compounds and maintain tissue EC in conditions of acute insult such as stroke. By controlling the depletion of EC, it might be possible to attenuate the initiation of destructive mechanisms at an early stage and avoid the later-onset processes causing longer-term tissue damage. This type of strategy offers

a more thorough approach to treating brain insult compared to those that only target individual late-onset events.

Appendix

I. Purine and Protein Analyses

II. Striatal Subregion Purine Analyses

III. Linear Regression Analysis of Adenosine-Energy Charge Relationships

IV. Individual Sleep Deprivation Studies

V. Expression Profiling of Adenosine-Related Genes - Supplemental Information.

Appendix I. – Purine and Protein Analyses

A. HPLC Equipment and Chromatograms

B. Protein Analysis – Method Validation

C. Tissue Homogenization Model

I.A. HPLC Equipment and Chromatograms

Component	Adenosine Analysis	Nucleotide Analysis
Injector	Waters 712 WISP*	Waters 710B WISP
Pump	Waters Model 510	Waters M6000A
Detector	Shimadzu RF-535 Fluorescence Detector	Waters 484 Tunable Absorbance Detector
Column	Waters C_{18} μBondapak (3.9 x 150 mm)	Waters C_{18} μBondapak (3.9 x 150 mm)
Mobile phase	0.04 M KH_2PO_4, 12% methanol, pH 5.0	0.1 M KH_2PO_4, 1% methanol, pH 6.0
Flow rate	1.5 ml/min	1.0 ml/min

Table I.A.1. HPLC Equipment. Listed are the HPLC components, mobile phases and flow rates used for analysis of adenosine and nucleotides. * - Waters Intelligent Sample Processor

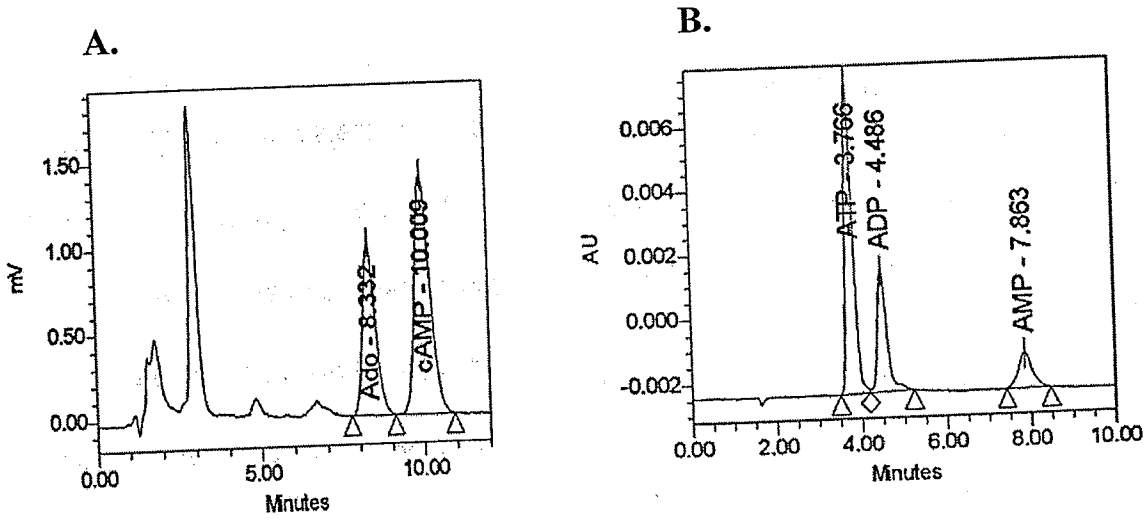

Figure I.A.1. HPLC Chromatograms. Shown are representative chromatograms from analysis of adenosine (Ado)/cAMP (A) and nucleotide (B) standards. Adenosine and cAMP peaks represent 10 pmol quantities (per 100 μl of original standard mixture) and ATP, ADP and AMP peaks represent 200, 100 and 50 pmol quantities, respectively.

I.B. Protein Analysis – Method Validation

Because we expressed our nucleotide and adenosine data in terms of nmol and pmol/mg protein, respectively, it was critical to verify the efficiency of our protein determinations to ensure that final purine levels were indeed accurate. The analysis described in Table I.B.1 was designed to determine both the efficiency of protein recovery and variations in this efficiency over the range of protein concentrations that we could expect with our standard method of tissue homogenization using 2% TCA. Our empirical data showed an average of approximately 8% protein content with wet tissue mass and an approximate mass range of 10-30 mg. From these estimates, and assuming a 1.0 ml homogenization volume, we selected the protein concentration range that was ultimately tested.

The final data shown in Figure 1.4 indicate a consistent 95% detection rate of BSA protein in the range from 1.0–3.0 mg/ml. The protein concentration values of tissue samples used in our tissue homogenization model, which are representative of protein measurements throughout all of our work, fell well within the 95% detection range. For protein analyses of $ZnSO_4$ homogenates, in cases where only tissue adenosine levels are analyzed, a minimum molar ratio of 1:3 $ZnSO_4$/NaOH is necessary to eliminate interference by $ZnSO_4$ when analyzing protein by the Bradford method.

Standard Number	Protein (mg/ml)	BSA (µl)	Water (µl)	2% TCA (µl)	Tot. Vol (µl)	0.1 M NaOH (µl)
1	0.25	15.6	184.4	800	1000	100
2	0.50	31.3	168.7	800	1000	200
3	0.75	46.9	153.1	800	1000	300
4	1.00	62.5	137.5	800	1000	400
5	1.25	78.1	121.9	800	1000	500
6	1.50	93.8	106.2	800	1000	700
7	1.75	109.4	90.6	800	1000	700
8	2.00	125.0	75.0	800	1000	800
9	2.25	140.4	59.4	800	1000	800
10	2.50	156.3	43.7	800	1000	900
11	2.75	171.9	28.1	800	1000	900
12	3.00	187.5	12.5	800	1000	1000

Table I.B.1. Preparation of Standards to Determine Protein Measurement Efficiency. BSA protein (16 mg/ml, prepared in water), was combined with water to produce 12, 200 µl protein standards. After each standard was combined with 2% TCA (1.6% final) to give a final volume of 1.0 ml, they were stored on ice for 20 min to facilitate protein precipitation. Protein was collected by centrifugation at 13,000 x g for 20 min at 4°C. After discarding supernatants, pellets were suspended in 0.1 M NaOH (see table for volumes) and incubated at 80°C for 15 min with periodic vortexing to facilitate dissolution of the pellets. Following incubation, samples were centrifuged at room temperature for 2 min at 13,000 x g and supernatants were then diluted 1:10 with 0.1 M NaOH for spectroscopic analysis. For further protein analysis details see the Methods section in Chapter 1.

I.C. Tissue Homogenization Model

This model was designed from empirical data collected from 260 rat brain samples. Using these data, projected homogenization volumes and dilution factors were determined that would maintain purine and protein analyses within detectable linear ranges given that both determinations were ultimately carried out spectroscopically. A sample of the full-form tissue homogenization model is shown in Figure I.C.1.

The first 12 columns contain empirical data. Columns 1-3 describe the type of tissue region (striatal subregions), the experimental treatment carried out on that tissue and the wet mass (mg) of the dissected tissue. The volume of 2% TCA (ml) used to homogenize the tissue sample is listed in column 4 and the tissue concentration (mg/ml) of the resulting homogenate is shown in column 5. Listed in columns 6, 7, 8, and 10 are pmol measurements of ATP, ADP, AMP and adenosine, respectively. The three columns of nucleotide data, showing raw values determined from peak areas and calibration curves resulting from HPLC analysis of a 10 µl injection were not adjusted for protein content. Listed in column 9 is the total sum of nucleotides ATP, ADP and AMP (Σ_{nuc}, pmol). The data in columns 11 and 12 came from the protein analysis of each sample. Immediately following tissue homogenization, 50 µl of homogenate was taken for protein analysis and stored on ice. These samples were then centrifuged and pellets were digested in 0.1 M NaOH. Because the protein contained in each tube came from 50 µl of original homogenate, the pellet, after removal of the TCA supernatant, was dissolved in a multiple of 50 µl volume of 0.1 M NaOH giving a dilution factor that was then used for final

calculation of protein concentration. In column 11 for example, a listing of 4 indicates that the protein pellet resulting from the original 50 µl of TCA homogenate was suspended in 200 µl of NaOH. Column 12 lists the protein content (µg) of a 10 µl aliquot of the protein sample in NaOH before accounting for dilution. With these data, the protein concentration (mg/ml) in the original TCA homogenate (col. 13) was calculated using the equation below:

$$\text{Protein (mg/ml)} = (\text{NaOH dil. factor}) \times \frac{(\mu g/10\ \mu l\ \text{value})}{10}$$

or in terms of column labels:

$$C_{13} = C_{11} \times \frac{C_{12}}{10}$$

One of the fundamental objectives of the model was to establish a criterion, based on wet tissue mass, to determine an appropriate homogenization volume that would result in adenosine and nucleotide values that would fall within detectable ranges. Because of the fluctuating nature of the single parameters of ATP, ADP, AMP or adenosine that occur with experimental treatments, we were unable to base the model on any one of these variables. Because the sum of ATP, ADP and AMP, however, does not change to any significant extent under our experimental conditions and time frames, we chose to use the Σ_{nuc} value to guide our determination of homogenization volume. The value of $\Sigma_{nuc} = 300$ was chosen as a target value because it would generally result from ATP, ADP and AMP values (pmol) of approximately 200, 100 and 25, respectively. These predicted values fell well within the linear detection range of the HPLC equipment. Using $\Sigma_{nuc} = 300$ as a target value,

column 14, the TCA homogenization volume (ml) required to yield a Σ_{nuc} value of 300 was calculated with the following equation:

$$\text{calc vol} = (\text{orig TCA vol.}) \times \frac{(\Sigma_{nuc})}{300}$$

Column 15 shows the difference between the calculated volume and the homogentation volume used experimentally. Columns 16, 17, 18, and 19 are the predicted values (pmol) of ATP, ADP, AMP, and adenosine, respectively if the calculated homogenization volume was used originally. These values were obtained by multiplying the corresponding values in columns 6, 7, 8, and 10 (empirical data) by the factor: (orig.vol./calc.vol.). In the same fashion, column 20, the new μg protein/10 μl value was determined by multiplying the data in column 12 by the factor: (orig.vol./calc.vol.).

Because it would be laborious and impractical to homogenize each sample in its own specific volume as dictated by the model, we assigned a single homogenization volume (column 21) for all tissue samples falling within a given range of tissue mass. The first volume, 575 μl, was chosen because that was the smallest volume that would provide enough homogenate to accommodate the nucleotide, adenosine and protein analyses. Given the designated homogenization volume, the predicted pmol values for ATP, ADP, AMP and adenosine were calculated (col.22-25) using the data in columns 6, 7, 8 and 10 and the dilution factor: (orig. TCA vol./desig. TCA vol.). Mass range cutoffs for designated homogenization

volumes were estimated where Σ_{nuc} (col. 26, pmol) values, calculated from columns 22-24, began to approach and exceed 300 pmol.

In addition to predicting a homogenization volume that would yield appropriate values from the purine analysis, it was necessary to include in the model criteria to predict the quantity of NaOH necessary to dissolve pellets for protein analysis. The NaOH dissolution volume necessary was dependent on the TCA quantity used to homogenize the original tissue sample and would determine whether samples were too concentrated or dilute to provide readings within a linear range. Using BSA standards and carrying out protein analyses in the same fashion as that used with tissue samples, we determined the linear range of our protein analysis and chose a value of 1.75 µg/10 µl as a target value for determining NaOH volumes. The value in column 27, analogous to that in column 11, represents the NaOH dilution factor necessary to yield a value of 1.75 µg/10 µl if the new TCA homogenization volume was used (col. 14). Also taken into account in this calculation were the original protein (col. 12), initial TCA homogenization volume (col. 4), and initial NaOH dilution (col.11) values. The equation used is outlined below:

$$\text{dil (col. 27)} = \frac{(\text{orig. TCA vol.} \times \text{orig. NaOH dil.}) \times (\text{orig. TCA vol./calc. TCA vol.})}{1.75}$$

in terms of columns:

$$C_{27} = \frac{(C_4 \times C_{11}) \times (C_3 / C_{14})}{1.75}$$

As with the TCA homogenization volume, it would be cumbersome to dilute each individual sample to obtain an exact protein value of 1.75 µg/10 µl. Therefore, we assigned a single NaOH dilution factor for sample masses that fell into designated

ranges. The range boundaries were determined by the magnitude of the predicted protein value in column 29. As values generally began to exceed 1.75 with increasing tissue mass, the designated NaOH dilution factor was increased accordingly.

The working form of the tissue homogenization model is shown in Figure 1.6. For each TCA homogenization volume, mean and standard deviation (SD) values were calculated from the projected ATP, ADP, AMP, adenosine and protein values. These statistics suggest that the calculations in model have indeed predicted TCA homogenization volumes and NaOH dilution factors that would provide raw data readings within the linear range of both purine and protein analyses.

A.

1	2	3	4	5	6	7	8	9	10	11	12	13	14	15
Region	Treat	Mass	TCA	Tis (mg/ml)	ATP	ADP	AMP	Σ_{nuc}	Ado	dil	µg/10µL	Pro (mg/ml)	calc vol	diff
2~4	Ctx.Stim.	4.70	0.750	6.27	54.7	28.9	15.0	98.6	14.1	4	1.30	0.52	0.247	-0.503
4~4	NMDA	5.10	0.700	7.29	90.3	41.1	17.8	149.2	7.0	4	1.63	0.65	0.348	-0.352
3~1	Glu	5.30	0.700	7.57	101.9	31.3	9.1	142.3	3.0	4	1.34	0.54	0.332	-0.368
2~6	aCSF	5.80	0.700	8.29	151.8	34.0	11.4	197.2	30.7	4	1.64	0.66	0.460	-0.240
9~1	no-vol	5.90	0.750	7.87	96.6	51.1	21.1	168.8	18.3	6	0.93	0.56	0.422	-0.328
2~6	Ctx.Stim.	6.10	0.750	8.13	101.6	56.1	22.3	180.0	15.5	4	1.88	0.75	0.450	-0.300

B.

1	3	16	17	18	19	20	21	22	23	24	25	26	27	28	29
Region	Mass	ATP	ADP	AMP	Ado	µg/10µl	des vol	ATP	ADP	AMP	Ado	Σ_{nuc}	dil	des dil	µg/10µl
2~4	4.70	166.3	88.0	45.7	42.9	3.96	0.575	71.3	37.8	19.6	18.4	128.6	4	5	1.36
4~4	5.10	181.7	82.6	35.7	14.1	3.28	0.575	110.0	50.0	21.6	8.5	181.6	5	5	1.59
3~1	5.30	214.8	66.0	19.2	6.2	2.83	0.575	124.1	38.1	11.1	3.6	173.3	4	5	1.31
2~6	5.80	230.9	51.8	17.3	46.7	2.49	0.575	184.7	41.4	13.9	37.4	240.1	5	5	1.60
9~1	5.90	171.8	90.8	37.4	32.5	1.65	0.575	126.0	66.6	27.5	23.8	220.1	4	5	1.45
2~6	6.10	169.3	93.4	37.2	25.8	3.13	0.575	132.5	73.1	29.1	20.2	234.7	6	5	1.96

Figure I.C.1. Tissue Homogenization Model Derivation. Shown are 6 representative data points of the 260 used in formulating the tissue homogenization model. The columns shown in B are a continuation of the table that begins in A. Columns 1 and 2 indicate tissue region and the experimental treatment carried out on that tissue, respectively. Shown in columns 3-13 are empirical data. The purine values (pmol) in these columns are not normalized for protein content. Values in the remaining columns are calculated ones derived from set target values, dilution factors and the empirical data. For complete details of the calculations used in this model, refer to the text in this appendix section.

Appendix II – Striatal Subregion Purine Analyses

A. Basal Purine Levels

B. No-Volume Injections

C. Tris Vehicle Injections

D. Salt Solution Injections

E. aCSF Vehicle Injections

F. Glutamate Injections (aCSF vehicle)

G. Glutamate Injections (with MK-801 ip)

H. NMDA Injections (Tris vehicle)

I. NMDA Injections (aCSF vehicle)

J. Cortex Stimulation

II.A. Basal Purine Levels

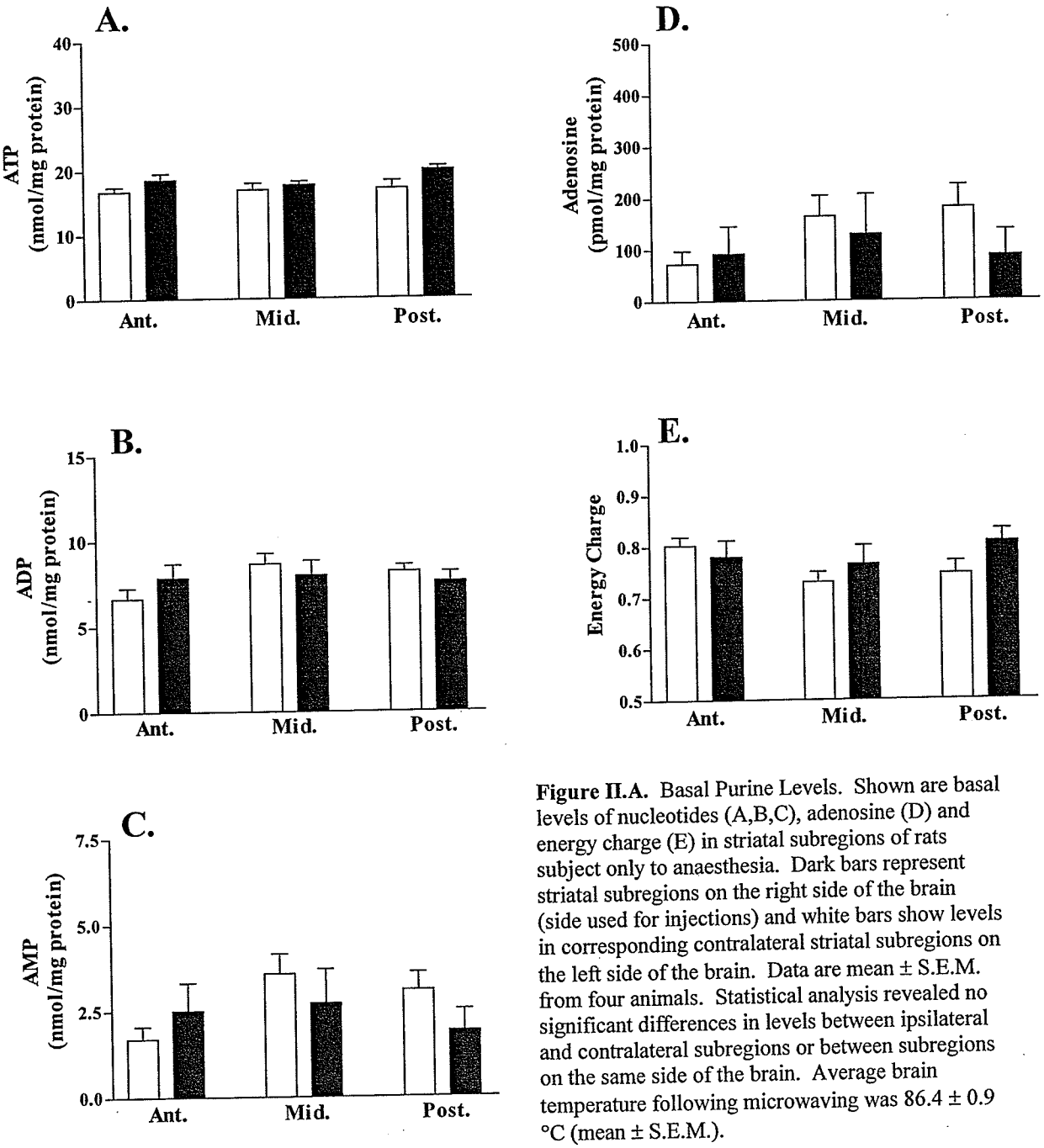

Figure II.A. Basal Purine Levels. Shown are basal levels of nucleotides (A,B,C), adenosine (D) and energy charge (E) in striatal subregions of rats subject only to anaesthesia. Dark bars represent striatal subregions on the right side of the brain (side used for injections) and white bars show levels in corresponding contralateral striatal subregions on the left side of the brain. Data are mean ± S.E.M. from four animals. Statistical analysis revealed no significant differences in levels between ipsilateral and contralateral subregions or between subregions on the same side of the brain. Average brain temperature following microwaving was 86.4 ± 0.9 °C (mean ± S.E.M.).

II.B. No-Volume Injections

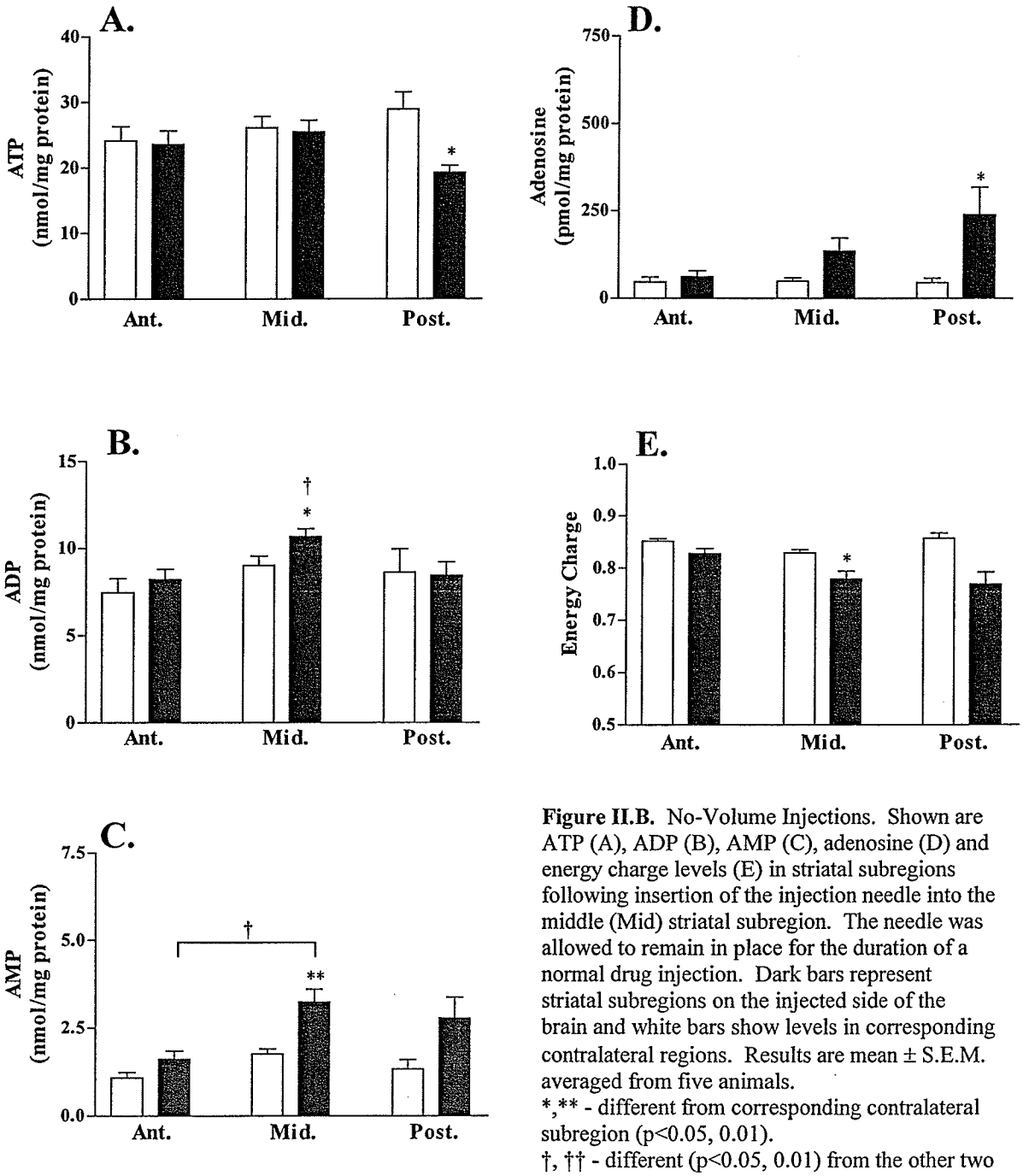

Figure II.B. No-Volume Injections. Shown are ATP (A), ADP (B), AMP (C), adenosine (D) and energy charge levels (E) in striatal subregions following insertion of the injection needle into the middle (Mid) striatal subregion. The needle was allowed to remain in place for the duration of a normal drug injection. Dark bars represent striatal subregions on the injected side of the brain and white bars show levels in corresponding contralateral regions. Results are mean ± S.E.M. averaged from five animals.
*,** - different from corresponding contralateral subregion ($p<0.05$, 0.01).
†, †† - different ($p<0.05$, 0.01) from the other two subregions of the same side of the brain or as otherwise annotated.

II.C. Tris Vehicle Injections

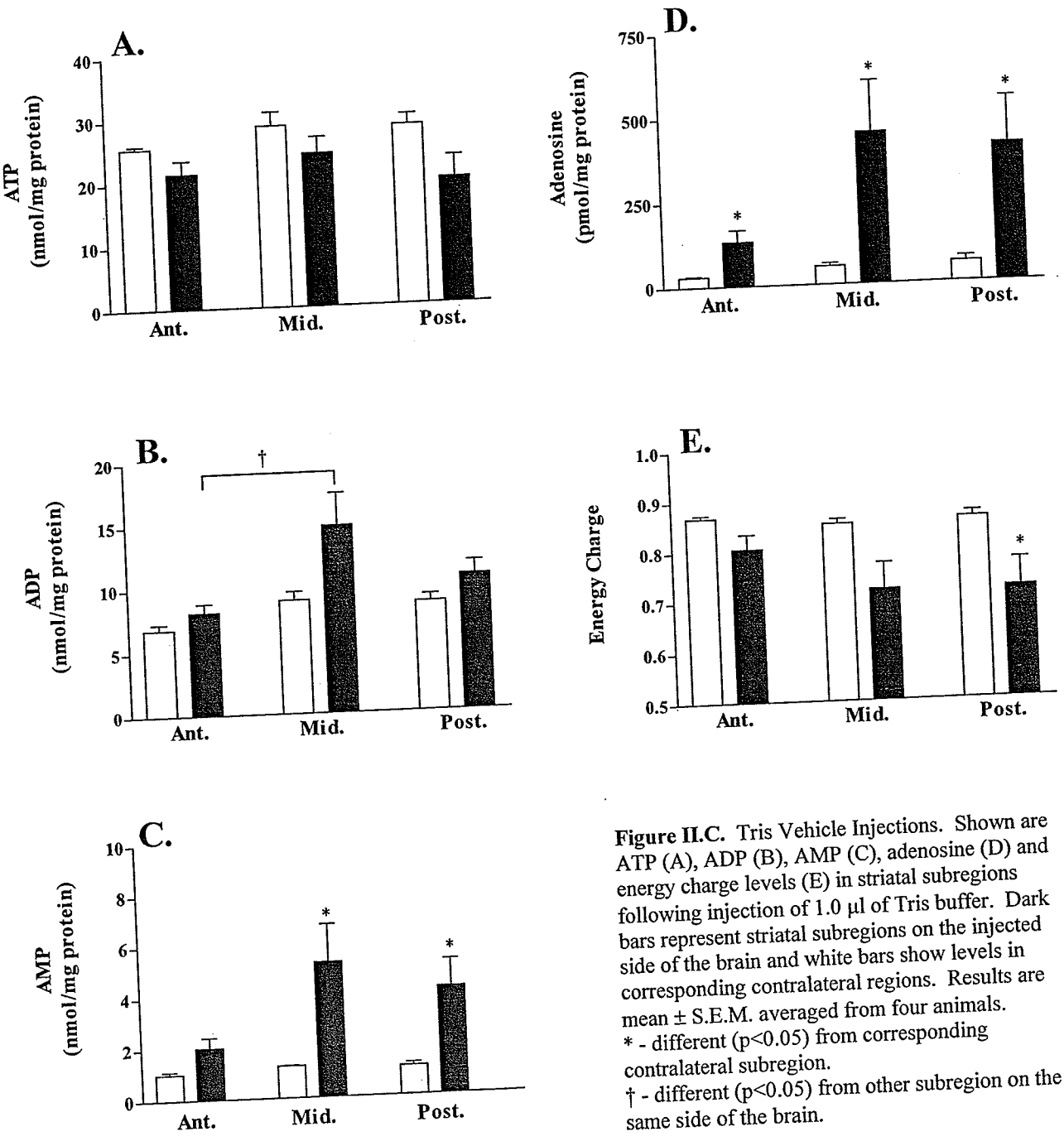

Figure II.C. Tris Vehicle Injections. Shown are ATP (A), ADP (B), AMP (C), adenosine (D) and energy charge levels (E) in striatal subregions following injection of 1.0 µl of Tris buffer. Dark bars represent striatal subregions on the injected side of the brain and white bars show levels in corresponding contralateral regions. Results are mean ± S.E.M. averaged from four animals.
* - different ($p<0.05$) from corresponding contralateral subregion.
† - different ($p<0.05$) from other subregion on the same side of the brain.

II.D. Salt Solution Injections

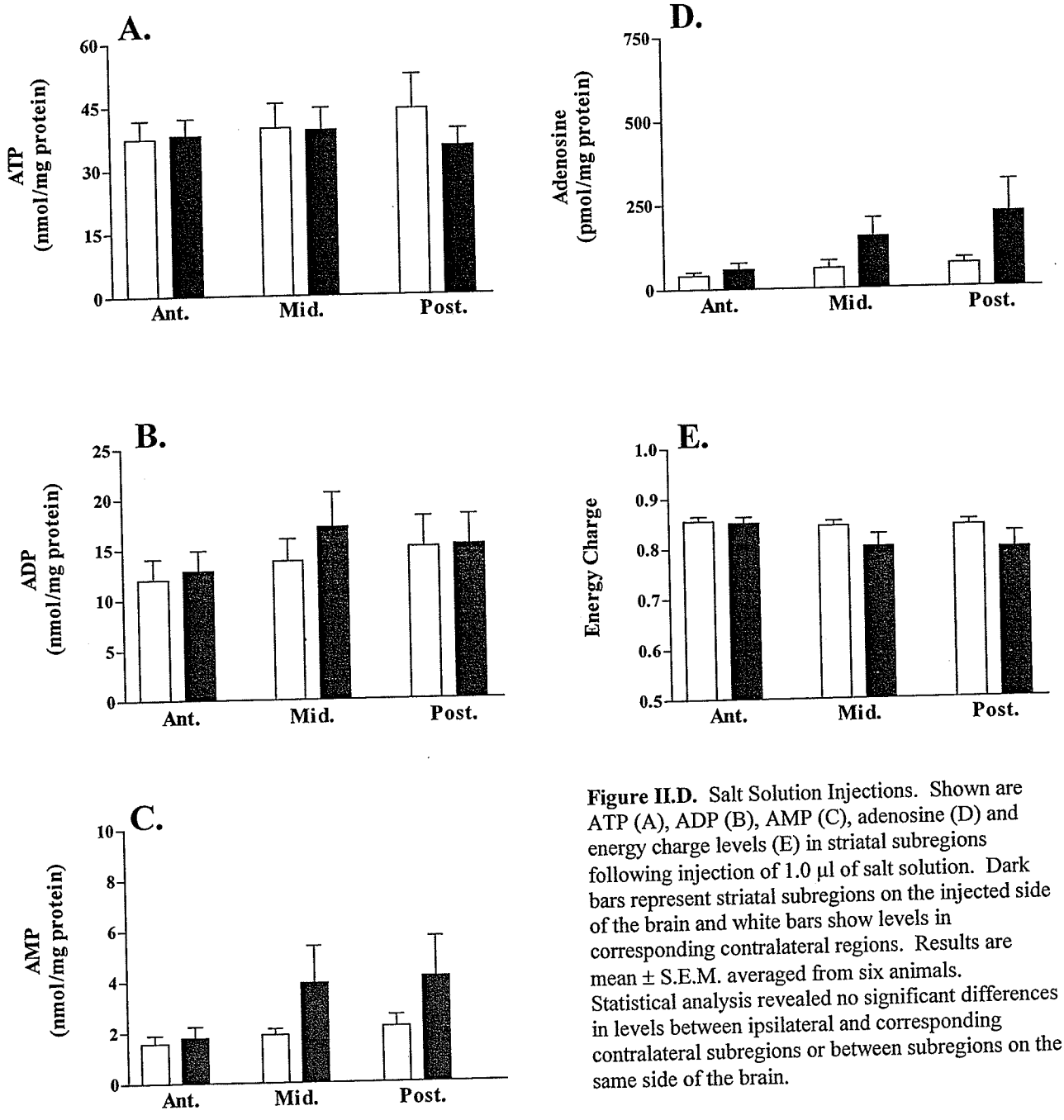

Figure II.D. Salt Solution Injections. Shown are ATP (A), ADP (B), AMP (C), adenosine (D) and energy charge levels (E) in striatal subregions following injection of 1.0 µl of salt solution. Dark bars represent striatal subregions on the injected side of the brain and white bars show levels in corresponding contralateral regions. Results are mean ± S.E.M. averaged from six animals. Statistical analysis revealed no significant differences in levels between ipsilateral and corresponding contralateral subregions or between subregions on the same side of the brain.

II.E. aCSF Vehicle Injections

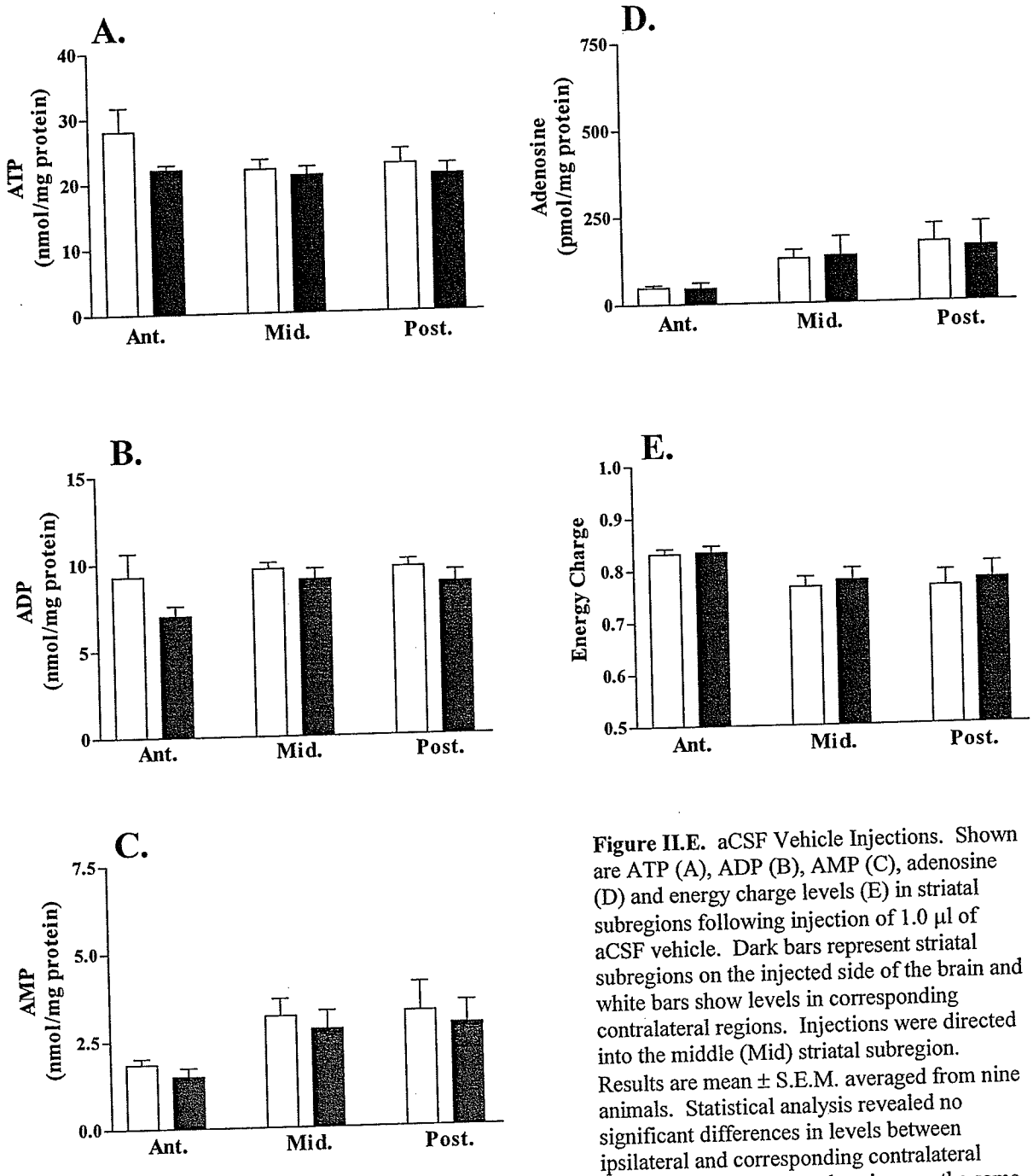

Figure II.E. aCSF Vehicle Injections. Shown are ATP (A), ADP (B), AMP (C), adenosine (D) and energy charge levels (E) in striatal subregions following injection of 1.0 μl of aCSF vehicle. Dark bars represent striatal subregions on the injected side of the brain and white bars show levels in corresponding contralateral regions. Injections were directed into the middle (Mid) striatal subregion. Results are mean ± S.E.M. averaged from nine animals. Statistical analysis revealed no significant differences in levels between ipsilateral and corresponding contralateral subregions or between subregions on the same side of the brain.

II.F. Glutamate Injections (aCSF Vehicle)

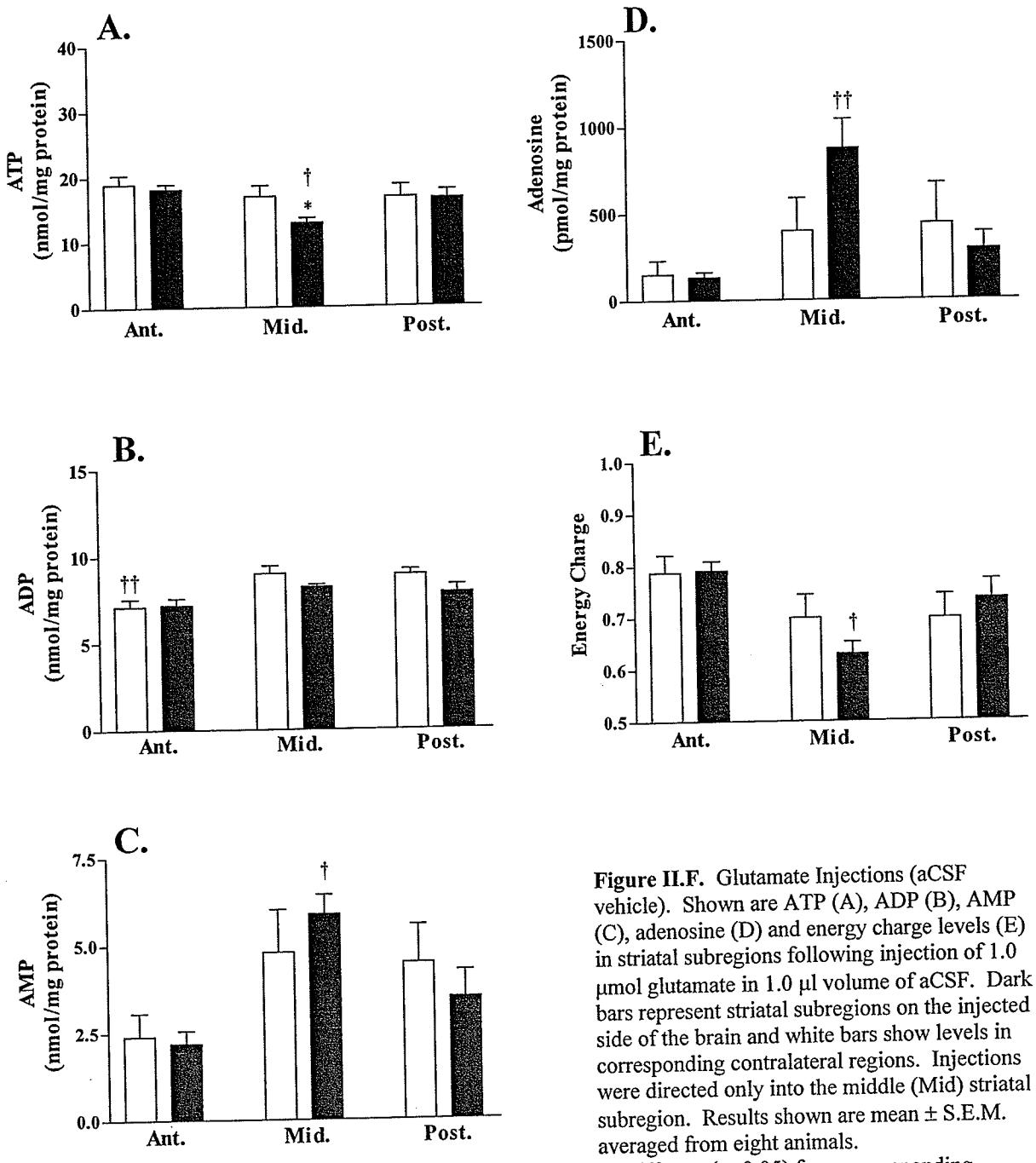

Figure II.F. Glutamate Injections (aCSF vehicle). Shown are ATP (A), ADP (B), AMP (C), adenosine (D) and energy charge levels (E) in striatal subregions following injection of 1.0 μmol glutamate in 1.0 μl volume of aCSF. Dark bars represent striatal subregions on the injected side of the brain and white bars show levels in corresponding contralateral regions. Injections were directed only into the middle (Mid) striatal subregion. Results shown are mean ± S.E.M. averaged from eight animals.
* - different ($p<0.05$) from corresponding contralateral region.
†, †† - different ($p<0.05$, 0.01) from the other two subregions of the same side of the brain.

II.G. Glutamate Injections (with MK-801 ip)

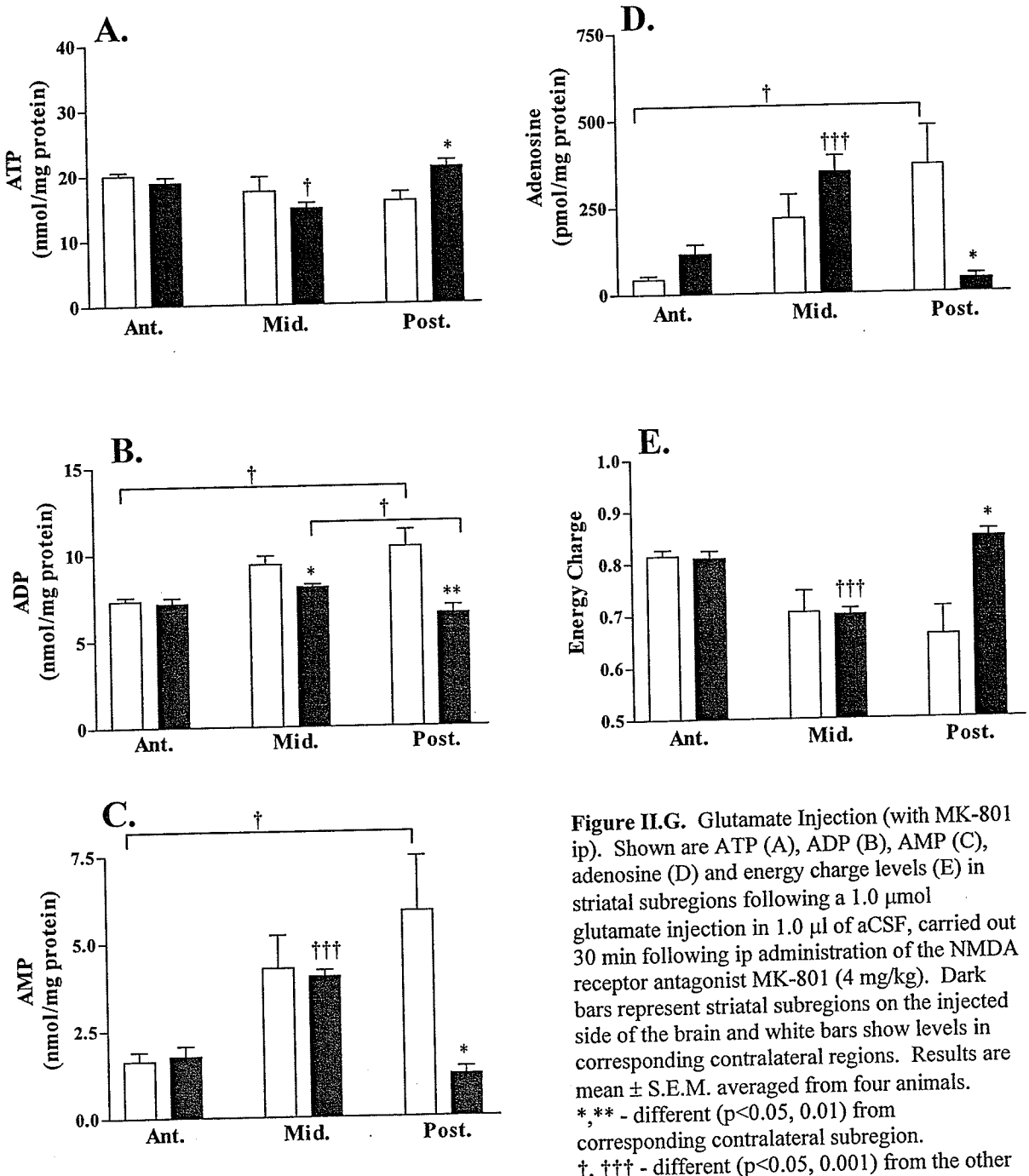

Figure II.G. Glutamate Injection (with MK-801 ip). Shown are ATP (A), ADP (B), AMP (C), adenosine (D) and energy charge levels (E) in striatal subregions following a 1.0 μmol glutamate injection in 1.0 μl of aCSF, carried out 30 min following ip administration of the NMDA receptor antagonist MK-801 (4 mg/kg). Dark bars represent striatal subregions on the injected side of the brain and white bars show levels in corresponding contralateral regions. Results are mean ± S.E.M. averaged from four animals.
*,** - different ($p<0.05$, 0.01) from corresponding contralateral subregion.
†, ††† - different ($p<0.05$, 0.001) from the other two subregions of the same side of the brain or as otherwise annotated.

II.H. NMDA Injections (Tris vehicle)

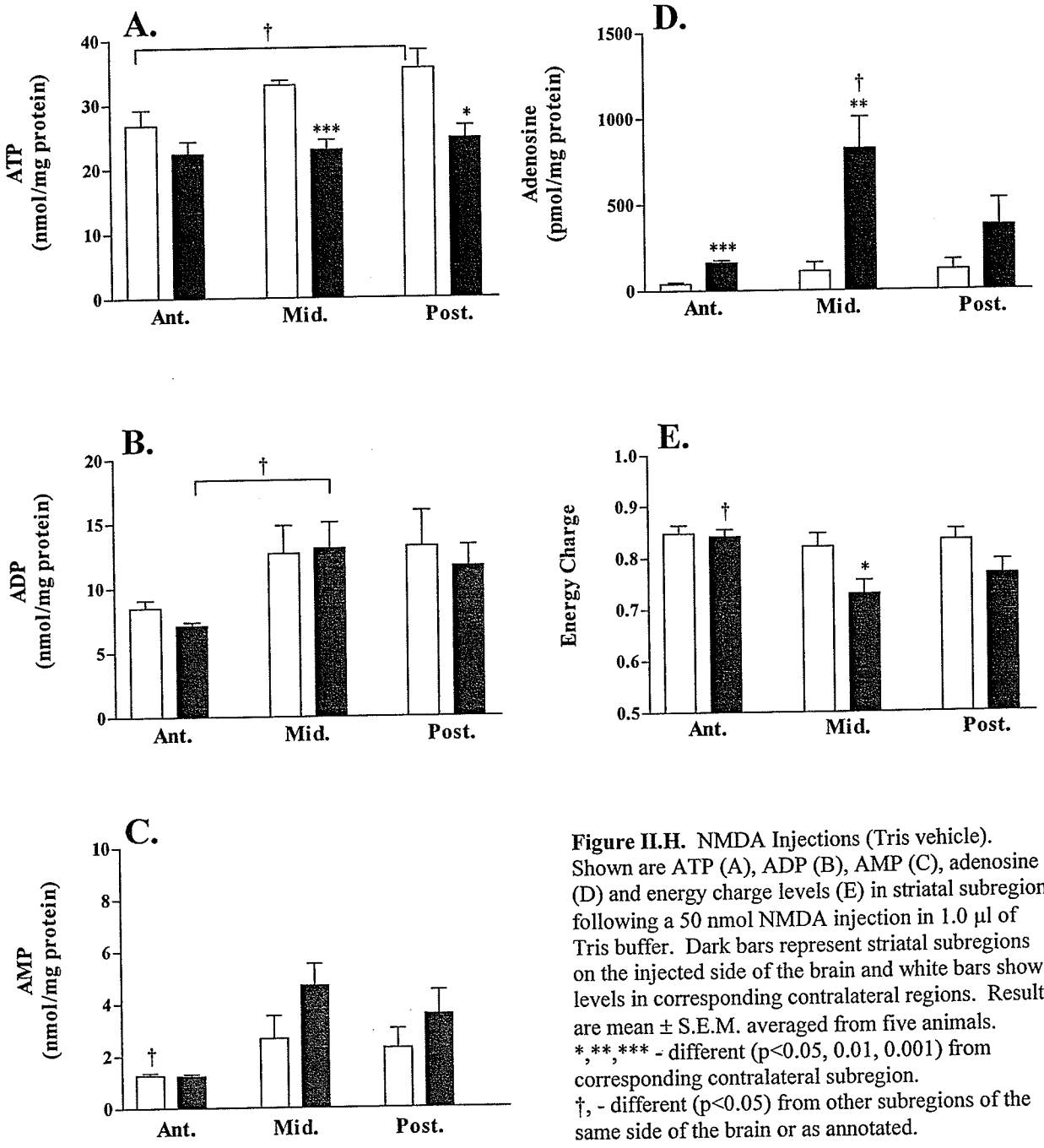

Figure II.H. NMDA Injections (Tris vehicle). Shown are ATP (A), ADP (B), AMP (C), adenosine (D) and energy charge levels (E) in striatal subregions following a 50 nmol NMDA injection in 1.0 µl of Tris buffer. Dark bars represent striatal subregions on the injected side of the brain and white bars show levels in corresponding contralateral regions. Results are mean ± S.E.M. averaged from five animals.
*,**,*** - different ($p<0.05$, 0.01, 0.001) from corresponding contralateral subregion.
†, - different ($p<0.05$) from other subregions of the same side of the brain or as annotated.

II.I. NMDA Injections (aCSF vehicle)

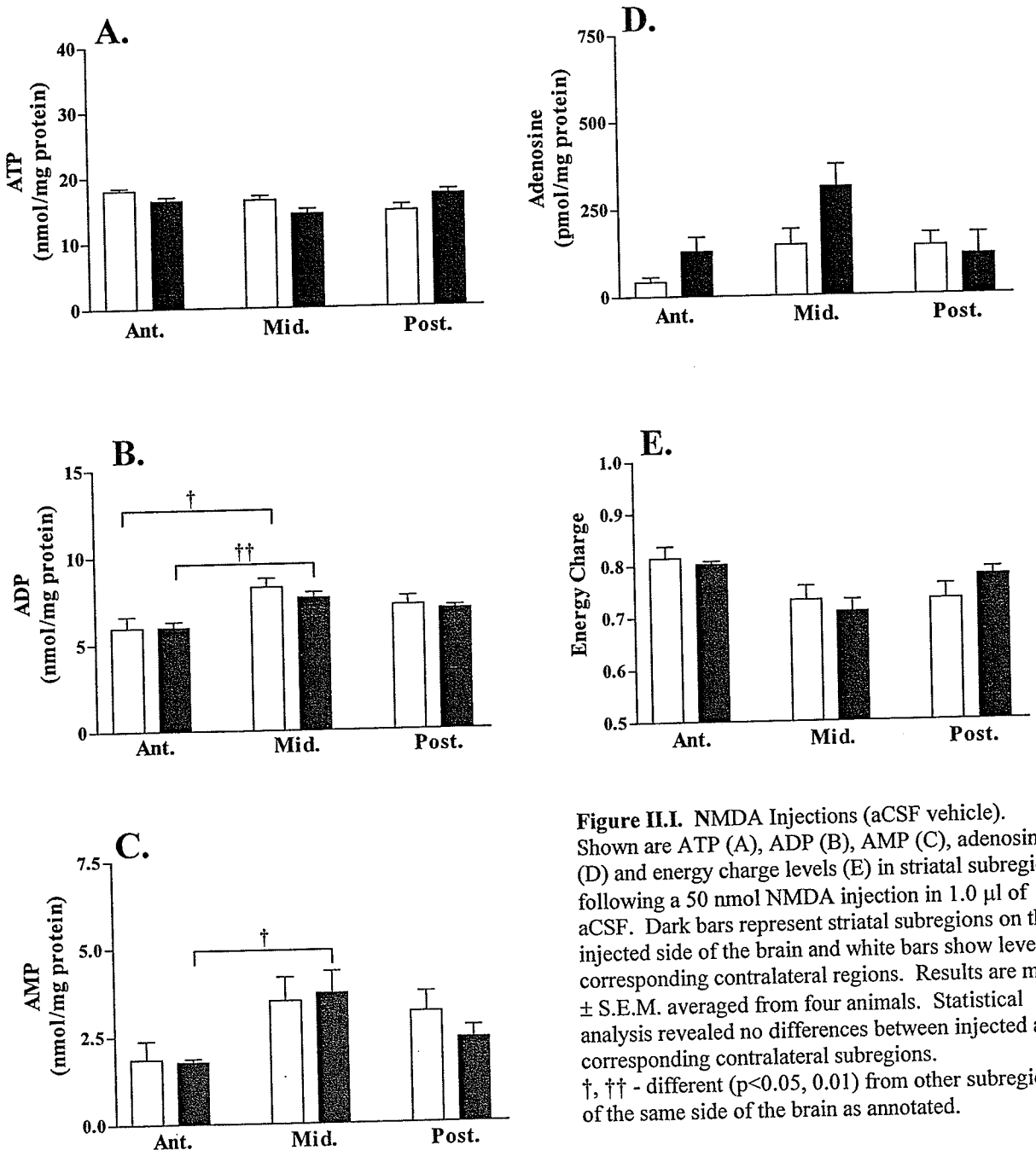

Figure II.I. NMDA Injections (aCSF vehicle). Shown are ATP (A), ADP (B), AMP (C), adenosine (D) and energy charge levels (E) in striatal subregions following a 50 nmol NMDA injection in 1.0 µl of aCSF. Dark bars represent striatal subregions on the injected side of the brain and white bars show levels in corresponding contralateral regions. Results are mean ± S.E.M. averaged from four animals. Statistical analysis revealed no differences between injected and corresponding contralateral subregions.
†, †† - different ($p<0.05$, 0.01) from other subregions of the same side of the brain as annotated.

II.J. Cortex Stimulation

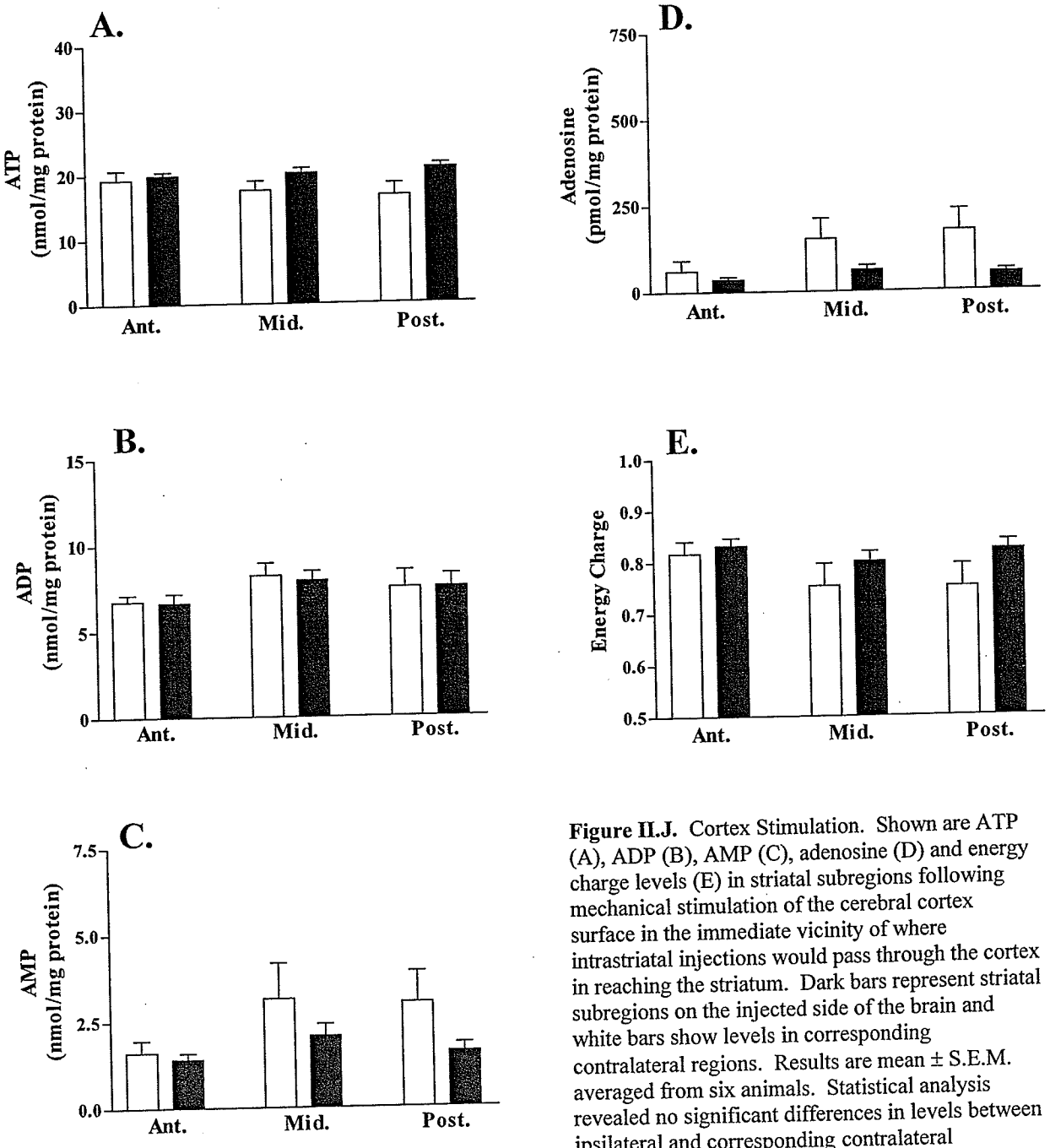

Figure II.J. Cortex Stimulation. Shown are ATP (A), ADP (B), AMP (C), adenosine (D) and energy charge levels (E) in striatal subregions following mechanical stimulation of the cerebral cortex surface in the immediate vicinity of where intrastriatal injections would pass through the cortex in reaching the striatum. Dark bars represent striatal subregions on the injected side of the brain and white bars show levels in corresponding contralateral regions. Results are mean ± S.E.M. averaged from six animals. Statistical analysis revealed no significant differences in levels between ipsilateral and corresponding contralateral subregions or between subregions on the same side of the brain.

Appendix III – Linear Regression Analyses of Adenosine – Energy Charge Relationships

A. Adenosine – EC Linear Regression #1

B. Adenosine – EC Linear Regression #2

III.A. Adenosine-EC Linear Regression #1

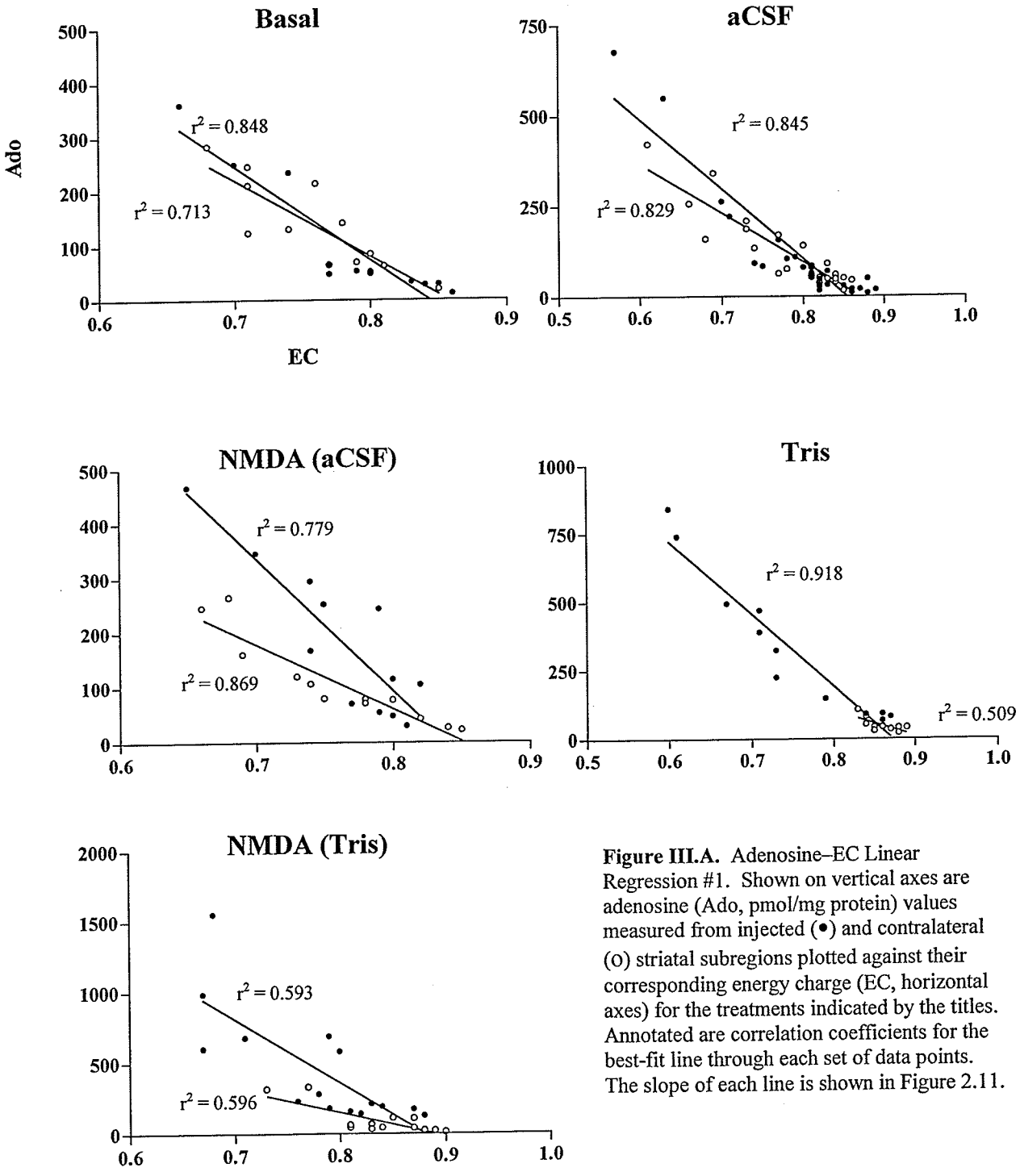

Figure III.A. Adenosine–EC Linear Regression #1. Shown on vertical axes are adenosine (Ado, pmol/mg protein) values measured from injected (•) and contralateral (o) striatal subregions plotted against their corresponding energy charge (EC, horizontal axes) for the treatments indicated by the titles. Annotated are correlation coefficients for the best-fit line through each set of data points. The slope of each line is shown in Figure 2.11.

III.B. Adenosine-EC Linear Regression #2

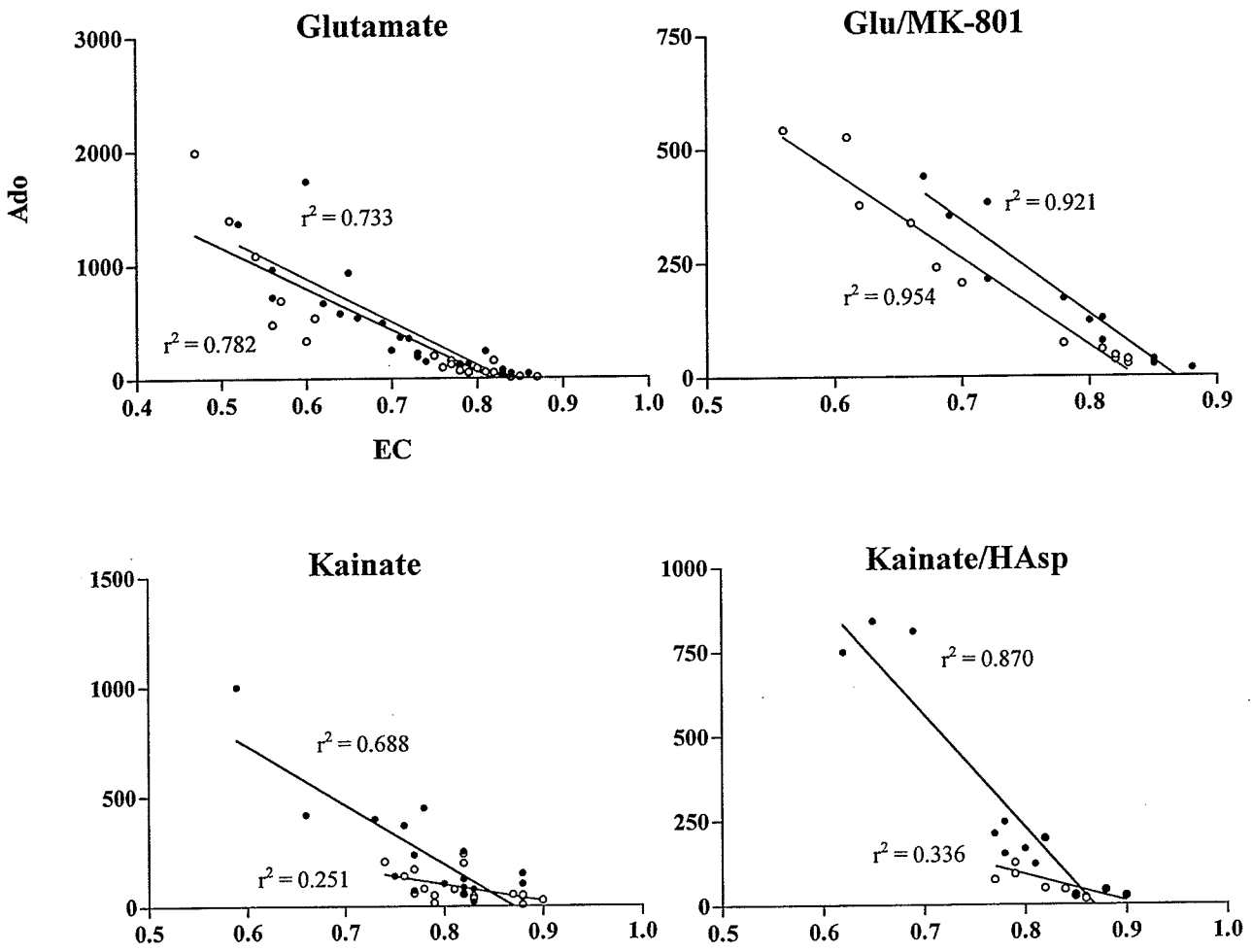

Figure III.B. Adenosine–EC Linear Regression #2. Shown on vertical axes are adenosine (Ado, pmol/mg protein) values measured from injected (•) and contralateral (o) striatal subregions plotted against their corresponding energy charge (EC, horizontal axes) for the treatments indicated by the titles. Annotated are correlation coefficients for the best-fit line through each set of data points. The slope of each line is shown in Figure 2.11.

Appendix IV – Individual Sleep Deprivation Studies

A. 24h Sleep Deprivation - Study #1

B. 24h Sleep Deprivation - Study #2

C. 24h Sleep Deprivation - Study #3

D. 12h Sleep Deprivation - Study #1

E. 12h Sleep Deprivation - Study #2

IV.A. 24h Sleep Deprivation - Study #1

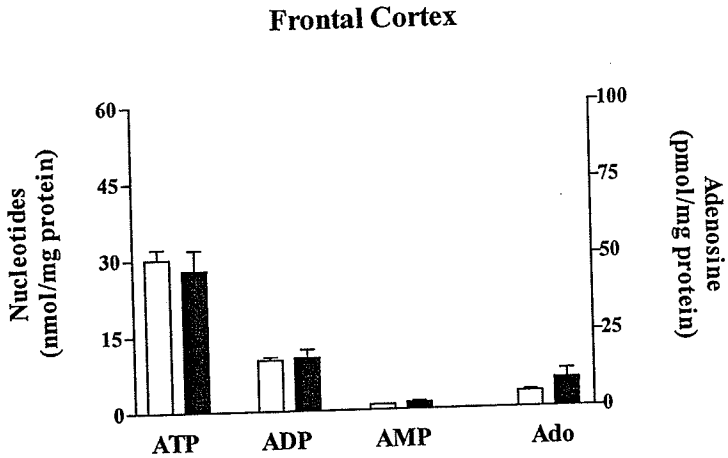

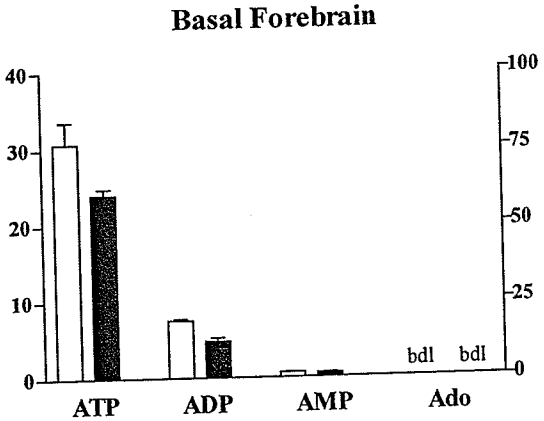

Figure IV.A. 24h Sleep Deprivation – Study #1. Shown are purine levels (mean ± S.E.M.) from control (n=4, light bars) and sleep deprived (n=4, dark bars) rats. All axes are presented in the same units as annotated in the frontal cortex figure. In some cases in this study adenosine levels were below detectable levels (bdl) given the analytical methods used at the time.

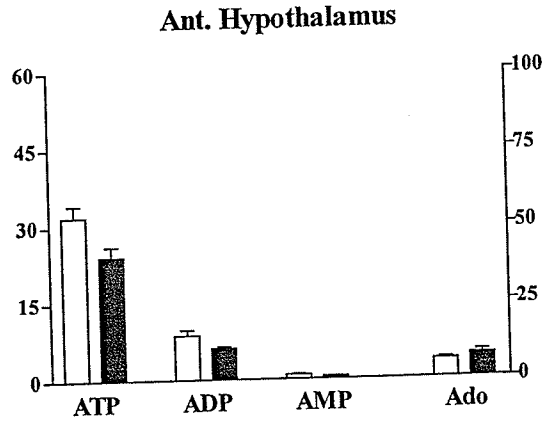

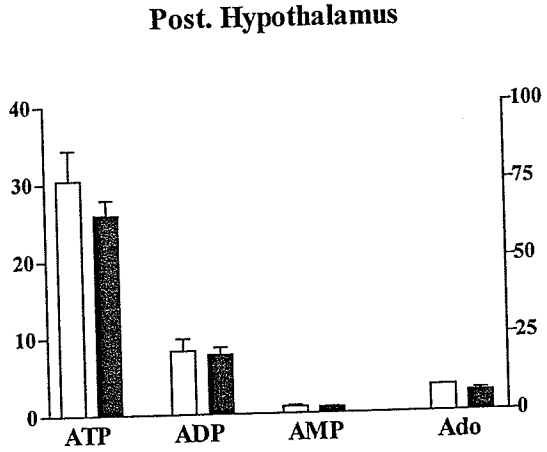

IV.B. 24h Sleep Deprivation - Study #2

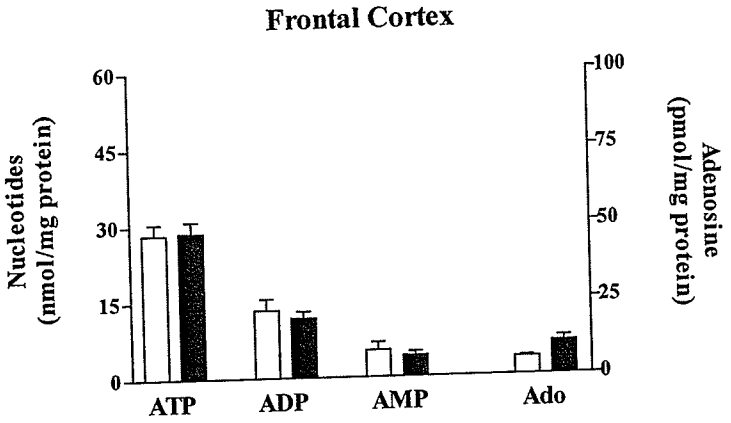

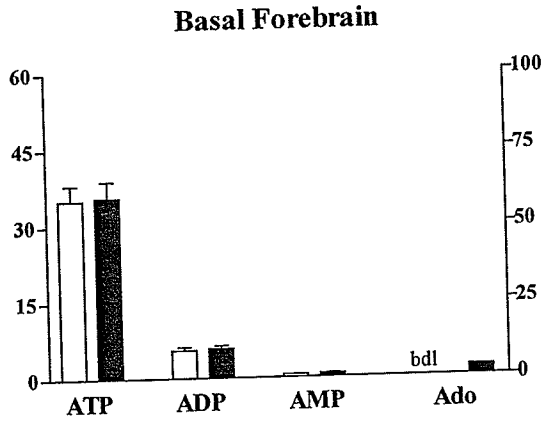

Figure IV.B. 24h Sleep Deprivation – Study #2. Shown are purine levels (mean ± S.E.M.) from control (n=8, light bars) and sleep deprived (n=8, dark bars) rats. All axes are presented in the same units as annotated in the frontal cortex figure. In some cases in this study adenosine levels were below detectable levels (bdl) given the analytical methods used at the time.

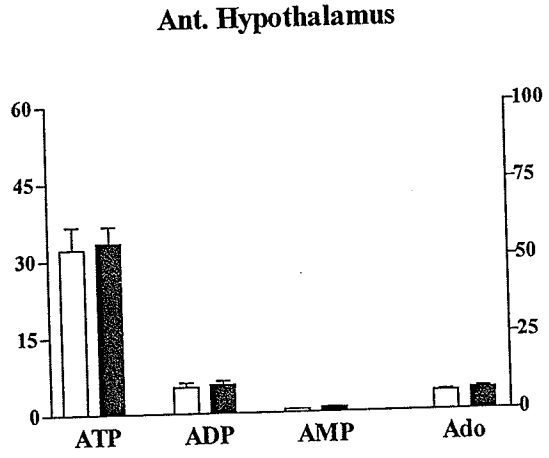

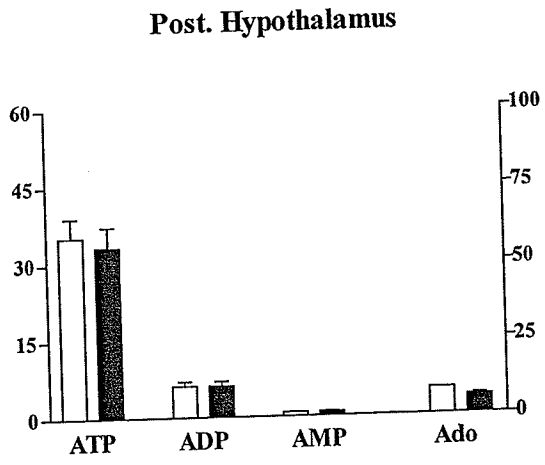

IV.C. 24h Sleep Deprivation - Study #3

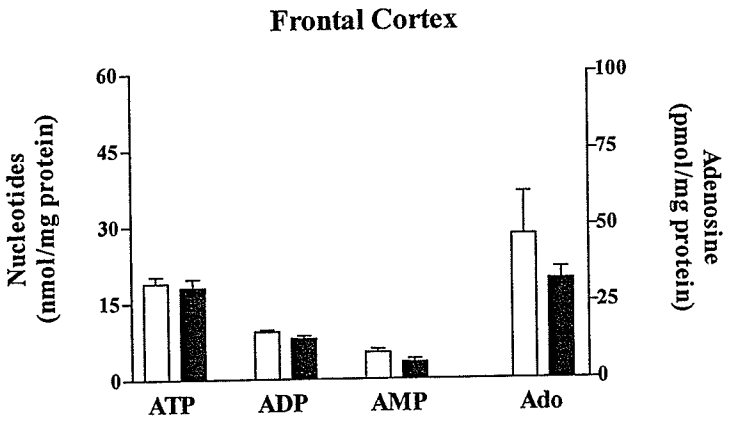

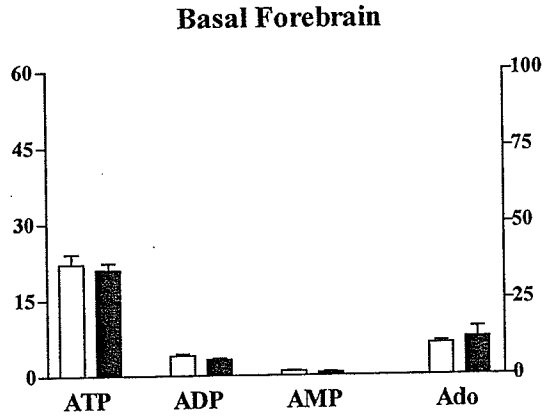

Figure IV.C. 24h Sleep Deprivation – Study #3. Shown are purine levels (mean ± S.E.M.) from control (n=5, light bars) and sleep deprived (n=5, dark bars) rats. All axes are presented in the same units as annotated in the frontal cortex figure. The modified analytical techniques used in this study allowed us to quantify all adenosine levels.

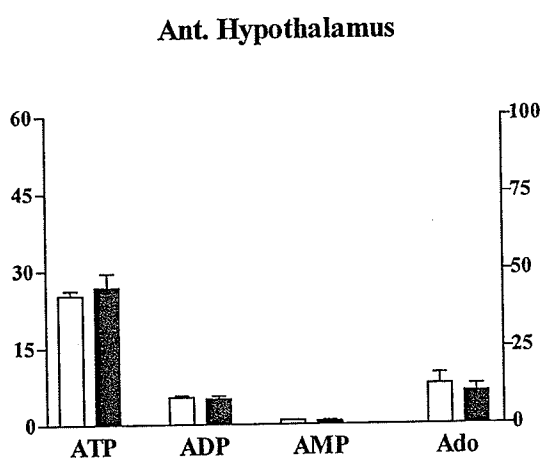

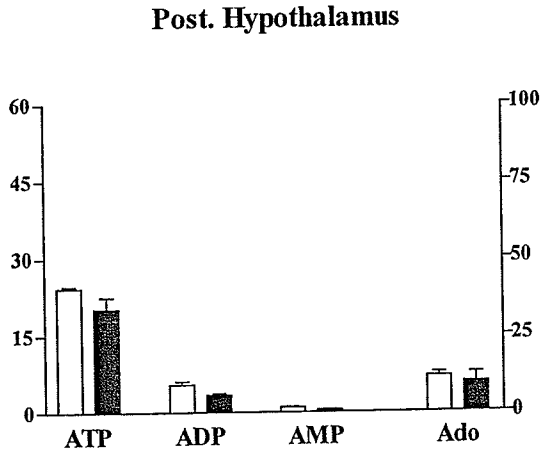

IV.D. 12h Sleep Deprivation - Study #1

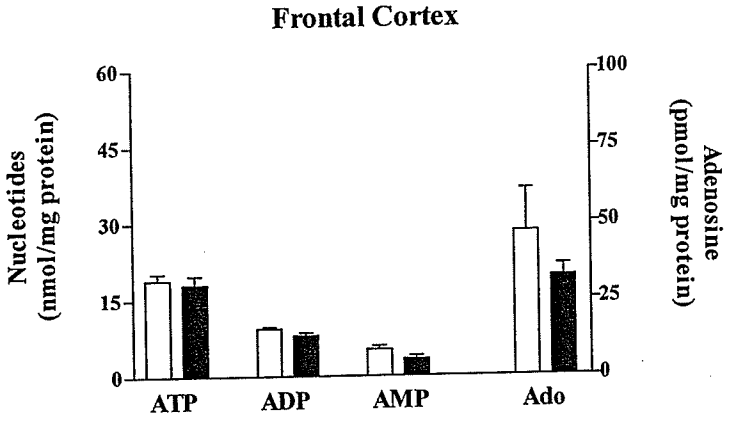

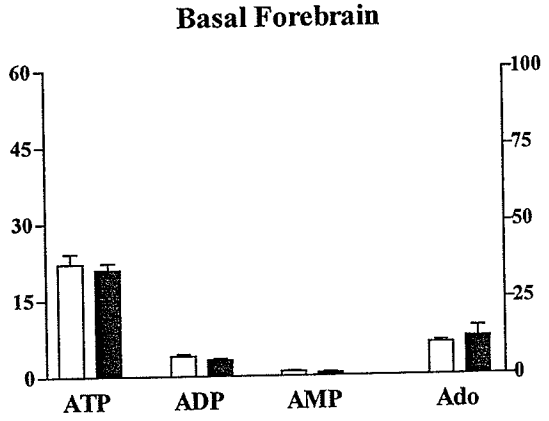

Figure IV.D. 12h Sleep Deprivation – Study #1. Shown are purine levels (mean ± S.E.M.) from control (n=3, light bars) and sleep deprived (n=5, dark bars) rats. All axes are presented in the same units as annotated in the frontal cortex figure.

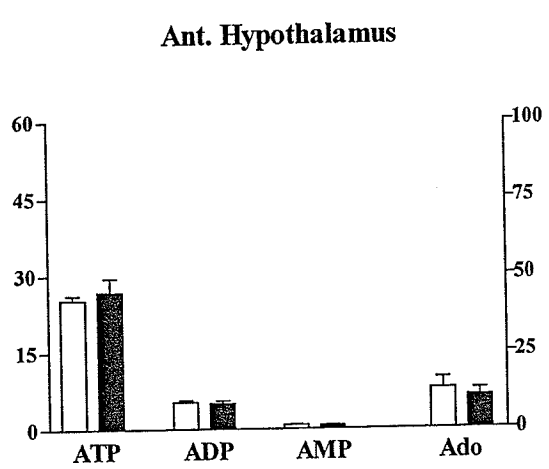

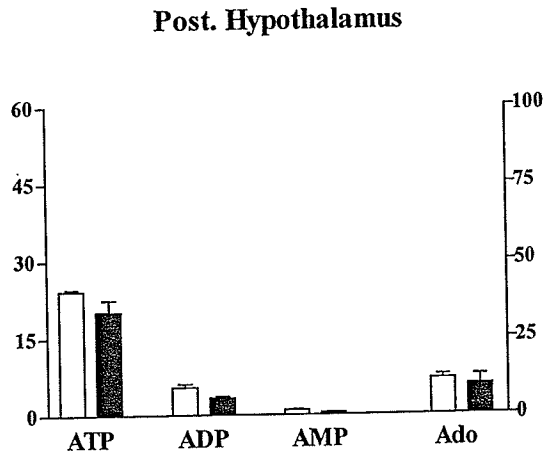

IV.E. 12h Sleep Deprivation - Study #2

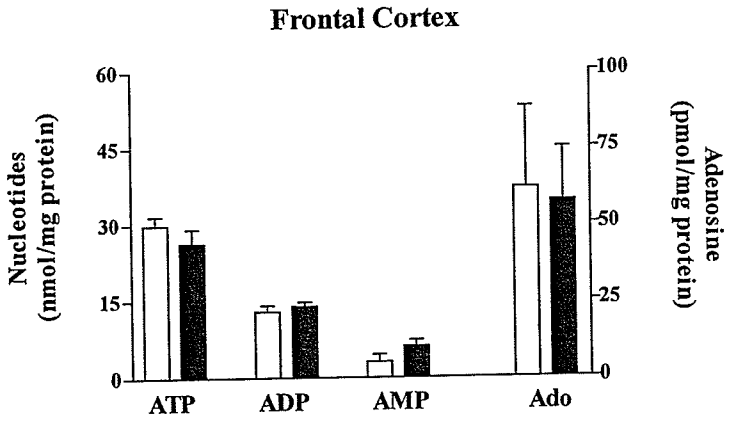

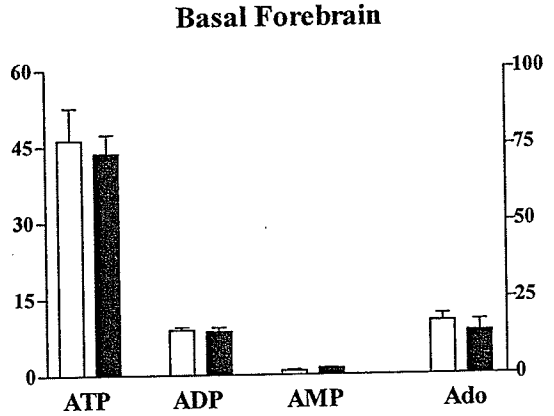

Figure IV.E. 12h Sleep Deprivation – Study #2. Shown are purine levels (mean ± S.E.M.) from control (n=5, light bars) and sleep deprived (n=5, dark bars) rats. All axes are presented in the same units as annotated in the frontal cortex figure.

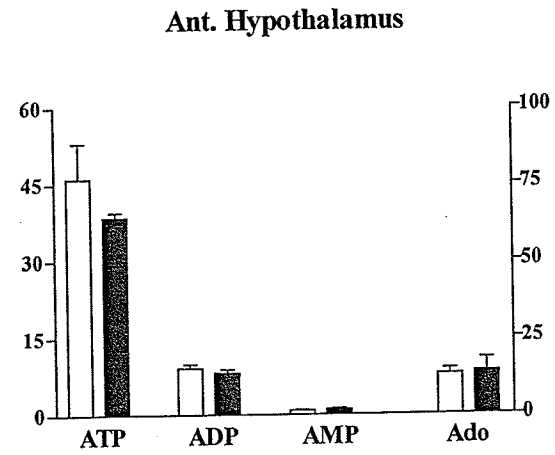

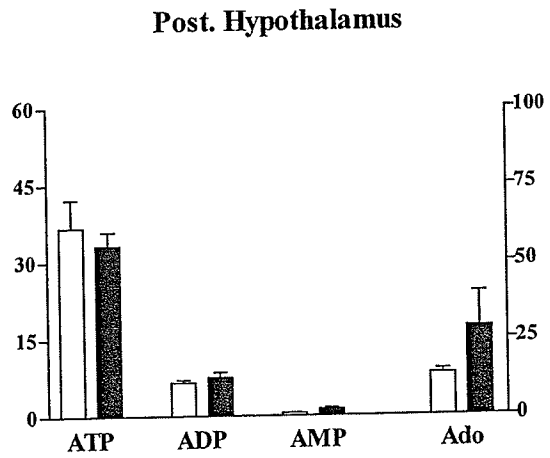

Appendix V - Expression Profiling of Adenosine-Related Genes - Supplemental Information

A. Oligonucleotide Primers

B. Atlas™ Gene Expression Array – Detected Genes

C. Reaction Enzymes

D. Commercial Nucleotides

E. Other Materials

F. Buffers

V.A. Oligonucleotide Primers

Gene	Sequence	Designed according to sequence reported by:
Housekeeping		
β-actin	5′ (113-132) 5′-GTG GGG CGC CCC AGG CAC CA-3′ 3′ (629-652) 5′-CTC CTT AAT GTC ACG CAC GAT TTC-3′	[157]
Glyceraldehyde-3-phosphate dehydrogenase (GAPDH)	5′ (546-570) 5′-CAT GAC CAC AGT CCA TGC CAT CAC T-3′ 3′ (1141-1165) 5′-ATG GGG TCT GGG ATG GAA TTG TGA G -3′	[206]
S29	5′ (1-23) 5′-CTC GTT CCT TTT CCT CCT TGG G-3′ 3′ (277-300) 5′-TAT TCT GTG TGC GCA AAG ACT AGC-3′	[30]
α-Tubulin	5′ (769-793) 5′-GTG TCT TCC ATC ACT GCT TCC CTC A-3′ 3′ (1296-1320) 5′-GAA CTC TCC CTC CTC CAT GCC CTC A-3′	[104]
Receptors		
A_1	5′ (766-788) 5′-TCG CTG GCC CTC ATC CTC TTC CT-3′ 3′ (1031-1052) 5′-GGC AGA GTC TAG TCC TCA GCT T-3′	[167]
A_{2a}	5′ (1208-1231) 5′-GGA GCG CCA GGA AGG CCA AGA GCA-3′ 3′ (1862-1886) 5′-GCC CTG TGA CTA AGT GCA TGG TAG C-3′	[64]
A_{2b}	5′ (1161-1184) 5′-CAG CTG GTG ACC TCA CTG TGG AGG-3′ 3′ (1716-1740) 5′-AGA GAA GCA AAC TCT AGT ACC TAG C-3′	[195]

V.A. Oligonucleotide Primers (con't)

Gene	Sequence	Designed according to sequence reported by:
Receptors con't		
A_3	5′ (1117-1139) 5′-CTG GGC ATC CTG TTG TCC CAT GC-3′ 3′ (1681-1703) 5′-CCT TCA ACG CAG GTT CTG TAC AT-3′	[239]
Enzymes		
Adenosine kinase	5′ (303-325) 5′-GGC TGA AGA CAA ACA CAA GGA AC-3′ 3′ (775-798) 5′-GAA CTG GCT AAT AAA CGG TGC AGA-3′	[194]
Adenosine deaminase	5′ (524-548) 5′-CTG TGC TGC ATG CGC CAC CAG CCC A-3′ 3′ (853-876) 5′-GTG AGG TAG CTG GAC CAG GGG CAG A-3′	[232]
5′-Nucleotidase	5′ (830-853) 5′-CGG GGG CCA CTA GCA CCT CAG ATA-3′ 3′ (na) 5′-TTG ATG GCT GCA TCT TCA CGA AT-3′	[126]
Transporters		
rCNT1	5′ (1698-1721) 5′-GGC TGA GGA GTG GCT TGG TGA CA-3′ 3′ (1996-2220) 5′-ACA TGG GAG CAG CGA TGA CCG TTG C-3′	[90]
E_i	5′ (1033-1059) 5′-GGC GCT GTG CCT TGT GTT GGT CTT C-3′ 3′ (1602-1624) 5′-CCA CAG ACC AAG AGA CCC GGT AT-3′	[231]
E_s	5′ (1040-1062) 5′-CGG AGC CTC ACA GCT ATT TGC AT-3′ 3′ (1521-1544) 5′-CCA ATC CCA AGT CCA TCC TCA GAG-3′	[231]

V.B. Atlas™ Gene Expression Array – Detected Genes

Intensity	Array Location	Gene Bank Accession #	Class	Gene Description
4	C 3 f	M11185	1	Myelin proteolipid protein (PLP) DM-20; lipophilin
3	C 6 g	J03754	1	Plasma membrane Ca-ATPase (brain isoform 2) EC 3.6.1.38
	D 5 a	M18547	2	40S ribosomal protein S12
2	A 7 d	Y00404	3	Superoxide dismutase 1 (SOD-1; Cu/Zn)
	B 4 d	M19007; X04440	4	(PKC-βI) + (PKC-βII)
	B 6 g	X13817	4	calmodulin
	B 6 i	D17615	4	PKC inhibitor protein-1; KCIP-1
	C 2 e	M64723	5	apolipoprotein J; clusterin
	C 5 d	AF019973	1	neuron-specific enolase
	C 5 k	M27925	1	synapsins 2A & 2B
	D 4 l	M27905	2	60S ribosomal protein L21
	D 4 m	J02650	2	60S ribosomal protein L20
	E 5 d	M28647	6	Na,K-ATPase α1 subunit
	F 3 g	U62326	7	macrophage migration inhibitory factor (MIF)
	F 5 I	M31602; J04625		carboxypeptidase E; carboxypeptidase H
1	A 1 a	D38629	8	adenomatous polyposis coli protein (APC)
	A 2 l	X17163	9	c-jun proto-oncogene; transcription factor AP-1 component.
	A 2 j	D26307	9	Jun-D; c-jun-related transcription factor
	A 3 c	X06942	10	A-raf proto-oncogene
	A 3 e	L15619	10	casein kinase II (β subunit)

V.B. Atlas™ Gene Expression Array – Detected Genes (con't)

Intensity	Array Location	Gene Bank Accession #	Class	Gene Description
1	A 3 l	D37880	11	Sky proto-oncogene; Tyro3; Rse; Dtk
	A 4 d	M13011	12	c-H-ras proto-oncogene; transforming G-protein p21
	A 6 c	M20035	13	Prothymosin α
	A 6 f	Y13380	13	amphiphysin II; Amph2
	B 1 d	U93306	14	KDR/flk1 vascular endothelial growth factor tyrosine kinase receptor (VEGFR2)
	B 2 f	U09307	4	Syp; SH-PTP2; adaptor protein tyrosine phosphatase
	B 4 g	M18331	4	PKC-ε
	B 4 i	M18332	4	PKC-zeta
	B 5 i	D85760	4	Gα12 guanine nucleotide regulatory protein
	B 5 k	U34959	4	transducin β-2 subunit; GTP binding proteinG(i)/G(s)/G(t) β subunit 2
	B 6 b	X06889	5	Rab-3a ras-related protein
	C 1 m	X02904	1	Glutathione S-transferase (class π)
	C 4 a	M17528	1	GTP-binding protein; G-α-i2; adenylate cyclase inhibiting
	C 4 h	M16736	1	Neuromodulin; axonal membrane protein GAP-43
	C 5 e	M63901	1	7B2 neuroendocrine protein
	C 5 j	M27812	1	synapsins IA & IB
	C 7 d	M93669	1	secretogranin II precursor (SGII); chromogranin C
	C 7 f	M24105	1	synaptobrevin-2 (SYB2); vesicle associated membrane protein 2 (VAMP-2)
	D 4 n	K03250	2	40S ribosomal protein S11

V.B. Atlas™ Gene Expression Array – Detected Genes (con't)

Intensity	Array Location	Gene Bank Accession #	Class	Gene Description
1	E 3 c	U72487	15	calcium-independent alpha-latrotoxin receptor
	E 5 n	M64373	6	calcium channel α1 subunit
	E 6 i	U15098	6	GluT and GluT-R glutamate transporter
	F 2 l	M25890	7	Somatostatin
	F 3 d	U25651	7	Testicular luteinizing hormone β-subunit (TLHB1)
	F 5 a	M76426	16	Dipeptidyl aminopeptidase related protein (DPP6)

Classifications:

1. nervous system-related proteins
2. translation
3. DNA synthesis, repair and recombination proteins
4. intracellular signal transduction
5. apoptosis related proteins
6. channels and transporters
7. cell-cell communication
8. tumor suppressors and related proteins
9. transcription factor-related oncogenes
10. serine-threonine protein kinase oncogenes
11. receptor protein tyrosine kinase oncogenes
12. intracellular signal transduction-related oncogenes
13. cell cycle regulatory proteins
14. receptors and cell-surface proteins
15. hormone receptors
16. protein turnover (proteases/inhibitors)

V.C. Reaction Enzymes

Product	Supplier	Catalog #	Concentration (U/µl)
AmpliTaq® DNA Polymerase	Perkin Elmer	N808-0160	5
DNA Polymerase (Klenow Fragment)	Promega	M2201*	5
DNase (RQ1, RNase-Free)	Promega	M6101	1
Moloney Murine Leukemia Virus Reverse Transcriptase (MMLV-RT)	Life Technologies	28025-013*	2
Ribonuclease inhibitor (recombinant Rnasin®)	Promega	N2511	40
S1 Nuclease	Promega	M5761*	30
T4 DNA Polymerase	Life Technologies	18005-017*	5
T7 RNA Polymerase	Epicentre Technologies	TH925K	1000
T7 RNA Polymerase*	Promega	P2075	20

* - supplied with concentrated reaction buffer

V.D. Commercial Nucleotides

Product	Supplier	Catalog #	Concentration (µg/µl)
DNTP Set (dATP, dCTP, dGTP, dTTP)	Pharmacia	27-2035-01	4 x 100 mM (25 µmol each)
NTP Set (ATP, CTP, GTP, UTP)	Pharmacia	27-2025-01	4 x 100 mM (25 µmol each)
Deoxyadenosine 5′-triphosphate [α^{32}P]	NEN	NEG012A	800 Ci/mmol (10mCi/ml)
Deoxyadenosine 5′-(α-thio) triphosphate [^{35}S]	NEN	NEG034S	500 Ci/mmol (10mCi/ml)
Deoxyadenosine 5′-triphosphate [α^{32}P]	NEN	NEG512H	3000 Ci/mmol (10mCi/ml)
Cytidine 5′-triphosphate [α^{32}P]	NEN	NEG508X	800 Ci/mmol (10mCi/ml)

V.E. Other Materials

Product	Supplier	Catalog #	Concentration (µg/µl)
BioMax Film MR-1 (8"x10")	Kodak	V8701302	n/a
Lambda DNA/*Hind* III (23,130 – 125 bp)	Promega	G1711°	0.5
ϕX174 DNA/*Hae* III (1353 – 72 bp)	Promega	G1761°	1
Atlas™ Rat cDNA Expression Array	Clontech	7738-1	n/a
Ultraspec™ RNA Reagent	Biotecx	BL-10050	n/a
Zeta-Probe® Blotting Membrane	Bio-Rad	162-0165	N/a

° - supplied with 6x blue/orange loading dye

V.F. Buffers

Buffer	Composition
5x first strand buffer*	250 mM Tris-HCl (pH8.3) 375 mM KCl 15 mM $MgCl_2$
10x PCR buffer*	contains 15 mM $MgCl_2$
5x T4 DNA Polymerase* buffer	165 mM Tris-acetate (pH 7.9) 330 mM sodium acetate 50 mM magnesium acetate 500 µg/ml BSA 2.5 mM DTT
Klenow 10x buffer*	500 mM Tris-HCl (pH7.2) 100 mM $MgSO_4$ 1.0 mM DTT
10x second strand buffer[a]	1.0 M Tris-HCl 200 mM KCl 100 mM $MgCl_2$ 50 mM DTT
S1 nuclease 10x reaction buffer*	500 mM sodium acetate (pH 4.5 at 25 °C) 2.8 M NaCl 45 mM $ZnSO_4$
10x KFI buffer[a]	200 mM Tris-HCl (pH 7.5) 100 mM $MgCl_2$ 50 mM NaCl 50 mM DTT
TE buffer	10 mM Tris-HCl (pH 8.0) 1 mM EDTA (pH 8.0)
5x RNA amplification buffer[b]	200 mM Tris (pH 7.9) 30 mM $MgCl_2$ 10 mM spermidine 50 mM NaCl

* - supplied with enzyme.
a – from Eberwine and Crino, 1997 [58].
b – used buffer provided with Promega T7 RNA polymerase.

References

[1] Abbracchio, M.P., Brambilla, R., Ceruti, S., Kim, H.O., von Lubitz, D.K., Jacobson, K.A. and Cattabeni, F., G protein-dependent activation of phospholipase C by adenosine A_3 receptors in rat brain, *Mol Pharmacol*, 48 (1995) 1038-45.

[2] Abbracchio, M.P. and Cattabeni, F., Brain adenosine receptors as targets for therapeutic intervention in neurodegenerative diseases, *Ann N Y Acad Sci*, 890 (1999) 79-92.

[3] Abbracchio, M.P., Ceruti, S., Brambilla, R., Franceschi, C., Malorni, W., Jacobson, K.A., von Lubitz, D.K. and Cattabeni, F., Modulation of apoptosis by adenosine in the central nervous system: a possible role for the A_3 receptor. Pathophysiological significance and therapeutic implications for neurodegenerative disorders, *Ann N Y Acad Sci*, 825 (1997) 11-22.

[4] Abbracchio, M.P., Rainaldi, G., Giammarioli, A.M., Ceruti, S., Brambilla, R., Cattabeni, F., Barbieri, D., Franceschi, C., Jacobson, K.A. and Malorni, W., The A_3 adenosine receptor mediates cell spreading, reorganization of actin cytoskeleton, and distribution of Bcl-XL: studies in human astroglioma cells, *Biochem Biophys Res Commun*, 241 (1997) 297-304.

[5] Abdul-Ghani, A.S., Attwell, P.J. and Bradford, H.F., The protective effect of 2-chloroadenosine against the development of amygdala kindling and on amygdala-kindled seizures, *Eur J Pharmacol*, 326 (1997) 7-14.

[6] Aizenman, E., Lipton, S.A. and Loring, R.H., Selective modulation of NMDA responses by reduction and oxidation, *Neuron*, 2 (1989) 1257-63.

[7] Arlinghaus, L. and Lee, K.S., Endogenous adenosine mediates the sustained inhibition of excitatory synaptic transmission during moderate hypoxia, *Brain Res*, 724 (1996) 265-8.

[8] Ascher, P. and Nowak, L., The role of divalent cations in the N-methyl-D-aspartate responses of mouse central neurones in culture, *J Physiol*, 399 (1988) 247-66.

[9] Aston-Jones, G., Chen, S., Zhu, Y. and Oshinsky, M.L., A neural circuit for circadian regulation of arousal, *Nat Neurosci*, 4 (2001) 732-8.

[10] Basheer, R., Sherin, J.E., Saper, C.B., Morgan, J.I., McCarley, R.W. and Shiromani, P.J., Effects of sleep on wake-induced c-fos expression, *J Neurosci*, 17 (1997) 9746-50.

[11] Basheer, R. and Shiromani, P.J., Effects of prolonged wakefulness on c-fos and AP1 activity in young and old rats, *Brain Res Mol Brain Res*, 89 (2001) 153-7.

[12] Beal, M.F., Mechanisms of excitotoxicity in neurologic diseases, *Faseb J*, 6 (1992) 3338-44.

[13] Ben-Ari, Y. and Cossart, R., Kainate, a double agent that generates seizures: two decades of progress, *Trends Neurosci*, 23 (2000) 580-7.

[14] Benington, J.H. and Heller, H.C., Restoration of brain energy metabolism as the function of sleep, *Prog Neurobiol*, 45 (1995) 347-60.

[15] Benington, J.H., Kodali, S.K. and Heller, H.C., Stimulation of A_1 adenosine receptors mimics the electroencephalographic effects of sleep deprivation, *Brain Res*, 692 (1995) 79-85.

[16] Bennett, G.C. and Boarder, M.R., The effect of nucleotides and adenosine on stimulus-evoked glutamate release from rat brain cortical slices, *Br J Pharmacol*, 131 (2000) 617-23.

[17] Berendse, H.W., Galis-de Graaf, Y. and Groenewegen, H.J., Topographical organization and relationship with ventral striatal compartments of prefrontal corticostriatal projections in the rat, *J Comp Neurol*, 316 (1992) 314-47.

[18] Bettler, B. and Mulle, C., Review: neurotransmitter receptors. II. AMPA and kainate receptors, *Neuropharmacology*, 34 (1995) 123-39.

[19] Bhardwaj, A., Northington, F.J., Koehler, R.C., Stiefel, T., Hanley, D.F. and Traystman, R.J., Adenosine modulates N-methyl-D-aspartate-stimulated hippocampal nitric oxide production in vivo, *Stroke*, 26 (1995) 1627-33.

[20] Bjorvatn, B., Fagerland, S., Eid, T. and Ursin, R., Sleep/waking effects of a selective 5-HT1A receptor agonist given systemically as well as perfused in the dorsal raphe nucleus in rats, *Brain Res*, 770 (1997) 81-8.

[21] Bradford, M.M., A rapid and sensitive method for the quantitation of microgram quantities of protein utilizing the principle of protein-dye binding, *Anal Biochem*, 72 (1976) 248-54.

[22] Brosh, S., Boer, P., Sperling, O. and Zoref-Shani, E., Elevated UTP and CTP content in cultured neurons from HPRT-deficient transgenic mice, *J Mol Neurosci*, 14 (2000) 87-91.

[23] Bruyn, R.P. and Stoof, J.C., The quinolinic acid hypothesis in Huntington's chorea, *J Neurol Sci*, 95 (1990) 29-38.

[24] Bundlie, S.R., Sleep in aging, *Geriatrics*, 53 Suppl 1 (1998) S41-3.

[25] Butcher, S.P. and Hamberger, A., In vivo studies on the extracellular, and veratrine-releasable, pools of endogenous amino acids in the rat striatum: effects of corticostriatal deafferentation and kainic acid lesion, *J Neurochem*, 48 (1987) 713-21.

[26] Capece, M.L. and Lydic, R., cAMP and protein kinase A modulate cholinergic rapid eye movement sleep generation, *Am J Physiol*, 273 (1997) R1430-40.

[27] Carboni, S., Melis, F., Pani, L., Hadjiconstantinou, M. and Rossetti, Z.L., The non-competitive NMDA-receptor antagonist MK-801 prevents the massive release of glutamate and aspartate from rat striatum induced by 1-methyl-4-phenylpyridinium (MPP+), *Neurosci Lett*, 117 (1990) 129-33.

[28] Carlsson, M. and Carlsson, A., Interactions between glutamatergic and monoaminergic systems within the basal ganglia--implications for schizophrenia and Parkinson's disease, *Trends Neurosci*, 13 (1990) 272-6.

[29] Chagoya de Sanchez, V., Hernandez Munoz, R., Suarez, J., Vidrio, S., Yanez, L. and Diaz Munoz, M., Day-night variations of adenosine and its metabolizing enzymes in the brain cortex of the rat--possible physiological significance for the energetic homeostasis and the sleep-wake cycle, *Brain Res*, 612 (1993) 115-21.

[30] Chan, Y.L., Suzuki, K., Olvera, J. and Wool, I.G., Zinc finger-like motifs in rat ribosomal proteins S27 and S29, *Nucleic Acids Res*, 21 (1993) 649-55.

[31] Cheng, J.T., Liu, I.M., Juang, S.W. and Jou, S.B., Decrease of adenosine A_1 receptor gene expression in cerebral cortex of aged rats, *Neurosci Lett*, 283 (2000) 227-9.

[32] Chittajallu, R., Braithwaite, S.P., Clarke, V.R. and Henley, J.M., Kainate receptors: subunits, synaptic localization and function, *Trends Pharmacol Sci*, 20 (1999) 26-35.

[33] Chittajallu, R., Vignes, M., Dev, K.K., Barnes, J.M., Collingridge, G.L. and Henley, J.M., Regulation of glutamate release by presynaptic kainate receptors in the hippocampus, *Nature*, 379 (1996) 78-81.

[34] Corradetti, R., Lo Conte, G., Moroni, F., Passani, M.B. and Pepeu, G., Adenosine decreases aspartate and glutamate release from rat hippocampal slices, *Eur J Pharmacol*, 104 (1984) 19-26.

[35] Corsi, C., Melani, A., Bianchi, L., Pepeu, G. and Pedata, F., Effect of adenosine A_{2A} receptor stimulation on GABA release from the striatum of young and aged rats in vivo, *Neuroreport*, 10 (1999) 3933-7.

[36] Corsi, C., Melani, A., Bianchi, L., Pepeu, G. and Pedata, F., Striatal A_{2A} adenosine receptors differentially regulate spontaneous and K+-evoked glutamate release in vivo in young and aged rats, *Neuroreport*, 10 (1999) 687-91.

[37] Cospito, J.A. and Kultas-Ilinsky, K., Synaptic organization of motor corticostriatal projections in the rat, *Exp Neurol*, 72 (1981) 257-66.

[38] Craig, A.M., Blackstone, C.D., Huganir, R.L. and Banker, G., The distribution of glutamate receptors in cultured rat hippocampal neurons: postsynaptic clustering of AMPA-selective subunits, *Neuron*, 10 (1993) 1055-68.

[39] Craig, C.G. and White, T.D., Low-level N-methyl-D-aspartate receptor activation provides a purinergic inhibitory threshold against further N-methyl-D-aspartate-mediated neurotransmission in the cortex, *J Pharmacol Exp Ther*, 260 (1992) 1278-84.

[40] Craig, C.G. and White, T.D., NMDA-evoked adenosine release from rat cortex does not require the intermediate formation of nitric oxide, *Neurosci Lett*, 158 (1993) 167-9.

[41] Craig, C.G. and White, T.D., N-methyl-D-aspartate- and non-N-methyl-D-aspartate-evoked adenosine release from rat cortical slices: distinct purinergic sources and mechanisms of release, *J Neurochem*, 60 (1993) 1073-80.

[42] Cronstein, B.N., Adenosine, an endogenous anti-inflammatory agent, *J Appl Physiol*, 76 (1994) 5-13.

[43] Cunha, R.A., Constantino, M.C., Sebastiao, A.M. and Ribeiro, J.A., Modification of A_1 and A_{2a} adenosine receptor binding in aged striatum, hippocampus and cortex of the rat, *Neuroreport*, 6 (1995) 1583-8.

[44] Cunha, R.A., Constantino, M.D., Fonseca, E. and Ribeiro, J.A., Age-dependent decrease in adenosine A_1 receptor binding sites in the rat brain. Effect of cis unsaturated free fatty acids, *Eur J Biochem*, 268 (2001) 2939-47.

[45] Cunha, R.A., Sebastiao, A.M. and Ribeiro, J.A., Ecto-5'-nucleotidase is associated with cholinergic nerve terminals in the hippocampus but not in the cerebral cortex of the rat, *J Neurochem*, 59 (1992) 657-66.

[46] de Mendonca, A. and Ribeiro, J.A., Influence of metabotropic glutamate receptor agonists on the inhibitory effects of adenosine A_1 receptor activation in the rat hippocampus, *Br J Pharmacol*, 121 (1997) 1541-8.

[47] Delaney, S.M. and Geiger, J.D., Enhancement of NMDA-induced increases in levels of endogenous adenosine by adenosine deaminase and adenosine transport inhibition in rat striatum, *Brain Res*, 702 (1995) 72-6.

[48] Delaney, S.M. and Geiger, J.D., Brain regional levels of adenosine and adenosine nucleotides in rats killed by high-energy focused microwave irradiation, *J Neurosci Methods*, 64 (1996) 151-6.

[49] Delaney, S.M. and Geiger, J.D., Levels of endogenous adenosine in rat striatum. II. Regulation of basal and N-methyl-D-aspartate-induced levels by inhibitors of adenosine transport and metabolism, *J Pharmacol Exp Ther*, 285 (1998) 568-72.

[50] Delaney, S.M., Shepel, P.N. and Geiger, J.D., Levels of endogenous adenosine in rat striatum. I. Regulation by ionotropic glutamate receptors, nitric oxide and free radicals, *J Pharmacol Exp Ther*, 285 (1998) 561-7.

[51] Di Iorio, P., Battaglia, G., Ciccarelli, R., Ballerini, P., Giuliani, P., Poli, A., Nicoletti, F. and Caciagli, F., Interaction between A_1 adenosine and class II metabotropic glutamate receptors in the regulation of purine and glutamate release from rat hippocampal slices, *J Neurochem*, 67 (1996) 302-9.

[52] Dixon, A.K., Widdowson, L. and Richardson, P.J., Desensitisation of the adenosine A_1 receptor by the A_{2A} receptor in the rat striatum, *J Neurochem*, 69 (1997) 315-21.

[53] Donoghue, J.P. and Wise, S.P., The motor cortex of the rat: cytoarchitecture and microstimulation mapping, *J Comp Neurol*, 212 (1982) 76-88.

[54] Dunnett, S.B. and Bjorklund, A., Prospects for new restorative and neuroprotective treatments in Parkinson's disease, *Nature*, 399 (1999) A32-9.

[55] Dunwiddie, T.V. and Diao, L., Regulation of extracellular adenosine in rat hippocampal slices is temperature dependent: role of adenosine transporters, *Neuroscience*, 95 (2000) 81-8.

[56] Dunwiddie, T.V., Diao, L., Kim, H.O., Jiang, J.L. and Jacobson, K.A., Activation of hippocampal adenosine A_3 receptors produces a desensitization of A_1 receptor-mediated responses in rat hippocampus, *J Neurosci*, 17 (1997) 607-14.

[57] During, M.J. and Spencer, D.D., Adenosine: a potential mediator of seizure arrest and postictal refractoriness, *Ann Neurol*, 32 (1992) 618-24.

[58] Eberwine, J. and Crino, P., Analysis of mRNA populations from single live and fixed cells of the central nervous system. , *Current Protocols in Neuroscience*, John Wiley & Sons, New York, 1997, pp. 5.3.1-5.3.15.

[59] Eberwine, J., Yeh, H., Miyashiro, K., Cao, Y., Nair, S., Finnell, R., Zettel, M. and Coleman, P., Analysis of gene expression in single live neurons, *Proc Natl Acad Sci U S A*, 89 (1992) 3010-4.

[60] Evans, M.C., Swan, J.H. and Meldrum, B.S., An adenosine analogue, 2-chloroadenosine, protects against long term development of ischaemic cell loss in the rat hippocampus, *Neurosci Lett*, 83 (1987) 287-92.

[61] Everts, I., Villmann, C. and Hollmann, M., N-Glycosylation is not a prerequisite for glutamate receptor function but Is essential for lectin modulation, *Mol Pharmacol*, 52 (1997) 861-73.

[62] Ferkany, J.W., Zaczek, R. and Coyle, J.T., Kainic acid stimulates excitatory amino acid neurotransmitter release at presynaptic receptors, *Nature*, 298 (1982) 757-9.

[63] Ferrante, R.J., Kowall, N.W., Cipolloni, P.B., Storey, E. and Beal, M.F., Excitotoxin lesions in primates as a model for Huntington's disease: histopathologic and neurochemical characterization, *Exp Neurol*, 119 (1993) 46-71.

[64] Fink, J.S., Weaver, D.R., Rivkees, S.A., Peterfreund, R.A., Pollack, A.E., Adler, E.M. and Reppert, S.M., Molecular cloning of the rat A_2 adenosine receptor: selective co- expression with D_2 dopamine receptors in rat striatum, *Brain Res Mol Brain Res*, 14 (1992) 186-95.

[65] Finn, S.F., Swartz, K.J. and Beal, M.F., 2-Chloroadenosine attenuates NMDA, kainate, and quisqualate toxicity, *Neurosci Lett*, 126 (1991) 191-4.

[66] Flagmeyer, I., Haas, H.L. and Stevens, D.R., Adenosine A_1 receptor-mediated depression of corticostriatal and thalamostriatal glutamatergic synaptic potentials in vitro, *Brain Res*, 778 (1997) 178-85.

[67] Fonnum, F., Storm-Mathisen, J. and Divac, I., Biochemical evidence for glutamate as neurotransmitter in corticostriatal and corticothalamic fibres in rat brain, *Neuroscience*, 6 (1981) 863-73.

[68] Foster, A.C., Miller, L.P. and J.B., W., Regulation of endogenous adenosine levels in the CNS: Potential for therapy in stroke, epilepsy and pain. In A. Sahota and M. Taylor (Eds.), *Purine and Pyrimidine Metabolism in Man*, Plenum Press, New York, 1995, pp. 427-430.

[69] Franklin, P.H., Zhang, G., Tripp, E.D. and Murray, T.F., Adenosine A_1 receptor activation mediates suppression of (-) bicuculline methiodide-induced seizures in rat prepiriform cortex, *J Pharmacol Exp Ther*, 251 (1989) 1229-36.

[70] Fredholm, B.B., Adenosine and neuroprotection, *Int Rev Neurobiol*, 40 (1997) 259-80.

[71] Fredholm, B.B., Abbracchio, M.P., Burnstock, G., Daly, J.W., Harden, T.K., Jacobson, K.A., Leff, P. and Williams, M., Nomenclature and classification of purinoceptors, *Pharmacol Rev*, 46 (1994) 143-56.

[72] Fuchs, J.L., 5'-Nucleotidase activity increases in aging rat brain, *Neurobiol Aging*, 12 (1991) 523-30.

[73] Gan, X.T., Cook, M.A., Moffat, M.P. and Karmazyn, M., Transient ischemia in the presence of an adenosine deaminase plus a nucleoside transport inhibitor confers protection against contractile depression produced by hydrogen peroxide. Possible role of glycogen, *J Mol Cell Cardiol*, 28 (1996) 1165-76.

[74] Gidday, J.M., Fitzgibbons, J.C., Shah, A.R., Kraujalis, M.J. and Park, T.S., Reduction in cerebral ischemic injury in the newborn rat by potentiation of endogenous adenosine, *Pediatr Res*, 38 (1995) 306-11.

[75] Girault, J.A., Barbeito, L., Spampinato, U., Gozlan, H., Glowinski, J. and Besson, M.J., In vivo release of endogenous amino acids from the rat striatum: further evidence for a role of glutamate and aspartate in corticostriatal neurotransmission [published erratum appears in J Neurochem 1987 Jan;48(1):327], *J Neurochem*, 47 (1986) 98-106.

[76] Grassi Zucconi, G., Menegazzi, M., Carcereri De Prati, A., Vescia, S., Ranucci, G. and Bentivoglio, M., Different programs of gene expression are associated with different phases of the 24h and sleep-wake cycles, *Chronobiologia*, 21 (1994) 93-7.

[77] Grassi-Zucconi, G., Menegazzi, M., De Prati, A.C., Bassetti, A., Montagnese, P., Mandile, P., Cosi, C. and Bentivoglio, M., c-fos mRNA is spontaneously induced in the rat brain during the activity period of the circadian cycle, *Eur J Neurosci*, 5 (1993) 1071-8.

[78] Graves, L., Pack, A. and Abel, T., Sleep and memory: a molecular perspective, *Trends Neurosci*, 24 (2001) 237-43.

[79] Gubitz, A.K., Widdowson, L., Kurokawa, M., Kirkpatrick, K.A. and Richardson, P.J., Dual signalling by the adenosine A_{2a} receptor involves activation of both N- and P-type calcium channels by different G proteins and protein kinases in the same striatal nerve terminals, *J Neurochem*, 67 (1996) 374-81.

[80] Haughey, N.J., Nath, A., Mattson, M.P., Slevin, J.T. and Geiger, J.D., HIV-1 Tat through phosphorylation of NMDA receptors potentiates glutamate excitotoxicity, *J Neurochem*, 78 (2001) 457-467.

[81] Heron, A., Lasbennes, F. and Seylaz, J., Adenosine modulation of amino acid release in rat hippocampus during ischemia and veratridine depolarization, *Brain Res*, 608 (1993) 27-32.

[82] Hoehn, K. and White, T.D., Role of excitatory amino acid receptors in K^+- and glutamate-evoked release of endogenous adenosine from rat cortical slices, *J Neurochem*, 54 (1990) 256-65.

[83] Hoehn, K. and White, T.D., Role of excitatory amino acid receptors in K^+- and glutamate-evoked release of endogenous adenosine from rat cortical slices, *J Neurochem*, 54 (1990) 256-65.

[84] Hollen, K.M., Nakabeppu, Y. and Davies, S.W., Changes in expression of delta FosB and the Fos family proteins following NMDA receptor activation in the rat striatum, *Brain Res Mol Brain Res*, 47 (1997) 31-43.

[85] Hollmann, M., Hartley, M. and Heinemann, S., Ca^{2+} permeability of KA-AMPA--gated glutamate receptor channels depends on subunit composition, *Science*, 252 (1991) 851-3.

[86] Hollmann, M. and Heinemann, S., Cloned glutamate receptors, *Annu Rev Neurosci*, 17 (1994) 31-108.

[87] Honore, T., Davies, S.N., Drejer, J., Fletcher, E.J., Jacobsen, P., Lodge, D. and Nielsen, F.E., Quinoxalinediones: potent competitive non-NMDA glutamate receptor antagonists, *Science*, 241 (1988) 701-3.

[88] Horner, R.L., Sanford, L.D., Annis, D., Pack, A.I. and Morrison, A.R., Serotonin at the laterodorsal tegmental nucleus suppresses rapid-eye- movement sleep in freely behaving rats, *J Neurosci*, 17 (1997) 7541-52.

[89] Houamed, K.M., Kuijper, J.L., Gilbert, T.L., Haldeman, B.A., O'Hara, P.J., Mulvihill, E.R., Almers, W. and Hagen, F.S., Cloning, expression, and gene structure of a G protein-coupled glutamate receptor from rat brain, *Science*, 252 (1991) 1318-21.

[90] Huang, Q.Q., Yao, S.Y., Ritzel, M.W., Paterson, A.R., Cass, C.E. and Young, J.D., Cloning and functional expression of a complementary DNA encoding a mammalian nucleoside transport protein, *J Biol Chem*, 269 (1994) 17757-60.

[91] Huston, J.P., Haas, H.L., Boix, F., Pfister, M., Decking, U., Schrader, J. and Schwarting, R.K., Extracellular adenosine levels in neostriatum and hippocampus during rest and activity periods of rats, *Neuroscience*, 73 (1996) 99-107.

[92] Jarvis, M.F. and Williams, M., Direct autoradiographic localization of adenosine A_2 receptors in the rat brain using the A_2-selective agonist, [3H]CGS 21680, *Eur J Pharmacol*, 168 (1989) 243-6.

[93] Jhamandas, K. and Dumbrille, A., Regional release of [^{3}H]adenosine derivatives from rat brain in vivo: effect of excitatory amino acids, opiate agonists, and benzodiazepines, *Can J Physiol Pharmacol*, 58 (1980) 1262-78.

[94] Jiang, N., Kowaluk, E.A., Lee, C.H., Mazdiyasni, H. and Chopp, M., Adenosine kinase inhibition protects brain against transient focal ischemia in rats, *Eur J Pharmacol*, 320 (1997) 131-7.

[95] Jin, Z.L., Lee, T.F., Zhou, S.J. and Wang, L.C., Age-dependent change in the inhibitory effect of an adenosine agonist on hippocampal acetylcholine release in rats, *Brain Res Bull*, 30 (1993) 149-52.

[96] Johnson, J.W. and Ascher, P., Glycine potentiates the NMDA response in cultured mouse brain neurons, *Nature*, 325 (1987) 529-31.

[97] Jones, B.E., The organization of central cholinergic systems and their functional importance in sleep-waking states, *Prog Brain Res*, 98 (1993) 61-71.

[98] Juvancz, P., The effect of raphe lesion on sleep in the rat, *Brain Res*, 194 (1980) 371-6.

[99] Kanai, Y. and Hediger, M.A., Primary structure and functional characterization of a high-affinity glutamate transporter, *Nature*, 360 (1992) 467-71.

[100] Kawaguchi, Y., Wilson, C.J., Augood, S.J. and Emson, P.C., Striatal interneurones: chemical, physiological and morphological characterization, *Trends Neurosci*, 18 (1995) 527-35.

[101] Kayama, Y., Ohta, M. and Jodo, E., Firing of 'possibly' cholinergic neurons in the rat laterodorsal tegmental nucleus during sleep and wakefulness, *Brain Res*, 569 (1992) 210-20.

[102] Knopfel, T., Kuhn, R. and Allgeier, H., Metabotropic glutamate receptors: novel targets for drug development, *J Med Chem*, 38 (1995) 1417-26.

[103] Kutsuwada, T., Kashiwabuchi, N., Mori, H., Sakimura, K., Kushiya, E., Araki, K., Meguro, H., Masaki, H., Kumanishi, T., Arakawa, M. and et al., Molecular diversity of the NMDA receptor channel, *Nature*, 358 (1992) 36-41.

[104] Lemischka, I.R., Farmer, S., Racaniello, V.R. and Sharp, P.A., Nucleotide sequence and evolution of a mammalian alpha-tubulin messenger RNA, *J Mol Biol*, 151 (1981) 101-20.

[105] Lerner-Natoli, M., Rondouin, G., Belaidi, M., Baldy-Moulinier, M. and Kamenka, J.M., N-[1-(2-thienyl)cyclohexyl]-piperidine (TCP) does not block kainic acid- induced status epilepticus but reduces secondary hippocampal damage, *Neurosci Lett*, 122 (1991) 174-8.

[106] Li, J. and Iadecola, C., Nitric oxide and adenosine mediate vasodilation during functional activation in cerebellar cortex, *Neuropharmacology*, 33 (1994) 1453-61.

[107] Lin, Y. and Phillis, J.W., Deoxycoformycin and oxypurinol: protection against focal ischemic brain injury in the rat, *Brain Res*, 571 (1992) 272-80.

[108] Link, A.A., Kino, T., Worth, J.A., McGuire, J.L., Crane, M.L., Chrousos, G.P., Wilder, R.L. and Elenkov, I.J., Ligand-activation of the adenosine A_{2a} receptors inhibits IL-12 production by human monocytes, *J Immunol*, 164 (2000) 436-42.

[109] Livesey, F.J. and Hunt, S.P., Differential display of mRNA by PCR. , *Current Protocols in Neuroscience*, John Wiley & Sons, New York, 1997, pp. 5.2.1-5.2.11.

[110] Lopes, L.V., Cunha, R.A. and Ribeiro, J.A., Increase in the number, G protein coupling, and efficiency of facilitatory adenosine A_{2A} receptors in the limbic cortex, but not striatum, of aged rats, *J Neurochem*, 73 (1999) 1733-8.

[111] Mackiewicz, M., Geiger, J.D. and Pack, A.I., Simultaneous assessment of ecto- and cytosolic-5'-nucleotidase activities in brain micropunches, *J Neurosci Methods*, 104 (2000) 9-18.

[112] Mackiewicz, M., Nikonova, E.V., Bell, C.C., Galante, R.J., Zhang, L., Geiger, J.D. and Pack, A.I., Activity of adenosine deaminase in the sleep regulatory areas of the rat CNS, *Brain Res Mol Brain Res*, 80 (2000) 252-5.

[113] Marangos, P.J., Adenosinergic approaches to stroke therapeutics, *Med Hypotheses*, 32 (1990) 45-9.

[114] Markowska, A.L., Stone, W.S., Ingram, D.K., Reynolds, J., Gold, P.E., Conti, L.H., Pontecorvo, M.J., Wenk, G.L. and Olton, D.S., Individual differences in aging: behavioral and neurobiological correlates, *Neurobiol Aging*, 10 (1989) 31-43.

[115] Martin, L.J., Al-Abdulla, N.A., Brambrink, A.M., Kirsch, J.R., Sieber, F.E. and Portera-Cailliau, C., Neurodegeneration in excitotoxicity, global cerebral ischemia, and target deprivation: A perspective on the contributions of apoptosis and necrosis, *Brain Res Bull*, 46 (1998) 281-309.

[116] Martin, L.J., Blackstone, C.D., Levey, A.I., Huganir, R.L. and Price, D.L., AMPA glutamate receptor subunits are differentially distributed in rat brain, *Neuroscience*, 53 (1993) 327-58.

[117] Masu, M., Tanabe, Y., Tsuchida, K., Shigemoto, R. and Nakanishi, S., Sequence and expression of a metabotropic glutamate receptor, *Nature*, 349 (1991) 760-5.

[118] Masubuchi, S., Honma, S., Abe, H., Ishizaki, K., Namihira, M., Ikeda, M. and Honma, K., Clock genes outside the suprachiasmatic nucleus involved in manifestation of locomotor activity rhythm in rats, *Eur J Neurosci*, 12 (2000) 4206-14.

[119] Mayne, M., Fotheringham, J., Yan, H.J., Power, C., Del Bigio, M.R., Peeling, J. and Geiger, J.D., Adenosine A_{2A} receptor activation reduces proinflammatory events and decreases cell death following intracerebral hemorrhage, *Ann Neurol*, 49 (2001) 727-35.

[120] Mayne, M., Shepel, P.N. and Geiger, J.D., Recovery of high-integrity mRNA from brains of rats killed by high-energy focused microwave irradiation, *Brain Res Brain Res Protoc*, 4 (1999) 295-302.

[121] McBean, G.J. and Roberts, P.J., Neurotoxicity of L-glutamate and DL-threo-3-hydroxyaspartate in the rat striatum, *J Neurochem*, 44 (1985) 247-54.

[122] McGeer, E.G. and McGeer, P.L., Duplication of biochemical changes of Huntington's chorea by intrastriatal injections of glutamic and kainic acids, *Nature*, 263 (1976) 517-9.

[123] McGurk, J.F., Bennett, M.V. and Zukin, R.S., Polyamines potentiate responses of N-methyl-D-aspartate receptors expressed in xenopus oocytes, *Proc Natl Acad Sci U S A*, 87 (1990) 9971-4.

[124] Meguro, H., Mori, H., Araki, K., Kushiya, E., Kutsuwada, T., Yamazaki, M., Kumanishi, T., Arakawa, M., Sakimura, K. and Mishina, M., Functional characterization of a heteromeric NMDA receptor channel expressed from cloned cDNAs, *Nature*, 357 (1992) 70-4.

[125] Menegazzi, M., Carcereri De Prati, A.C. and Zucconi, G.G., Differential expression pattern of jun B and c-jun in the rat brain during the 24-h cycle, *Neurosci Lett*, 182 (1994) 295-8.

[126] Misumi, Y., Ogata, S., Hirose, S. and Ikehara, Y., Primary structure of rat liver 5'-nucleotidase deduced from the cDNA. Presence of the COOH-terminal hydrophobic domain for possible post- translational modification by glycophospholipid, *J Biol Chem*, 265 (1990) 2178-83.

[127] Mori, A., Shindou, T., Ichimura, M., Nonaka, H. and Kase, H., The role of adenosine A_{2a} receptors in regulating GABAergic synaptic transmission in striatal medium spiny neurons, *J Neurosci*, 16 (1996) 605-11.

[128] Mori, A., Takahashi, T., Miyashita, Y. and Kasai, H., Quantal properties of H-type glutamatergic synaptic input to the striatal medium spiny neurons, *Brain Res*, 654 (1994) 177-9.

[129] Mori, H. and Mishina, M., Structure and function of the NMDA receptor channel, *Neuropharmacology*, 34 (1995) 1219-37.

[130] Moriyoshi, K., Masu, M., Ishii, T., Shigemoto, R., Mizuno, N. and Nakanishi, S., Molecular cloning and characterization of the rat NMDA receptor, *Nature*, 354 (1991) 31-7.

[131] Nagy, J.I., Geiger, J.D. and Staines, W.A., Adenosine deaminase and purinergic neuroprotection, *Neurochem Int*, 16 (1990) 211-221.

[132] Nakanishi, S., Molecular diversity of glutamate receptors and implications for brain function, *Science*, 258 (1992) 597-603.

[133] Newby, A.C., Adenosine and the concept of 'retaliatory metabolites', *Trends Biochem Sci*, 9 (1984) 42-44.

[134] Newby, A.C., Worku, Y. and Meghji, P., Critical evaluation of the role of ecto- and cytosolic 5'-nucleotidase in adenosine formation. In E. Gerlach and B.F. Becker (Eds.), *Topics and perspectives in adenosine research*, Springer-Verlag, Berlin, 1987, pp. 155-169.

[135] Nowak, L., Bregestovski, P., Ascher, P., Herbet, A. and Prochiantz, A., Magnesium gates glutamate-activated channels in mouse central neurones, *Nature*, 307 (1984) 462-5.

[136] Nusser, Z., Mulvihill, E., Streit, P. and Somogyi, P., Subsynaptic segregation of metabotropic and ionotropic glutamate receptors as revealed by immunogold localization, *Neuroscience*, 61 (1994) 421-7.

[137] Oguro, K., Oguro, N., Kojima, T., Grooms, S.Y., Calderone, A., Zheng, X., Bennett, M.V. and Zukin, R.S., Knockdown of AMPA receptor GluR2 expression causes delayed neurodegeneration and increases damage by sublethal ischemia in hippocampal CA1 and CA3 neurons, *J Neurosci*, 19 (1999) 9218-27.

[138] Onodera, H., Iijima, K. and Kogure, K., Mononucleotide metabolism in the rat brain after transient ischemia, *J Neurochem*, 46 (1986) 1704-10.

[139] Orford, M., Mazurkiewicz, D. and Saggerson, D., Soluble 5'-nucleotidase activities in rat brain, *J Neurochem*, 56 (1991) 141-6.

[140] Parkinson, F.E., Rudolphi, K.A. and Fredholm, B.B., Propentofylline: a nucleoside transport inhibitor with neuroprotective effects in cerebral ischemia, *Gen Pharmacol*, 25 (1994) 1053-8.

[141] Parkinson, F.E., Zhang, Y.W., Shepel, P.N., Greenway, S.C., Peeling, J. and Geiger, J.D., Effects of nitrobenzylthioinosine on neuronal injury, adenosine levels, and adenosine receptor activity in rat forebrain ischemia, *J Neurochem*, 75 (2000) 795-802.

[142] Partin, K.M., Patneau, D.K., Winters, C.A., Mayer, M.L. and Buonanno, A., Selective modulation of desensitization at AMPA versus kainate receptors by cyclothiazide and concanavalin A, *Neuron*, 11 (1993) 1069-82.

[143] Paxinos, G. and Watson, C., *The Rat Brain in Stereotaxic Coordinates*, Academic Press, New York, 1986.

[144] Pazzagli, M., Corsi, C., Fratti, S., Pedata, F. and Pepeu, G., Regulation of extracellular adenosine levels in the striatum of aging rats, *Brain Res*, 684 (1995) 103-6.

[145] Pazzagli, M., Pedata, F. and Pepeu, G., Effect of K^+ depolarization, tetrodotoxin, and NMDA receptor inhibition on extracellular adenosine levels in rat striatum, *Eur J Pharmacol*, 234 (1993) 61-5.

[146] Pedata, F., Magnani, M. and Pepeu, G., Muscarinic modulation of purine release from electrically stimulated rat cortical slices, *J Neurochem*, 50 (1988) 1074-9.

[147] Pedata, F., Pazzagli, M. and Pepeu, G., Endogenous adenosine release from hippocampal slices: excitatory amino acid agonists stimulate release, antagonists reduce the electrically-evoked release, *Naunyn Schmiedebergs Arch Pharmacol*, 344 (1991) 538-43.

[148] Pelled, D., Sperling, O. and Zoref-Shani, E., Abnormal purine and pyrimidine nucleotide content in primary astroglia cultures from hypoxanthine-guanine phosphoribosyltransferase-deficient transgenic mice, *J Neurochem*, 72 (1999) 1139-45.

[149] Pelligrino, D.A., Wang, Q., Koenig, H.M. and Albrecht, R.F., Role of nitric oxide, adenosine, N-methyl-D-aspartate receptors, and neuronal activation in hypoxia-induced pial arteriolar dilation in rats, *Brain Res*, 704 (1995) 61-70.

[150] Perez-Pinzon, M.A., Mumford, P.L., Rosenthal, M. and Sick, T.J., Anoxic preconditioning in hippocampal slices: role of adenosine, *Neuroscience*, 75 (1996) 687-94.

[151] Perkins, M.N. and Stone, T.W., In vivo release of [3H]-purines by quinolinic acid and related compounds, *Br J Pharmacol*, 80 (1983) 263-7.

[152] Perkinton, M.S. and Sihra, T.S., A high-affinity presynaptic kainate-type glutamate receptor facilitates glutamate exocytosis from cerebral cortex nerve terminals (synaptosomes), *Neuroscience*, 90 (1999) 1281-92.

[153] Pin, J.P. and Duvoisin, R., The metabotropic glutamate receptors: structure and functions, *Neuropharmacology*, 34 (1995) 1-26.

[154] Pines, G., Danbolt, N.C., Bjoras, M., Zhang, Y., Bendahan, A., Eide, L., Koepsell, H., Storm-Mathisen, J., Seeberg, E. and Kanner, B.I., Cloning and expression of a rat brain L-glutamate transporter, *Nature*, 360 (1992) 464-7.

[155] Pisani, A., Calabresi, P., Centonze, D. and Bernardi, G., Activation of group III metabotropic glutamate receptors depresses glutamatergic transmission at corticostriatal synapse, *Neuropharmacology*, 36 (1997) 845-51.

[156] Pompeiano, M., Cirelli, C. and Tononi, G., Immediate-early genes in spontaneous wakefulness and sleep: expression of c-fos and NGFI-A mRNA and protein, *J Sleep Res*, 3 (1994) 80-96.

[157] Ponte, P., Ng, S.Y., Engel, J., Gunning, P. and Kedes, L., Evolutionary conservation in the untranslated regions of actin mRNAs: DNA sequence of a human beta-actin cDNA, *Nucleic Acids Res*, 12 (1984) 1687-96.

[158] Popoli, P., Betto, P., Reggio, R. and Ricciarello, G., Adenosine A_{2A} receptor stimulation enhances striatal extracellular glutamate levels in rats, *Eur J Pharmacol*, 287 (1995) 215-7.

[159] Popoli, P., Betto, P., Rimondini, R., Reggio, R., Pezzola, A., Ricciarello, G., Fuxe, K. and Ferre, S., Age-related alteration of the adenosine/dopamine balance in the rat striatum, *Brain Res*, 795 (1998) 297-300.

[160] Porkka-Heiskanen, T., Strecker, R.E. and McCarley, R.W., Brain site-specificity of extracellular adenosine concentration changes during sleep deprivation and spontaneous sleep: an in vivo microdialysis study, *Neuroscience*, 99 (2000) 507-17.

[161] Porkka-Heiskanen, T., Strecker, R.E., Thakkar, M., Bjorkum, A.A., Greene, R.W. and McCarley, R.W., Adenosine: a mediator of the sleep-inducing effects of prolonged wakefulness, *Science*, 276 (1997) 1265-8.

[162] Portas, C.M., Thakkar, M., Rainnie, D.G., Greene, R.W. and McCarley, R.W., Role of adenosine in behavioral state modulation: a microdialysis study in the freely moving cat, *Neuroscience*, 79 (1997) 225-35.

[163] Prince, D.A. and Stevens, C.F., Adenosine decreases neurotransmitter release at central synapses, *Proc Natl Acad Sci U S A*, 89 (1992) 8586-90.

[164] Purkiss, R.J., Legg, M.D., Hunt, S.P. and Davies, S.W., Immediate early gene expression in the rat forebrain following striatal infusion of quinolinic acid, *Eur J Neurosci*, 5 (1993) 1653-62.

[165] Radulovacki, M., Virus, R.M., Djuricic-Nedelson, M. and Green, R.D., Adenosine analogs and sleep in rats, *J Pharmacol Exp Ther*, 228 (1984) 268-74.

[166] Rainnie, D.G., Grunze, H.C., McCarley, R.W. and Greene, R.W., Adenosine inhibition of mesopontine cholinergic neurons: implications for EEG arousal, *Science*, 263 (1994) 689-92.

[167] Reppert, S.M., Weaver, D.R., Stehle, J.H. and Rivkees, S.A., Molecular cloning and characterization of a rat A_1-adenosine receptor that is widely expressed in brain and spinal cord, *Mol Endocrinol*, 5 (1991) 1037-48.

[168] Roche, K.W., Tingley, W.G. and Huganir, R.L., Glutamate receptor phosphorylation and synaptic plasticity, *Curr Opin Neurobiol*, 4 (1994) 383-8.

[169] Rodriguez-Moreno, A. and Lerma, J., Kainate receptor modulation of GABA release involves a metabotropic function, *Neuron*, 20 (1998) 1211-8.

[170] Rosati, A.M., Traversa, U., Florio, C. and Vertua, R., Circadian rhythm of cortical and striatal adenosine receptors, *Life Sci*, 52 (1993) 1677-84.

[171] Rothstein, J.D., Martin, L., Levey, A.I., Dykes-Hoberg, M., Jin, L., Wu, D., Nash, N. and Kuncl, R.W., Localization of neuronal and glial glutamate transporters, *Neuron*, 13 (1994) 713-25.

[172] Roucher, P., Meric, P., Correze, J.L., Mispelter, J., Tiffon, B., Lhoste, J.M. and Seylaz, J., Metabolic effects of R-phenylisopropyladenosine during reversible forebrain ischemia studied by in vivo ^{31}P nuclear magnetic resonance spectroscopy, *J Cereb Blood Flow Metab*, 11 (1991) 453-8.

[173] Rudolphi, K.A., Schubert, P., Parkinson, F.E. and Fredholm, B.B., Adenosine and brain ischemia, *Cerebrovasc Brain Metab Rev*, 4 (1992) 346-69.

[174] Satoh, S., Matsumura, H. and Hayaishi, O., Involvement of adenosine A_{2A} receptor in sleep promotion, *Eur J Pharmacol*, 351 (1998) 155-62.

[175] Satoh, S., Matsumura, H., Suzuki, F. and Hayaishi, O., Promotion of sleep mediated by the A_{2a}-adenosine receptor and possible involvement of this receptor in the sleep induced by prostaglandin D2 in rats, *Proc Natl Acad Sci U S A*, 93 (1996) 5980-4.

[176] Sattler, R., Charlton, M.P., Hafner, M. and Tymianski, M., Distinct influx pathways, not calcium load, determine neuronal vulnerability to calcium neurotoxicity, *J Neurochem*, 71 (1998) 2349-64.

[177] Sattler, R., Xiong, Z., Lu, W.Y., Hafner, M., MacDonald, J.F. and Tymianski, M., Specific coupling of NMDA receptor activation to nitric oxide neurotoxicity by PSD-95 protein, *Science*, 284 (1999) 1845-8.

[178] Schiffmann, S.N. and Vanderhaeghen, J.J., Age-related loss of mRNA encoding adenosine A_2 receptor in the rat striatum, *Neurosci Lett*, 158 (1993) 121-4.

[179] Schmitz, D., Mellor, J. and Nicoll, R.A., Presynaptic kainate receptor mediation of frequency facilitation at hippocampal mossy fiber synapses, *Science*, 291 (2001) 1972-6.

[180] Scholz, K.P. and Miller, R.J., Analysis of adenosine actions on Ca^{2+} currents and synaptic transmission in cultured rat hippocampal pyramidal neurones, *J Physiol*, 435 (1991) 373-93.

[181] Schousboe, A., Frandsen, A. and Drejer, J., Evidence for evoked release of adenosine and glutamate from cultured cerebellar granule cells, *Neurochem Res*, 14 (1989) 871-5.

[182] Sebastiao, A.M., Cunha, R.A., de Mendonca, A. and Ribeiro, J.A., Modification of adenosine modulation of synaptic transmission in the hippocampus of aged rats, *Br J Pharmacol*, 131 (2000) 1629-34.

[183] Sebastiao, A.M. and Ribeiro, J.A., Adenosine A_2 receptor-mediated excitatory actions on the nervous system, *Prog Neurobiol*, 48 (1996) 167-89.

[184] Seki, Y., Feustel, P.J., Keller, R.W., Jr., Tranmer, B.I. and Kimelberg, H.K., Inhibition of ischemia-induced glutamate release in rat striatum by dihydrokinate and an anion channel blocker, *Stroke*, 30 (1999) 433-40.

[185] Sheardown, M.J., Nielsen, E.O., Hansen, A.J., Jacobsen, P. and Honore, T., 2,3-Dihydroxy-6-nitro-7-sulfamoyl-benzo(F)quinoxaline: a neuroprotectant for cerebral ischemia, *Science*, 247 (1990) 571-4.

[186] Simpson, R.E., O'Regan, M.H., Perkins, L.M. and Phillis, J.W., Excitatory transmitter amino acid release from the ischemic rat cerebral cortex: effects of adenosine receptor agonists and antagonists, *J Neurochem*, 58 (1992) 1683-90.

[187] Sinclair, C.J., Shepel, P.N., Geiger, J.D. and Parkinson, F.E., Stimulation of nucleoside efflux and inhibition of adenosine kinase by A1 adenosine receptor activation, *Biochem Pharmacol*, 59 (2000) 477-83.

[188] Sladeczek, F., Pin, J.P., Recasens, M., Bockaert, J. and Weiss, S., Glutamate stimulates inositol phosphate formation in striatal neurones, *Nature*, 317 (1985) 717-9.

[189] Smith, A.D. and Bolam, J.P., The neural network of the basal ganglia as revealed by the study of synaptic connections of identified neurones, *Trends Neurosci*, 13 (1990) 259-65.

[190] Smith, I.D. and Beninger, R.J., Contralateral turning caused by metabotropic glutamate receptor stimulation in the dorsal striatum is reversed by MCPG, TTX, and cis- flupenthixol, *Behav Neurosci*, 110 (1996) 282-9.

[191] Smith, I.D., Todd, M.J. and Beninger, R.J., Glutamate receptor agonist injections into the dorsal striatum cause contralateral turning in the rat: involvement of kainate and AMPA receptors, *Eur J Pharmacol*, 301 (1996) 7-17.

[192] Smolders, I., Sarre, S., Vanhaesendonck, C., Ebinger, G. and Michotte, Y., Extracellular striatal dopamine and glutamate after decortication and kainate receptor stimulation, as measured by microdialysis, *J Neurochem*, 66 (1996) 2373-80.

[193] Sperlagh, B., Zsilla, G., Baranyi, M., Kekes-Szabo, A. and Vizi, E.S., Age-dependent changes of presynaptic neuromodulation via A1-adenosine receptors in rat hippocampal slices, *Int J Dev Neurosci*, 15 (1997) 739-47.

[194] Spychala, J., Datta, N.S., Takabayashi, K., Datta, M., Fox, I.H., Gribbin, T. and Mitchell, B.S., Cloning of human adenosine kinase cDNA: sequence similarity to microbial ribokinases and fructokinases, *Proc Natl Acad Sci U S A*, 93 (1996) 1232-7.

[195] Stehle, J.H., Rivkees, S.A., Lee, J.J., Weaver, D.R., Deeds, J.D. and Reppert, S.M., Molecular cloning and expression of the cDNA for a novel A_2-adenosine receptor subtype, *Mol Endocrinol*, 6 (1992) 384-93.

[196] Steriade, M., Datta, S., Pare, D., Oakson, G. and Curro Dossi, R.C., Neuronal activities in brain-stem cholinergic nuclei related to tonic activation processes in thalamocortical systems, *J Neurosci*, 10 (1990) 2541-59.

[197] Storck, T., Schulte, S., Hofmann, K. and Stoffel, W., Structure, expression, and functional analysis of a Na(+)-dependent glutamate/aspartate transporter from rat brain, *Proc Natl Acad Sci U S A*, 89 (1992) 10955-9.

[198] Strong, R., Neurochemical changes in the aging human brain: implications for behavioral impairment and neurodegenerative disease, *Geriatrics*, 53 Suppl 1 (1998) S9-12.

[199] Szatkowski, M. and Attwell, D., Triggering and execution of neuronal death in brain ischaemia: two phases of glutamate release by different mechanisms, *Trends Neurosci*, 17 (1994) 359-65.

[200] Szymusiak, R., Alam, N., Steininger, T.L. and McGinty, D., Sleep-waking discharge patterns of ventrolateral preoptic/anterior hypothalamic neurons in rats, *Brain Res*, 803 (1998) 178-88.

[201] Tani, Y. and Ishihara, T., Changes in EEG associated with sleep-awake behavior in young adult versus aged adult Fischer-344 rats, *Physiol Behav*, 44 (1988) 389-92.

[202] Tarazi, F.I., Campbell, A., Yeghiayan, S.K. and Baldessarini, R.J., Localization of ionotropic glutamate receptors in caudate-putamen and nucleus accumbens septi of rat brain: comparison of NMDA, AMPA, and kainate receptors, *Synapse*, 30 (1998) 227-35.

[203] Testa, C.M., Standaert, D.G., Young, A.B. and Penney, J.B., Jr., Metabotropic glutamate receptor mRNA expression in the basal ganglia of the rat, *J Neurosci*, 14 (1994) 3005-18.

[204] Trotti, D., Rossi, D., Gjesdal, O., Levy, L.M., Racagni, G., Danbolt, N.C. and Volterra, A., Peroxynitrite inhibits glutamate transporter subtypes, *J Biol Chem*, 271 (1996) 5976-9.

[205] Trussell, L.O. and Jackson, M.B., Adenosine-activated potassium conductance in cultured striatal neurons, *Proc Natl Acad Sci U S A*, 82 (1985) 4857-61.

[206] Tso, J.Y., Sun, X.H., Kao, T.H., Reece, K.S. and Wu, R., Isolation and characterization of rat and human glyceraldehyde-3- phosphate dehydrogenase cDNAs: genomic complexity and molecular evolution of the gene, *Nucleic Acids Res*, 13 (1985) 2485-502.

[207] Tymianski, M., Charlton, M.P., Carlen, P.L. and Tator, C.H., Source specificity of early calcium neurotoxicity in cultured embryonic spinal neurons, *J Neurosci*, 13 (1993) 2085-104.

[208] Van den Noort, S. and Brine, K., Effect of sleep on brain labile phosphates and metabolic rate, *Am J Physiol*, 218 (1970) 1434-9.

[209] Van Gelder, R.N., von Zastrow, M.E., Yool, A., Dement, W.C., Barchas, J.D. and Eberwine, J.H., Amplified RNA synthesized from limited quantities of heterogeneous cDNA, *Proc Natl Acad Sci U S A*, 87 (1990) 1663-7.

[210] van Gool, W.A. and Mirmiran, M., Effects of aging and housing in an enriched environment on sleep-wake patterns in rats, *Sleep*, 9 (1986) 335-47.

[211] Veech, R.L., Harris, R.L., Veloso, D. and Veech, E.H., Freeze-blowing: A technique for the study of brain *in vivo*, *J Neurochem*, 20 (1973) 183-188.

[212] Verhaegen, M., Iaizzo, P.A. and Todd, M.M., A comparison of the effects of hypothermia, pentobarbital, and isoflurane on cerebral energy stores at the time of ischemic depolarization, *Anesthesiology*, 82 (1995) 1209-15.

[213] Virus, R.M., Baglajewski, T. and Radulovacki, M., Circadian variation of [3H]N6-(L-phenylisopropyl)adenosine binding in rat brain, *Neurosci Lett*, 46 (1984) 219-22.

[214] von Lubitz, D.K., Carter, M.F., Beenhakker, M., Lin, R.C. and Jacobson, K.A., Adenosine: a prototherapeutic concept in neurodegeneration, *Ann N Y Acad Sci*, 765 (1995) 163-78; discussion 196-7.

[215] von Lubitz, D.K., Ye, W., McClellan, J. and Lin, R.C., Stimulation of adenosine A3 receptors in cerebral ischemia. Neuronal death, recovery, or both?, *Ann N Y Acad Sci*, 890 (1999) 93-106.

[216] Wahl, F., Obrenovitch, T.P., Hardy, A.M., Plotkine, M., Boulu, R. and Symon, L., Extracellular glutamate during focal cerebral ischaemia in rats: time course and calcium dependency, *J Neurochem*, 63 (1994) 1003-11.

[217] Wakade, A.R., Guo, X., Palmer, K.C., Kulkarni, J.S., Przywara, D.A. and Wakade, T.D., 2'-deoxyadenosine induces apoptosis in rat chromaffin cells, *J Neurochem*, 67 (1996) 2273-81.

[218] Walker, B.A., Rocchini, C., Boone, R.H., Ip, S. and Jacobson, M.A., Adenosine A_{2a} receptor activation delays apoptosis in human neutrophils, *J Immunol*, 158 (1997) 2926-31.

[219] Walker, P.D. and Carlock, L.R., Immediate early gene activation during the initial phases of the excitotoxic cascade, *J Neurosci Res*, 36 (1993) 588-95.

[220] Wang, J.Q., Regulation of immediate early gene c-fos and zif/268 mRNA expression in rat striatum by metabotropic glutamate receptor, *Brain Res Mol Brain Res*, 57 (1998) 46-53.

[221] Watanabe, M., Inoue, Y., Sakimura, K. and Mishina, M., Distinct distributions of five N-methyl-D-aspartate receptor channel subunit mRNAs in the forebrain, *J Comp Neurol*, 338 (1993) 377-90.

[222] White, T.D., Potentiation of excitatory amino acid-evoked adenosine release from rat cortex by inhibitors of adenosine kinase and adenosine deaminase and by acadesine, *Eur J Pharmacol*, 303 (1996) 27-38.

[223] White, T.D., Craig, C.G. and Hoehn, K., Extracellular adenosine, formed during low level NMDA receptor activation, provides an inhibitory threshold against further NMDA receptor-mediated neurotransmission in the cortex, *Drug Dev Res*, 28 (1993) 406-409.

[224] Williams, M., Purinergic Drugs: Opportunities in the 1990s, *Drug Dev Res*, 28 (1993) 438-444.

[225] Wilson, C.J., Morphology and synaptic connections of crossed corticostriatal neurons in the rat, *J Comp Neurol*, 263 (1987) 567-80.

[226] Wisden, W. and Seeburg, P.H., A complex mosaic of high-affinity kainate receptors in rat brain, *J Neurosci*, 13 (1993) 3582-98.

[227] Wojcik, W., Olianas, M., Parenti, M., Gentleman, S. and Neff, N.H., A simple fluorometric method for cAMP: application to studies of brain adenylate cyclase activity, *J Cyclic Nucleotide Res*, 7 (1981) 27-35.

[228] Wojcik, W.J. and Neff, N.H., Adenosine measurement by a rapid HPLC-fluorometric method: induced changes of adenosine content in regions of rat brain, *J Neurochem*, 39 (1982) 280-2.

[229] Wojcik, W.J. and Neff, N.H., Differential location of adenosine A_1 and A_2 receptors in striatum, *Neurosci Lett*, 41 (1983) 55-60.

[230] Yan, L., Takekida, S., Shigeyoshi, Y. and Okamura, H., Per1 and Per2 gene expression in the rat suprachiasmatic nucleus: circadian profile and the compartment-specific response to light, *Neuroscience*, 94 (1999) 141-50.

[231] Yao, S.Y., Ng, A.M., Muzyka, W.R., Griffiths, M., Cass, C.E., Baldwin, S.A. and Young, J.D., Molecular cloning and functional characterization of nitrobenzylthioinosine (NBMPR)-sensitive (es) and NBMPR-insensitive (ei) equilibrative nucleoside transporter proteins (rENT1 and rENT2) from rat tissues, *J Biol Chem*, 272 (1997) 28423-30.

[232] Yeung, C.Y., Ingolia, D.E., Roth, D.B., Shoemaker, C., Al-Ubaidi, M.R., Yen, J.Y., Ching, C., Bobonis, C., Kaufman, R.J. and Kellems, R.E., Identification of functional murine adenosine deaminase cDNA clones by complementation in Escherichia coli, *J Biol Chem*, 260 (1985) 10299-307.

[233] Yoon, K.W. and Rothman, S.M., Adenosine inhibits excitatory but not inhibitory synaptic transmission in the hippocampus, *J Neurosci*, 11 (1991) 1375-80.

[234] Young, A.M., Crowder, J.M. and Bradford, H.F., Potentiation by kainate of excitatory amino acid release in striatum: complementary in vivo and in vitro experiments, *J Neurochem*, 50 (1988) 337-45.

[235] Yu, X.M., Askalan, R., Keil, G.J., 2nd and Salter, M.W., NMDA channel regulation by channel-associated protein tyrosine kinase Src, *Science*, 275 (1997) 674-8.

[236] Zhang, G., Franklin, P.H. and Murray, T.F., Manipulation of endogenous adenosine in the rat prepiriform cortex modulates seizure susceptibility, *J Pharmacol Exp Ther*, 264 (1993) 1415-24.

[237] Zhang, L., Rzigalinski, B.A., Ellis, E.F. and Satin, L.S., Reduction of voltage-dependent Mg^{2+} blockade of NMDA current in mechanically injured neurons, *Science*, 274 (1996) 1921-3.

[238] Zhang, Y., Geiger, J.D. and Lautt, W.W., Improved high-pressure liquid chromatographic-fluorometric assay for measurement of adenosine in plasma, *Am J Physiol*, 260 (1991) G658-64.

[239] Zhou, Q.Y., Li, C., Olah, M.E., Johnson, R.A., Stiles, G.L. and Civelli, O., Molecular cloning and characterization of an adenosine receptor: the A3 adenosine receptor, *Proc Natl Acad Sci U S A*, 89 (1992) 7432-6.